Astrocyte-specific function of A20 and FasL in experimental autoimmune encephalomyelitis

Dissertation

zur Erlangung des akademischen Grades

doctor rerum naturalium

(Dr. rer. nat.)

genehmigt durch die Fakultät für Naturwissenschaften

der Otto-von-Guericke-Universität Magdeburg

von M.Sc. Xu Wang

geb. am 16. Feburar 1986 in Shandong, China

Gutachter:	**Prof. Dr. med. Dirk Schlüter**
	Prof. Dr. Lydia Sorokin
eingereicht am:	**10.12.2014**
verteidigt am:	**04.05.2015**

Acknowledgements

First of all, I would like to give my special thanks to my supervisor Prof. Dirk Schlüter for giving me the opportunity to do my doctoral thesis in his laboratory. His immense knowledge and professional supervision enables me to finish my PhD study. I would also like to thank him for encouraging and supporting me to attend various conferences, which greatly broaden my scientific horizons and spark new ideas. As a knowlegable scientist, Prof. Schlüter sets a good example for me, which helps me develop interest in science and will have a long-lasting influence on my future career.

I would like to deeply thank my second supervisor Prof. Michael Naumann for his constructive suggestions and valuable discussions during the thesis committee meetings. I thank Prof. Naumann for accepting me to join the graduate school GRK1167 directed by him. The GRK1167 provides me with interesting lectures, seminars, workshops and retreats, which are of particular help for my study.

I am grateful to Prof. Martina Deckert and Elena Fischer for their help with histology. I would like to thank Prof. Ari Waisman for the helpful discussions.

I appreciate Ms. Annette Sohnekind, Ms. Nadja Schlüter and Ms. Anita Marquardt for their excellent technical assistance. I would like to express my gratitude to other members in our lab, including Dr. Nikolaus Koniszewski, Dr. Nishanth Gopala, Dr. Nguyen Thi Xuan, Ms. Shanshan Song, and Miss. Sissy Just for their help and support.

Last but not the least, I would like to sincerely thank my parents and my wife Ms. Jing Ruan for their constant love, encouragement and support. I love you all.

Publications

This work is published under the following titles:

<u>**Wang X**</u>, Haroon F, Karray S, Deckert M, Schlüter D. (2013). Astrocytic Fas ligand expression is required to induce T-cell apoptosis and recovery from experimental autoimmune encephalomyelitis. *Eur. J. Immunol*. Jan; 43(1): 115-124

<u>**Wang X**</u>, Deckert M, Xuan NT, Nishanth G, Just S, Waisman A, Naumann M, Schlüter D. (2013) Astrocytic A20 ameliorates experimental autoimmune encephalomyelitis by inhibiting NF-κB- and STAT1-dependent chemokine production in astrocytes. *Acta Neuropathol*. Nov; 126(5): 711-724

<u>**Other Publications**</u>

Xuan NT*, <u>**Wang X**</u>*, Nishanth G, Waisman A, Borucki K, Isermann B, Naumann M, Deckert M, Schlüter D. (2014) A20 expression in dendritic cells protects mice from LPS-induced mortality. *Eur. J. Immunol*. DOI: 10.1002/eji.201444795   *These authors contributed equally to this work

Table of Contents

Abbreviations

A

ABIN-1	A20 binding and inhibitor of NF-κB
Ag	Antigen
Apaf-1	Apoptotic protease-activating factor 1
APC	Antigen-presenting cell
APO-1	Apoptosis antigen 1
ASK1	Apoptosis signal-regulating kinase 1
ATP	Adenosine triphosphate

B

BAFF	B-cell activating factor
BBB	Blood brain barrier
BMDC	Bone marrow-derived dendritic cell
BMDM	Bone marrow-derived macrophage
BSA	Bovine serum albumin

C

CBA	Cytometric Bead Arrays
CCL	Chemokine (C-C motif) ligand
CD	Cluster of differentiation
CFA	Complete Freund's adjuvant
CNS	Central nervous system
CRDs	Cysteine rich domains
CSF	Cerebrospinal fluid
CTLA-4	Cytotoxic T lymphocyte-associated antigen-4
CXCL	Chemokine (C-X-C motif) ligand
CYLD	Cylindromatosis

D

DC	Dendritic cell
DED	Death effector domain
DISC	Death inducing signaling complex
DSS	dextran sulphate sodium
DUBs	Deubiquitinating enzymes

E

EAE	Experimental autoimmune encephalomyelitis
EBV	Epstein-Barr virus
ERK	Extracellular signal-regulated kinases

F

FADD	Fas-associated death domain protein

FasL Fas ligand

G
GM-CSF Granulocyte-macrophage colony-stimulating factor
GFAP Glial fibrillary acidic protein
gld generalized lymphoproliferative disease
GWAS Genome-wide association study

H
HBSS Hank's Balanced Salt Solution
HDAC Histone deacetylase
HEPES (4-(2-Hydroxyethyl)-1-piperazineethanesulfonic acid
HPRT Hypoxanthine phosphoribosyltransferase
HUVEC Human umbilical vein endothelial cell

I
IBD Inflammatory bowel disease
IEC Intestinal epithelial cell
IFN Interferon
IKK IκB kinase
IL Interleukin
i.p. Intraperitoneal
IRAK1 Interleukin-1 receptor-associated kinase 1
IRF Interferon regulatory factor
i.v. Intravenous
IκB Inhibitor of NF-κB

J
JNK c-Jun N-terminal kinase

K
K Lysine

L
lpr lymphoproliferation
LPS Lipopolysaccharide
LUBAC Linear ubiquitin chain assembly complex

M
MACS Magnetic-activated cell sorting
MAPK Mitogen-activated protein kinase
MBP Myelin basic protein
MDP Muramyl dipeptide
MEF Mouse embryonic fibroblast

MOG	Myelin oligodendrocyte glycoprotein
MS	Multiple Sclerosis
MyD88	Myeloid differentiation primary response gene 88

N

NEMO	NF-kappa-B essential modulator
NF-κB	Nuclear factor 'kappa-light-chain-enhancer' of activated B-cells
NIK	NF-κB inducing kinase
NK	Natural killer
NO	Nitric oxide
NOD2	Nucleotide-binding oligomerization domain containing 2
NOS	Nitric oxide synthase

O

OTUs	Ovarian tumour-related proteases

P

PFA	Paraformaldehyde
PMA	Phorbol 12-myristate 13-acetate
PBS	Phosphate buffered saline
PLP	Proteolipid protein
PRR	Pattern recognition receptor
PRD	Proline rich domain

Q

qRT-PCR	quantitative real time-PCR

R

RHD	Rel homology domain
RIP1	Receptor-Interacting Protein 1
RNF11	Ring finger protein 11
ROS	Reactive oxygen species

S

siRNA	Small interfering RNA
SLE	Systemic lupus erythematosus
SNP	Single-nucleotide polymorphism
STAT1	Signal transducer and activator of transcription 1

T

TAD	Transactivation domain
TAX1BP1	Tax1 binding protein 1
TGF-β	Transforming growth factor beta
Th	T helper
THD	TNF homology domain
TIMPs	Tissue inhibitors of metalloproteinases

TLR   Toll like receptor
TNF   Tumor necrosis factor
TNFAIP3   TNF alpha-induced protein 3
TNFRSF6   TNF receptor superfamily member 6
TRAF   TNF receptor-associated factor
TRAIL   TNF-related apoptosis-inducing ligand
TWEAK   TNF-related weak inducer of apoptosis

U
Ub   Ubiquitin
UBA   Ubiquitin-like modifier activating enzyme
UCHs   Ubiquitin carboxy-terminal hydrolases
USPs   Ubiquitin-specific proteases

W
WB   Western blot
WT   Wildtype

7
7-AAD   7-amino actinomycin D

1. Introduction

Multiple sclerosis (MS) is an inflammatory demyelinating disease of the central nervous system (CNS). It is estimated that between 2 and 2.5 million people are affected by MS in the world and the disease is twice as common in women as in men (Milo and Kahana, 2010). MS is pathologically characterized by perivascular infiltrates of inflammatory cells, demyelination, and axonal damage, with the formation of multiple plaques in the brain and spinal cord. Clinically, MS patients show symptoms of visual disturbances, paresthesias, muscle weakness and ataxia. MS usually begins between the age of 20 and 50 and is the leading cause of disability resulting from CNS inflammation in young adults in western countries. So far, the cause of MS is still unclear, and not a single genetic or environmental factor has been unambiguously identified as the causative agent of MS. It is generally accepted that MS is a multifactorial disease caused by complex interactions between susceptibility genes and environmental factors. The leading environmental factor candidates are infectious agents, particularly Epstein-Barr virus (EBV), and vitamin D (Ascherio and Munger, 2007b; Ascherio and Munger, 2007a).

Experimental autoimmune encephalomyelitis (EAE) is a widely used animal model to study MS. Both EAE and MS are inflammatory demyelinating diseases mediated by infiltration of T lymphocytes and macrophages in the CNS (McFarland and Martin, 2007; Baxter, 2007). EAE can be induced in mice by active immunization with myelin antigens such as myelin oligodendrocyte glycoprotein (MOG) peptide or passive transfer of myelin-reactive $CD4^+$ T lymphocytes, which are both initiators and effectors of EAE. Among $CD4^+$ T cells, T helper 1 (Th1), T helper 17 (Th17), and granulocyte-macrophage colony-stimulating factor (GM-CSF)-producing $CD4^+$ T cells have been identified as important mediators in the immunopathogenesis of EAE and all of them can induce EAE independently (Lees et al., 2008; Stromnes et al., 2008; Codarri et al., 2011; Domingues et al., 2010). To some extent, T cell responses can be regulated by CNS-resident cells; therefore, some CNS-resident cell populations may play a critical role in the pathogenesis of MS and EAE. Neurons, though often neglected as immune-regulating cells, contribute to the suppression of EAE by controlling the conversion of encephalitogenic T cells to $CD25^+$ $Foxp3^+$ regulatory T cells (Liu et al., 2006). As active players in CNS innate immunity, astrocytes may play various roles in EAE. In our study, we are interested in elucidating the function of astrocyte-derived A20 and FasL in the pathogenesis and development of EAE.

1.1 Astrocytes

 Astrocytes, also called astroglia, are star-shaped glial cells of the central nervous system (CNS) and are, therefore, named with the ancient Greek root word 'astro', which means star. Astrocytes are a major cellular constituent of the CNS. Astrocytes are characterized by their specific intermediate filament glial fibrillary acidic protein (GFAP) (Eng, 1985). Based on the morphology and location, rodent astrocytes can be classified into two distinct groups: highly ramified protoplasmic astrocytes in the grey matter, which ensheath synapses and blood vessels with their membraneous processes and fibrous astrocytes in the white matter, which are in contact with blood vessels and nodes of ranvier (Barres, 2008). Functionally, astrocytes provide an optimal physical and metabolic environment for neuronal activities. They play an important role in controlling potassium homeostasis in the extracellular space of the CNS. Active neurons release potassium, resulting in the local increase of extracellular potassium concentration. Astrocytes, which express potassium channels at a high density, rapidly clear potassium from the extracellular space (Walz, 2000). Upon stimulation by neurotransmitters, astrocytes produce neuroactive substances and trophic factors, thereby controlling development and function of synapses and neuronal survival. Purified retinal ganglion cells, a type of CNS neurons, cultured in the absence of astrocytes exhibit little synaptic activity although they express dendrites and axons and are electrically excitable. However, synaptic activity is strongly enhanced in retinal ganglion cells cocultured with astrocytes or cultured in culture medium conditioned by astrocytes (Pfrieger and Barres, 1997). Ullian et al. found that only few functionally immature synapses were formed between retinal ganglion cells cultured in the absence of astrocytes. Coculture with astrocytes strongly increases the number of synapses, and more importantly, astrocytes also enhance the presynaptic and postsynaptic functions of formed synapses (Ullian et al., 2001). Christopherson et al identified that astrocytes promoted CNS synaptogenesis by releasing thrombospondin (Christopherson et al., 2005). Thrombospondin is able to induce the formation of synapses that are ultrastructurally normal. *In vivo*, synapse number is significantly decreased in thrombospondin 1/2-deficient brains (Christopherson et al., 2005). In addition to promoting the formation and function of synapses, astrocytes also contribute to the survival of neurons. Astrocytes promote the growth and prolong the survival of neurons by producing neurotrophic factors (Banker, 1980). Neuronal survival is reduced in epidermal growth factor receptor (EGFR)-deficient mice, in which cortical astrocytes display increased apoptosis (Wagner et al.,

2006). In addition to the important functions mentioned above, astrocytes also play important roles in CNS diseases. Astrocytes are activated during CNS diseases, leading to astrogliosis, which is usually beneficial because it helps to encapsulate infection and seal damaged blood brain barrier. In this regard, we have found that gp130-dependent astrocyte survival and astrogliosis are critical to restrict CNS inflammation in *Toxoplasma* encephalitis and EAE (Drogemuller et al., 2008; Haroon et al., 2011).

1.1.1 Role of astrocytes in EAE

According to the three stage theory of EAE (McFarland and Martin, 2007; Zepp et al., 2011), EAE includes (1) an initiation stage, in which myelin-reactive T cells are expanded in the periphery; (2) an effector stage, in which myelin-specific T cells are recruited to and reactivated in the CNS and start tissue destruction; and (3) a recovery stage, in which immune responses in the CNS are suppressed. Astrocytes are substantially involved in all three stages of EAE and play both beneficial and detrimental roles in this CNS autoimmune disease.

Initiation stage

In the initiation stage, astrocytes contribute to CNS immune privilege by forming the blood brain barrier (BBB), the location where first interaction between immune cells and CNS happens during neuroinflammation. The BBB is a composition of several different barriers that include tight junctions between CNS endothelial cells, low rates of endocytosis in endothelial cells, and high levels of export and import transporters (Zlokovic, 2008). The importance of astrocytes in the formation of BBB is presented by their ability to induce various BBB properties in endothelial cells of non-neural origin (Janzer and Raff, 1987; Kuchler-Bopp et al., 1999; Hayashi et al., 1997). In addition, the BBB-inducing function of astrocytes is conserved among species and rat astrocytes are able to induce neural endothelium-specific functions in human non-neural endothelial cells (Kuchler-Bopp et al., 1999; Hayashi et al., 1997). In addition to inducing other cells to form BBB, astrocytes themselves are also involved in the construction of BBB by building the glia limitans with their end-feet. As part of the BBB, astrocytes protect the CNS parenchyma from the invasion of encephalitogenic T cells in at least two ways: mechanical and functional. Due to specificities of glial basal lamina composition, the glia limitans is impermeable to T cells (Miljkovic et al., 2011; Bechmann et al., 2007). In order to migrate into the CNS parenchyma, T cells have to penetrate the glia limitans in cooperation with

macrophages/microglia (Tran et al., 1998). In addition to stopping T cells mechanically, astrocytes can also induce the apoptosis of T cells. The death ligand CD95L/FasL is constitutively expressed on the astrocytic end-feet and astrocytes can induce apoptosis of T cells in a FasL dependent way, thereby preventing the invasion of T cells into the CNS parenchyma (Bechmann et al., 1999; Bechmann et al., 2002). Although BBB is impermeable to most leukocytes, it can be crossed by low numbers of activated T cells that patrol the CNS. In the late phase of initiation stage, myelin-reactive T cells penetrate BBB nonspecifically and get reactivated by CNS antigens, leading to the effector stage.

Effector stage

The effector stage of EAE involves two waves of leukocyte invasion, which are associated with the initiation of EAE symptoms. After expansion in the periphery, myelin-specific T cells traffic through the choroid plexus to the subarachnoid space (Wave 1) where they are restimulated by antigens presented by menigeal APCs, including dendritic cells, macrophages and microglia (Engelhardt and Sorokin, 2009; Kebir et al., 2007; Reboldi et al., 2009). Since astrocytes can also express MHC class II, it is possible that astrocytes might also be able to present autoantigens to invading T cells in the CNS (Zeinstra et al., 2000). It has been shown that, during EAE, astrocytes can process and present MOG, proteolipid protein (PLP), and myelin basic protein (MBP) to encephalitogenic CD4$^+$ T cells (Tan et al., 1998; Kort et al., 2006).

As a result, T cells undergo clonal expansion and produce inflammatory cytokines, which stimulate adjacent CNS resident cells, in particular astrocytes, to produce leukocyte-recruiting chemokines and cytokines. Consequently, a large amount of perivascular leukocytes is recruited to the CNS parenchyma, leading to an explosive inflammatory cascade that is associated with the onset of EAE. At the effector stage, the large numbers of inflammatory cells, including T cells, migrate to the white matter of the CNS and initiate tissue destruction, including demyelination and axonal damage. As a major source of chemokines and cytokines in the CNS, astrocytes produce a large variety of chemokines and cytokines, including BAFF, GM-CSF, IFN-β, IL-1β, IL-6, TGF-β, TNF, CCL2, CCL5, CCL20, CXCL1, CXCL2, ,CXCL9, CXCL10, CXCL11, and CXCL12 (Brambilla et al., 2005; Kang et al., 2010; Zhou et al., 2011; Mason et al., 2001; Lieberman et al., 1989; Krumbholz et al., 2005; Diniz et al., 2012; Van Wagoner et al., 1999). Chemokines produced by astrocytes are of particular importance for the progression from Wave 1 to Wave 2. The NF-κB signaling pathway, in synergy with MAPK and other signaling

pathways, plays a key role in modulating chemokine expression in astrocytes (Fig. 1). Inactivation of astroglial NF-κB significantly reduces CCL2 and CXCL10 expression in mouse ischemic injury (Dvoriantchikova et al., 2009). Ablation of NF-κB activators NEMO or IKK2 in astrocytes reduces the expression of proinflammatory chemokines including CCL5 and CXCL10, as well as the adhesion molecule VCAM1. As a result, CNS-restricted deletion of NEMO or IKK2 ameliorates EAE in mice (van et al., 2006). Consistently, Brambilla et al. also found that transgenic inactivation of NF-κB resulted in reduced disease severity and improved functional recovery during MOG_{35-55}-induced EAE (Brambilla et al., 2009). Act1, an ubiquitinase capable of activating TRAF6 through K63-linked ubiquitination (Liu et al., 2009), is indispensable for the activation of the NF-κB cascade induced by IL-17 (Qian et al., 2007). In CNS-restricted Act1 knockout mice, IL-17 mediated NF-κB activation in astrocytes was abolished, leading to compromised production of chemokines, such as CXCL1, CXCL2 and CCL20, in the CNS and ameliorated EAE symptoms (Kang et al., 2010). TRAF3 is identified as a receptor proximal negative regulator of IL-17 receptor signaling and interferes with the formation of IL-17R-Act1-TRAF6 activation complex by competitive binding with the IL-17 receptor. TRAF3 inhibits IL-17 induced NF-κB and mitogen-activated protein kinase activation and subsequent production of chemokines and cytokines. Similar to CNS-restricted ablation of Act1, over-expression of TRAF3 in the CNS can also ameliorate EAE (Zhu et al., 2010). Estradiol has been shown to inhibit NF-κB-dependent CCL2 expression in astrocytes *in vitro*. Consistently, *in vivo*, treatment with Estradiol decreases astrocytic CCL2 expression and ameliorates ongoing EAE (Giraud et al., 2010). However, not all the chemokines and cytokines produced by astrocytes during EAE are detrimental. In sharp contrast, CXCL12, which is upregulated in the CNS of MS patients, particularly produced by astrocytes, suppresses EAE by redirecting the polarization of Th1 cells into regulatory T cells (Meiron et al., 2008). In addition to producing T cell-manipulating cytokines and chemokines, astrocytes can also express iNOS, which produces NO and causes direct damage in the CNS. Blocking NO production by inhibition of iNOS reduces the severity of EAE (Zhao et al., 1996). Astrocytes are one of the most important sources of iNOS in the CNS during EAE (Tran et al., 1997) and their production of NO can be stimulated by fingerprint cytokines of encephalitogenic Th1 and Th17 cells, including IFN-γ , TNF, and IL-17 (Trajkovic et al., 2001; Saha and Pahan, 2006). Demyelination is a major feature of EAE, and astrocytes contribute to demyelination through phagocytosis of

myelin (Lee et al., 1990) and production of molecules, such as redox reactants, that are toxic to oligodendrocytes (Antony et al., 2004).
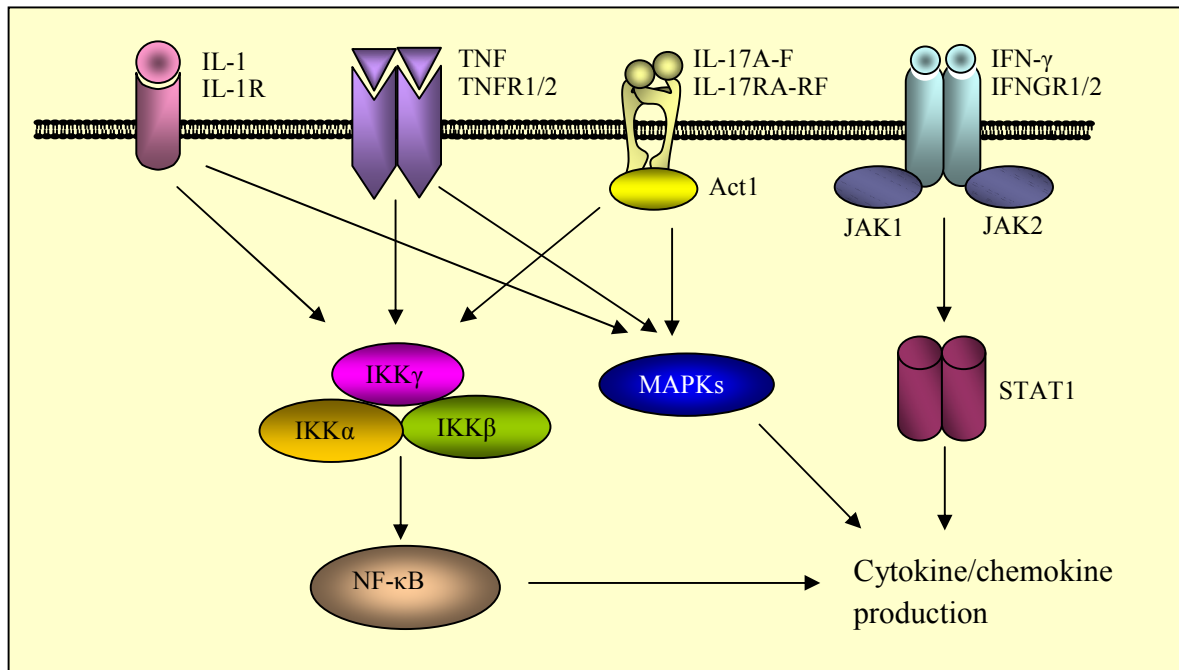
Figure 1. Signaling pathways induced by cytokines produced by encephalitic T cells
T cells are effector cells of EAE and they produce various cytokines such as IL-1, TNF, IL-17, and IFN-γ. These cytokines activate multiple signaling pathways, including NF-κB, MAPKs, and STAT1, in astrocytes, leading to the production of various cytokines and chemokines, which are critical for the progression from wave 1 to wave 2 of T cell recruitment.

Recovery stage

The recovery stage, in which inflammation in the CNS is inhibited, is associated with elimination of invading leukocytes in the CNS and remyelination. Astrocytes contribute substantially to the recovery from EAE. After EAE onset, reactive astrogliosis is formed, in which astrocytes intensively proliferate and migrate to the lesions. Astrogliosis can be detrimental because the scar formed by astrocytes, characterized as a physical barrier around the demyelinated area, inhibits remyelination and neuro-regeneration (Bannerman et al., 2007; Nair et al., 2008). During EAE, astrogliosis and scar formation is absent in GFAP-TK transgenic mice, in which reactive and dividing astrocytes can be inducibly deleted (Voskuhl et al., 2009). However, due to the absence of scar-like perivascular barrier formed by astrocytes, inflammation and demyelination is more prominent and widespread in these mice, showing that astrogliosis is beneficial during EAE. We have shown that, during EAE, loss of gp130 expression results in apoptosis of astrocytes in inflammatory lesions of GFAP-Cre gp130$^{fl/fl}$ mice, in which gp130 was specifically

deleted in astrocytes. Due to astrocyte loss, GFAP-Cre gp130$^{fl/fl}$ mice are unable to mount astrogliosis in EAE, leading to larger areas of demyelination and increased CD4^{+} T cell infiltration in the CNS (Haroon et al., 2011). Apoptotic elimination of encephalitogenic T cells in the CNS has been shown to be important for EAE resolution (Pender et al., 1991; Schmied et al., 1993). Among CNS-resident cells, astrocytes may be key inducers of T cell apoptosis because (1) astrocytes express apoptosis-inducing FasL and autoreactive CD4^{+} T cells are Fas^{+} (Kohji and Matsumoto, 2000; Bonetti et al., 1997); (2) astrocytes are in intimate contact with apoptotic T cells during EAE (Kohji and Matsumoto, 2000); (3) astrocytes induce apoptosis of CD4^{+} T cells *in vitro* in a FasL dependent way (Bechmann et al., 2002). Therefore, astrocytes might contribute to EAE recovery by inducing apoptotic elimination of infiltrating autoreactive T cells. As a major source of cytokines, astrocytes can also promote EAE recovery by producing immunosuppressive cytokines, such as IL-27 (Hindinger et al., 2012; Fitzgerald et al., 2007). The costimulatory molecule cytotoxic T lymphocyte-associated antigen-4 (CTLA-4, CD152) provides inhibitory signals leading to inhibition of T cell activation and suppression of ongoing responses (Egen et al., 2002). Blocking CTLA-4 during the onset of EAE markedly exacerbates the diseases (Perrin et al., 1996). It was shown that astrocytes inhibited MBP-specific T cell activation, proliferation and effector function by enhancing CTLA-4 expression on T cells (Gimsa et al., 2004), indicating that astrocytes can also ameliorate EAE by inhibiting T cell responses. In sharp contrast to EAE-promoting Th1 and Th17 cells, regulatory T cells are protective in EAE. Astrocytes can also induce a regulatory phenotype among infiltrating autoreactive T cells, thereby mitigating the disease (Trajkovic et al., 2004). In addition, astrocytes can also contribute to EAE recovery by enhancing myelin repair. Astrocytes express matrix metalloproteinase 9 (MMP-9), which has been shown to mediate oligodendrocyte process growth (Uhm et al., 1998). MMP-9-deficient mice show impaired remyelination after a demyelinating insult (Larsen et al., 2003). MMP activity is inhibited by tissue inhibitors of metalloproteinases (TIMPs), which are also produced by astrocytes in demyelinating areas in EAE (Pagenstecher et al., 1998). Ablation of TIMP-1 in mice results in enhanced immune cell invasion and deficiency in myelin repair (Crocker et al., 2006).

1.2 Fas-FasL

Fas, also called apoptosis antigen 1 (APO-1), cluster of differentiation 95 (CD95) or tumor necrosis factor receptor superfamily member 6 (TNFRSF6), is a death receptor on the cell surface that leads to apoptosis (Itoh et al., 1991). Mature Fas is a type I transmembrane protein of 319 aa, consisting of a 157 aa extracellular domain and a 145 aa intracellular domain (Fig. 2). The extracellular domain contains three cysteine rich domains (CRDs), which are required for ligand binding (Orlinick et al., 1997). The intracellular domain contains a death domain, which is required for apoptosis induction (Itoh and Nagata, 1993). Expression of Fas has been detected on various cell populations, including cells of the hematopoietic system, epithelial cells, and fibroblasts. Fas ligand (FasL, also called APO-1L, CD95L, TNFSF6; CD178) is type II transmembrane protein that belongs to the tumor necrosis factor (TNF) family (Suda et al., 1993). Structurally, FasL also consists of a 179 aa extracellular domain, which contains a TNF homology domain (THD) (Bodmer et al., 2002), and a 80 aa intracellular domain, which contains a proline rich domain (PRD). The receptor binding site (RB) is located at the very C terminus of FasL and mediates specific binding to the CRDs of Fas. FasL exists in two forms, either soluble or membrane-bound. Interestingly, only membrane-bound FasL triggers death induction, whereas soluble FasL counteracts it (O' Reilly et al., 2009). In fact, soluble FasL is chemoattractant and recruits neutrophils and phagocytes to the site of inflammation (Ottonello et al., 1999; Seino et al., 1998).
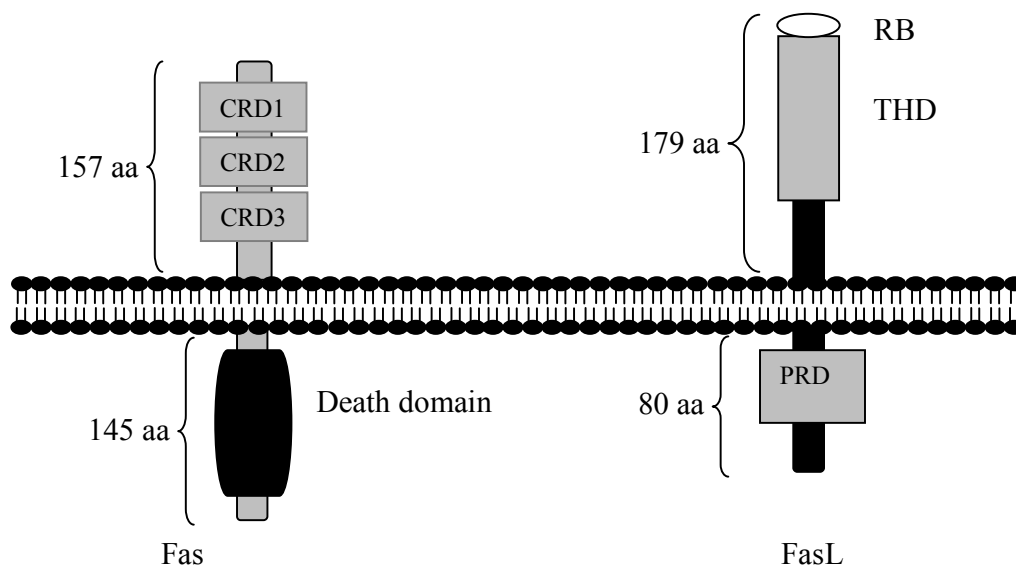
Figure 2. Domain structure of Fas and FasL
Both Fas and FasL are transmembrane proteins, and consists of an extracellular domain and an intracellular domain, respectively. CRD, cysteine rich domain; RB, receptor binding site; THD, TNF homology domain; PRD, proline rich domain (modified from (Ehrenschwender and Wajant, 2009))

Binding of FasL with Fas induces the assembly of death inducing signaling complex (DISC). One crucial part of DISC is the receptor adaptor protein Fas-associated death domain protein (FADD), which bridges Fas with procaspase-8 (Chinnaiyan et al., 1995; Boldin et al., 1996; Muzio et al., 1996) (Fig. 3). FADD directly binds to the death domain of Fas via its C-terminal death domain and interact with procaspase-8 via its N-terminal death effector domain (DED), thereby mediating the recruitment of procaspase-8 to the DISC (Chinnaiyan et al., 1995; Boldin et al., 1995). Within the DISC, procaspase-8 is processed into mature heterotetrameric caspase-8 following its initial activation by dimerization, which is negatively regulated by FLICE-inhibitory protein (FLIP) (Wajant et al., 2003; Donepudi et al., 2003; Boatright et al., 2003). Active caspase-8 is released from the DISC and induce the activation of effector caspases, in particular caspase-3, to mediate cell apoptosis. If caspase-8 levels are high, it directly activates effector caspases to trigger apoptosis (Maher et al., 2002; Peter and Krammer, 2003). However, in certain cells, caspase-8 expression is low. In these cells, caspase-8 cleaves Bid into tBid, which translocates to the outer mitochondrial membrane and activates Bak. Activated Bak oligomerizes and forms pores in the outer mitochondrial membrane allowing the release of proapoptotic proteins, including cytochrome c, to the cytoplasm (Barnhart et al., 2003).

Cytochrome c interacts with apoptotic protease-activating factor 1 (Apaf-1), ATP, and procaspase-9 to mediate capase-9 activation. Similar to caspase-8, active caspase-9 cleaves and activates caspase-3 to trigger the cell death machinery (Riedl and Salvesen, 2007).

Expression of FasL is linked to the establishment of immunoprivilege and is essential for deletion of infiltrating inflammatory cells in immunoprivileged organs including the eye, brain, testicle and placenta (Griffith et al., 1995; Bellgrau et al., 1995; Hunt et al., 1997; Suvannavejh et al., 2000). Fas/FasL interaction is important for homeostasis of the immune system and its dysregulation leads to various autoimmune diseases. Naturally occurring mutant mice defective for Fas (lymphoproliferation, lpr) and FasL (generalized lymphoproliferative disease, gld) develop lymphadenopathy and suffer from an autoimmune syndrome similar to human systemic lupus erythematosus (Takahashi et al., 1994; Watanabe-Fukunaga et al., 1992). FasL knockout mice exhibit a severe autoimmune phenotype with splenomegaly and lymphadenopathy and die early after birth (Karray et al., 2004).

Fas and FasL are also involved in the pathogenesis of EAE, as EAE symptoms are ameliorated in *lpr* and *gld* mice in terms of disease incidence and mean clinical score (Waldner et al., 1997). Apoptosis of oligodendrocytes mediated by Fas/FasL plays a central role in EAE. Selective ablation of Fas or FADD in oligodendrocytes ameliorates EAE (Mc et al., 2010; Hovelmeyer et al., 2005). In addition, elimination of infiltrating T cells in the CNS by apoptosis is crucial for resolution of EAE (Schmied et al., 1993; Pender et al., 1991). Intrathecal infusion of recombinant FasL induces apoptosis of CNS-infiltrating inflammatory cells, including T cells and macrophages, but does not exert cytotoxicity against CNS-resident cells, resulting in mitigated EAE manifestations (Zhu et al., 2002). FasL-deficient *gld* recipients develop prolonged EAE after adoptive transfer of myelin basic protein (MBP)-reactive wild-type Fas[+] T lymphocytes, indicating that Fas/FasL-mediated apoptotic elimination of T cells from the CNS is important for EAE recovery (Sabelko-Downes et al., 1999). However, the CNS-resident cell population which induces apoptosis of CD4^{+} T cells in EAE still remains to be identified. We hypothesise that astrocytes, which constitutively express FasL, may play a key role given that FasL-expressing astrocytes are in intimate contact with apoptotic T cells in EAE and can induce apoptosis of activated CD4^{+} T cells *in vitro* (Bechmann et al., 2002; Kohji and Matsumoto, 2000).
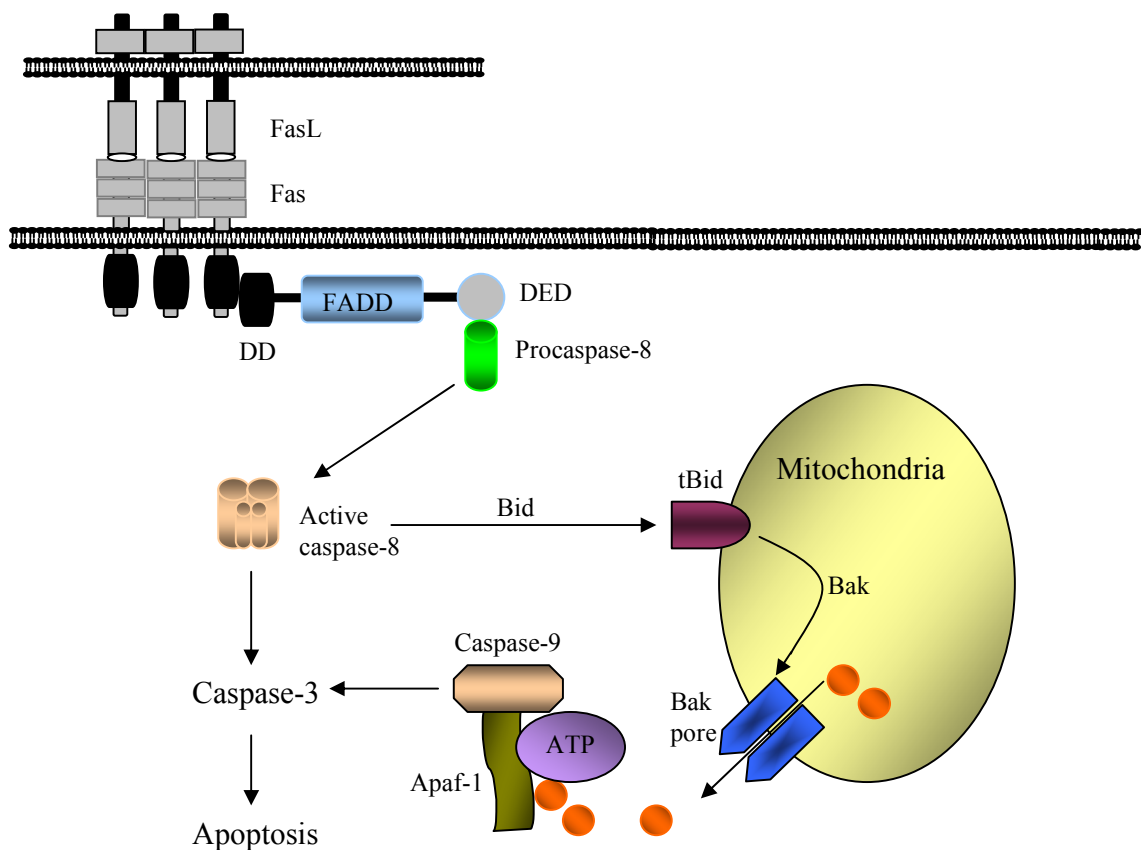
Figure 3. Fas mediated apoptosis-inducing pathway
Upon binding with FasL, Fas activates proapoptotic signaling pathways. In cells with affluent caspase 8, effector caspases, including caspase 3, is activated directly by caspase 8. In cells where caspase-8 expression is low, caspase-8 truncates Bid to produce tBid, which further activate Bak. Cytochrome c is released from Bak pores formed in the outer mitochondrial membrane and activate caspase-9, which further activates caspase-3. DD, death domain; DED, death effector domain

1.3 NF-κB pathway

NF-κB is a family of transcription factors that regulates various biological functions, including immune response, cell differentiation, proliferation and survival (Hayden and Ghosh, 2008; Vallabhapurapu and Karin, 2009). Upon bacterial and viral infection, stimulation with inflammatory cytokines, and activation of antigen receptors, NF-κB transcription factors regulate gene transcription by binding as dimers to κB enhancers or promoters. In mammals, the NF-κB family is composed of five members: RelA (p65), RelB, c-Rel, NF-κB1 p50 (processed from precursor protein NF-κB1 p105), and NF-κB2 p52 (processed from precursor protein NF-κB2 p100) (Oeckinghaus et al., 2011) (Fig. 4). All NF-κB proteins share a conserved Rel homology domain (RHD), which is required for dimerization, DNA binding, IκB interaction, and nuclear translocation (Ghosh et al., 1998). Based on their transactivation potential, NF-κB transcription

factors can be further divided into two groups because only RelA, RelB, and c-Rel have a transactivation domain (TAD). p50 and p52 do not have the TAD and they positively regulate transcription by interacting with RelA, RelB, c-Rel, or other co-activators (Hayden and Ghosh, 2011). Overall, two main NF-κB pathways exist in cells, i.e., the canonical NF-κB pathway and the noncanonical NF-κB pathway.
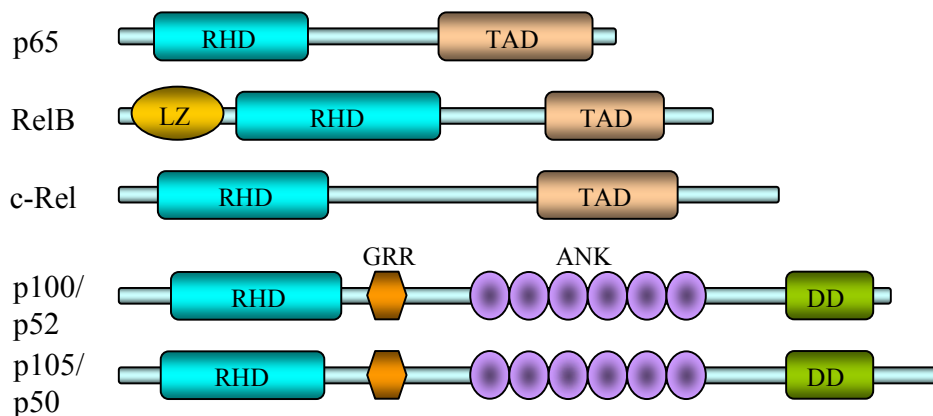
Figure 4. NF-κB members
Structure of the NF-κB family members. ANK, ankyrin-repeat; DD, death domain; GRR, glycine-rich region; RHD, Rel homology domain; TAD, transactivation domain.

1.3.1 The canonical NF-κB pathway

The canonical NF-κB pathway is dependent on NF-κB transcription factors RelA and p50. In resting cells, RelA and p50 dimers are sequestered in the cytoplasm by inhibitory IκB proteins. The canonical pathway is activated in response to activation of specific cytokine receptors, antigen receptors, and pattern-recognition receptors (Fig. 5). Upon NF-κB activation, IκB is phosphorylated by the trimeric IκB kinase (IKK) complex, which comprises two catalytically active kinases, IKKα and IKKβ, and the regulatory/scaffold subunit IKKγ (NEMO) (Karin and Ben-Neriah, 2000). Phosphorylated IκB is subsequently K48-ubiquitinated and degraded by 26S proteasome. As a result, the RelA/p50 dime is free to translocate to the nucleus to initiate the transcription of target genes. It is of note that ubiquitination is important for regulating canonical NF-κB activation and key signaling molecules, including TRAF6, IRAK1, RIP1, IκB, and NEMO, are all targets of ubiquitination (Wertz and Dixit, 2010).

1.3.2 The non-canonical NF-κB pathway

A subset of TNF superfamily ligands, such as BAFF, lymphotoxin, LIGHT, CD40L, RANKL, and TWEAK, activate the non-canonical NF-κB pathway (Claudio et al., 2002; Coope et al., 2002; Dejardin et al., 2002; Novack et al., 2003; Wicovsky et al., 2009) (Fig. 5). The non-canonical NF-κB pathway regulates various biological activities, including lymphoid organ development, B cell survival and activation, dendritic cell activation, and osteoclastogenesis (Dejardin, 2006; Sun, 2011). Upon non-canonical NF-κB activation, NIK is stabilized and phosphorylates IKKα. Phosphorylated IKKα homodimer induces the processing of p100, which forms a dimer with RelB. The p100/RelB dimer is sequestered in the cytoplasm because p100 functions as an IκB-like molecule and inhibits RelB nuclear translocation (Solan et al., 2002). In an ubiquitination-dependent way, p100 is processed to p52. The newly generated RelB/p52 complex then translocates to the nucleus to start gene transcription. Stabilization of NIK is essential for non-canonical NF-κB activation. In resting cells, the level of NIK is extremely low because it is constantly ubiquitinated by cIAP, which leads to its proteasomal degradation (Zarnegar et al., 2008).
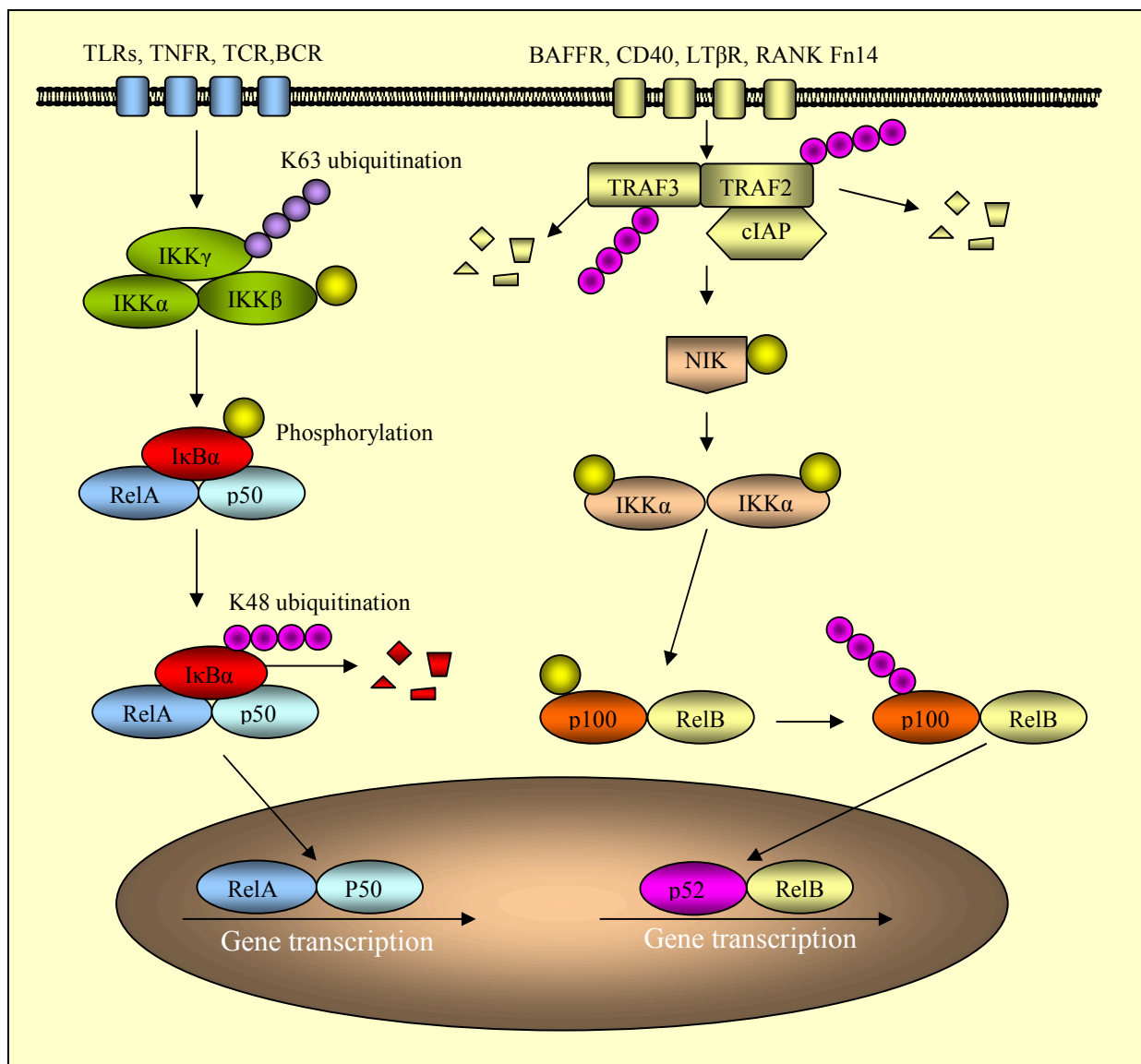
Figure 5. The NF-κB pathway
The canonical NF-κB pathway is dependent on activation of IKKα, IKKβ, and IKKγ. Activation of the trimeric IKK complex leads to the phosphorylation of IκBα, which is further K48-ubiquitinated and subsequently degraded by the 26S proteasome. The RelA/p50 dimer is then free to translocate to the nucleus and initiates transcription. Activation of the noncanonical NF-κB is NIK-dependent. Accumulation and activation of NIK causes the activation of IKKα. Activated IKKα induces the processing of p100 to p52. The RelB/p52 dimer then translocate to the nucleus to start gene transcription.

1.4 Ubiquitination/ Deubiquitination

Ubiquitin, an 8.6 KD protein consisting of 76 amino acids, is highly conserved among eukaryotic species. Ubiquitination is an important post-translational modification and catalyzed by a cascade of three different kinds of enzymes: ubiquitin-activating enzymes (E1s), ubiquitin-conjugating enzymes (E2s), and ubiquitin-ligases (E3s) (Fig. 6). Utilizing ATP, E1s generate a

thioester bond between the carboxyl terminus of ubiquitin and the E1 cysteine sulfhydryl group (Schulman and Harper, 2009). The activated ubiquitin is then transferred to the cysteine in the active site of an E2. Ubiquitin is finally transferred to a target protein catalyzed by an E3, which interacts with both the E2 and the target protein. So far, 2 E1s (UBA1 and UBA6), 38 E2s, and at least 600 E3s have been discovered in human (Deshaies and Joazeiro, 2009).
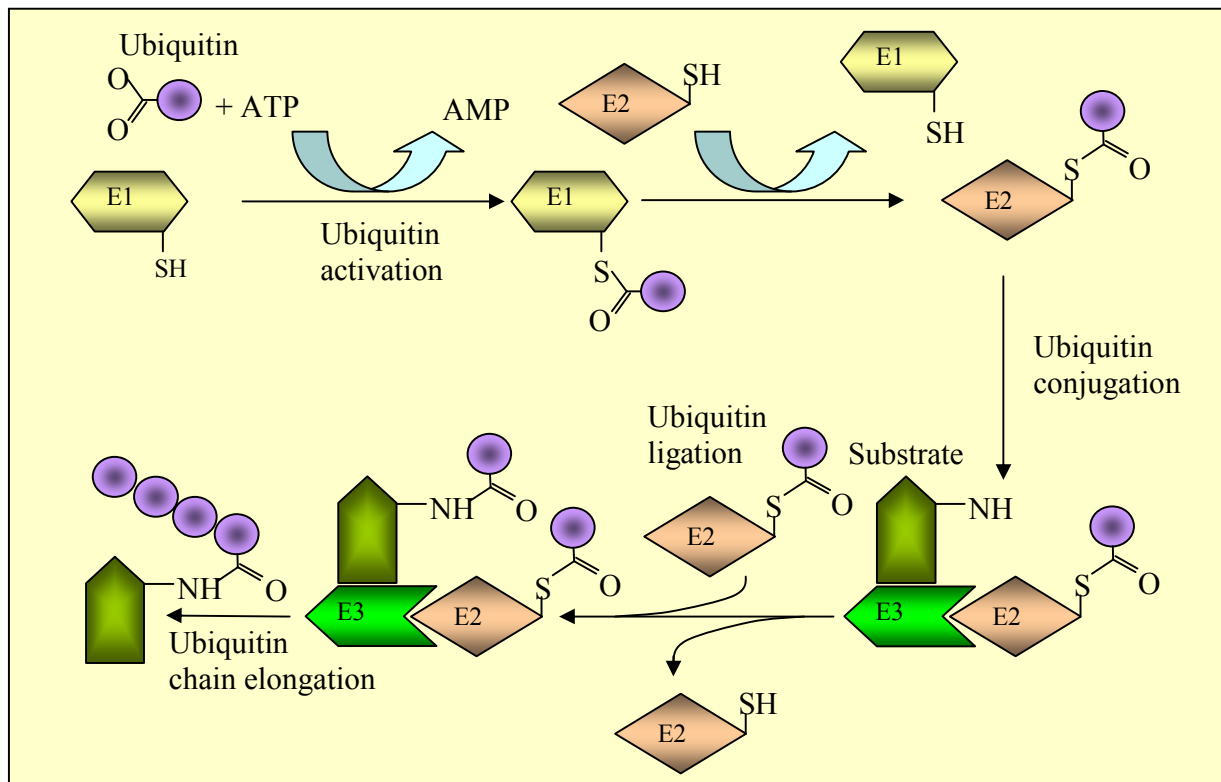
Figure 6. Ubiquitination process
The ubiquitination process involves a cascade of three enzymes. Ubiquitin-activating enzymes (E1s) activate ubiquitin. Ubiquitin-conjugating enzymes (E2s) transfer ubiquitin to ubiquitin ligases (E3s). E3s attach ubiquitin to substrates. The elongation of polyubiquitin chains is mediated by both E2s and E3s.

Ubiquitination was initially characterized as a mechanism to trigger proteasomal degradation of target proteins. However, ubiquitination is also involved in other cellular functions, including membrane trafficking, endocytosis, and, in particular, signal transduction. The functions of ubiquitination are decided by the patterns of ubiquitin linkage to target proteins. Ubiquitination of a substrate may be mediated by a single ubiquitin molecule (monoubiquitination) or a chain of covalently linked polyubiquitin molecules (polyubiquitination) (Fig. 7). Monoubiquitination and multi-monoubiquitinations are important for membrane trafficking, endocytosis, and viral budding (Miranda and Sorkin, 2007; Ikeda and

Dikic, 2008). Polyubiquitination is mediated by seven internal Lys residues, i.e., K6, K11, K27, K29, K33, K48, and K63. A mass spectrometry analysis has shown that K6-, K11-, K27-, K29, and K48-linked ubiquitin chains can all mediate proteasomal degradation (Dammer et al., 2011). Indeed, K48-linked ubiquitination has been well characterized as a mechanism inducing degradation of target proteins by 26S proteasome (Hershko and Ciechanover, 1998). In addition, K11-linked ubiquitin chains are characterized as degradative signals in cell cycle regulation (Jin et al., 2008; Kirkpatrick et al., 2006; Matsumoto et al., 2010). In sharp contrast, K63-linked polyubiquitin chain regulates non-degradative activities such as signal transduction (Adhikari et al., 2007; Hershko and Ciechanover, 1998).
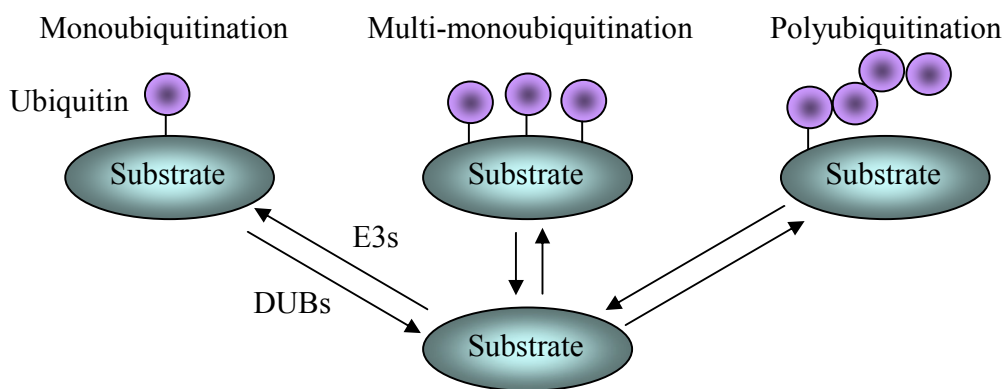
Figure 7. Forms of ubiquitination
There are three forms of ubiquitination: monoubiquitination, multi-monoubiquitination, and polyubiquitination. Polyubiquitination chains are linked by K6, K11, K27, K29, K33, K48, and K63 residues, respectively.

Ubiquitination is reversible and can be counter-regulated by a family of deubiquitinating enzymes (deubiquitinases, DUBs). The human genome encodes nearly 100 DUBs, which can be classified into 5 distinct subfamilies based on structural domains: ubiquitin-specific proteases (USPs), ubiquitin C-terminal hydrolases (UCHs), ovarian tumour proteases (OTUs), Josephins, and JAB1/MPN/MOV34 metalloenzymes (JAMMs, also known as MPN$^+$) (Skaug et al., 2009; Reyes-Turcu et al., 2009). USPs, UCHs, OTUs, and Josephins are cysteine proteases, whereas JAMMs/ MPN$^+$ are zinc^{2+} metalloproteases. The largest subfamily of DUBs is the USP subfamily, which consists of more than 50 members including Cylindromatosis (CYLD) (Sun, 2010; Sun, 2008). The OTU subfamily is the second largest, comprising many important NF-κB regulators such as A20, Cezanne (OTUD7B), and Otubain-1 (Enesa et al., 2008; Hu et al., 2013; Li et al., 2010).

1.5 Regulation of immune responses by A20

A20, also known as tumor necrosis factor alpha-induced protein 3 (TNFAIP3), was originally identified as a TNF-inducible gene in human umbilical vein endothelial cells (HUVECs) (Opipari, Jr. et al., 1990). In many cell types, expression of A20 is kept at low levels but can be rapidly enhanced by proinflammatory cytokines or mitogens. In contrast, thymocytes and T cells express relatively high levels of A20 and A20 expression in these cells can be downregulated upon stimulation with T cell receptor agonists (Tewari et al., 1995). As a zinc finger protein, A20 has seven zinc finger domains (C_2H_2) in the C-terminus and an ovarian tumor (OTU) domain, which exerts the deubiquitinase activity, in the N-terminus (Evans et al., 2004; Wertz et al., 2004) (Fig. 8). Initially, A20 was found to play a pro-survival role in protecting cells from TNF-induced cytotoxicity (Opipari, Jr. et al., 1992), and subsequent studies gradually revealed its function as a negative regulator of the NF-κB signaling pathway induced by various stimuli, such as IL-1, TNF, CD40, and PRRs (Jaattela et al., 1996; Lee et al., 2000; Beyaert et al., 2000). Both findings were further confirmed by studying A20-deficient (*Tnfaip3$^{-/-}$*) mice (Lee et al., 2000). *Tnfaip3$^{-/-}$* mice are hypersensitive to proinflammatory stimuli, including TNF and LPS, and die prematurely due to unfettered multi-organ inflammation and cathexia. Activation of NF-κB induced by TNF and IL-1 persisted in A20-deficient mouse embryonic fibroblasts (MEFs) as indicated by prolonged IKK activation and IκBα degradation. In addition, its anti-apoptotic function was also confirmed by showing that A20-deficient MEFs were sensitive to TNF-induced programmed cell death (Lee et al., 2000). In addition to its well studied role in restricting the canonical NF-κB signaling, A20 has been shown to regulate other signaling pathways, such as non-canonical NF-κB signaling, interferon regulatory factor (IRF) pathway and Wnt pathway (Yamaguchi et al., 2013; Saitoh et al., 2005; Shao et al., 2013). Mechanistically, A20 is an ubiquitin-modifying enzyme. A20 cleaves K63-linked polyubiquitin chains via its DUB activity and can also build K48-linked polyubiquitin chains through its E3 activity.
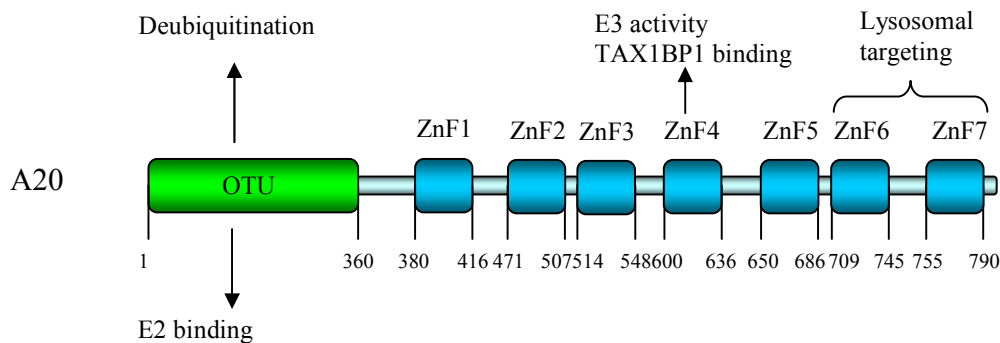
Figure 8. Domain structure of A20
In the N-terminus of A20, there is an OTU domain that is responsible for the DUB activity of A20. There are 7 zinc finger domains (ZnF) in the C-terminus of A20. ZnF4 confers A20 E3 ligase activity. ZnF6 and ZnF7 are involved in lysosomal targeting.

1.5.1 Function of A20 in apoptosis

A20 has both pro- and anti-apoptotic functions. Initially, A20 was found to be anti-apoptotic (Opipari, Jr. et al., 1992). Indeed, A20 functions as an anti-apoptotic protein in many cell types. A20 protects endothelial cells from TNF- and Fas-induced apoptosis by inhibiting caspase 8 activation (Daniel et al., 2004). Activation of the TNF-related apoptosis-inducing ligand (TRAIL) death receptor induces ubiquitination of caspase-8 by a cullin-3 (CUL3)-based E3 ligase (Jin et al., 2009). Overexpression of CUL3 increases ubiquitination and activity of caspase-8. Interestingly, A20 was found to be part of the DISC and physically interact with caspase-8. Overexpression of A20 reverses CUL3-mediated polyubiquitination of caspase-8 and inhibits caspase-8 activity, indicating that A20 excerts its anti-apoptotic function through deubiquitination and inhibition of caspase-8 (Jin et al., 2009). In the DISC induced by TRAIL, the C-terminal ZnF domain of A20 mediates polyubiquitination of RIP1 through K63-linked polyubiquitin chains. RIP1 and K63-linked polyubiquitin chains bind to the protease domain of caspase-8 and inhibit its dimerization and cleavage, resulting in inhibition of TRAIL-induced apoptosis (Bellail et al., 2012). Upon TNF stimulation, A20 binds to apoptosis signal-regulating kinase-1 (ASK1), an important upstream kinase in the JNK signaling pathway, and promotes its degradation through K48 ubiquitination, leading to inhibition of JNK signaling and eventually blockage of apoptosis (Won et al., 2010). In addition, overexpression of A20 protects islets of Langerhans from apoptosis induced by IL-1β and IFN-γ, and this is dependent on its inhibitory function in cytokine-induced NO production (Grey et al., 1999).

However, in several cell types, A20 plays a pro-apoptotic role. In the absence of A20, bone marrow-derived dendritic cells (BMDCs) survive better under CD40 and RANKL stimulation due to the enhanced production of anti-apoptotic Bcl-2 and Bcl-x (Kool et al., 2011). A20-deficient B cells also produce more Bcl-x and, therefore, are more resistant to Fas-mediated cell death (Tavares et al., 2010). Similarly, A20-deficient mast cells are resistant to LPS- and IL-33-mediated apoptosis due to enhanced Bcl-2 and Bcl-x production (Heger et al., 2014). In summary, the function of A20 in apoptosis is highly dependent on the cell type as well as the balance between its anti-apoptotic properties and its regulation of anti-apoptotic genes.

1.5.2 Function of A20 in NF-κB signaling

Activation of the NF-κB signaling cascade is dependent on the K63-linked polyubiquitination of various signaling molecules such as TRAF6, RIP1, and NEMO. As an ubiquitin-editing enzyme, A20 target these proteins for deubiquitination and inactivation, thereby downregulating the NF-κB signaling (Fig. 9). Upon TNF stimulation, A20 expression is rapidly induced in an NF-κB-dependent way and targets RIP1, which is ubiquitinated with K63-linked polyubiquitin chains by cIAP1/2, for inactivation in two sequential steps (Bertrand et al., 2008). As a DUB, A20 first inactivate RIP1 by removing the K63-linked polyubiquitin chains. Then, utilizing its E3 ligase activity, A20 attaches K48-linked polyubiquitin chains to RIP1 for proteasome-mediated degradation (Wertz et al., 2004). The E3 ligase activity of A20 is dependent on the fourth zinc finger domain (ZnF4). Thus, A20 plays dual roles in ubiquitin-editing of RIP1 via its DUB and E3 activities. In addition to RIP1, A20 inhibits TNF-induced NF-κB signaling by deubiquitinating NEMO (Mauro et al., 2006). Recently, linear polyubiquitination, which is generated by the E3 ligase complex called linear ubiquitin chain assembly complex (LUBAC), is considered to be important for canonical NF-κB activation (Tokunaga et al., 2009; Tokunaga et al., 2011; Ikeda et al., 2011). A20 can also disrupt TNF-induced interaction between LUBAC and NEMO by competitive binding to the linear polyubiquitin through its ZnF7 domain, resulting in NF-κB inhibition (Verhelst et al., 2012; Tokunaga et al., 2012).

$Tnfaip3^{-/-}$ mice are protected from lethal inflammation by crossing with $Myd88^{-/-}$ mice, suggesting that the spontaneous inflammation in A20-deficient mice is driven by TLR signaling. Consistently, treatment with broad-spectrum antibiotics protects $Tnfaip3^{-/-}$ mice from lethal inflammation, indicating that A20-deficiency causes hyperactivation of the TLR signaling to

commensal intestinal flora (Turer et al., 2008). Thus, A20 might be a negative regulator of the TLR signaling. In the absence of A20, bone marrow-derived macrophages (BMDMs) exhibit elevated and persistent NF-κB activation and produce more inflammatory cytokines in response to LPS, suggesting that A20 is a negative regulator of the TLR4 signaling (Boone et al., 2004). As a DUB, A20 downregulates LPS-induced NF-κB signaling through removing K63-linked polyubiquitin chains from TRAF6. Deubiquitination of TRAF6 by A20 is also an important mechanism in the inhibition of signaling pathways induced by IL-1 or TGF-β (Jung et al., 2013; Shembade et al., 2010). In addition to deubiquitination, A20 can also inhibit LPS-induced NF-κB signaling by disrupting the ubiquitination process. For example, A20 inhibits the E3 ligase activities of TRAF6, TRAF2, and cIAP1 by disrupting their interaction with the E2 ubiquitin conjugating enzymes (Shembade et al., 2010).

A20 expression can be induced by treatment with IL-17 (Garg et al., 2013). Upon IL-17 stimulation, A20-deficient cells display enhanced expression of inflammatory genes. Mechanistically, in response to IL-17, A20 interacts and deubiquitinates TRAF6 and restricts IL-17-induced NF-κB and MAPK pathways (Garg et al., 2013).

A20 can also inhibit the NF-κB signaling induced by nucleotide-binding oligomerization domain containing 2 (NOD2), which is activated by muramyl dipeptide (MDP), a product of bacterial cell wall peptidoglycan (Hitotsumatsu et al., 2008). NOD2-mediated IKK activation is critically dependent on the K63-linked polyubiquitination of RIP2. Using its DUB activity, A20 inhibits NOD2 signaling by romoving K63-linked polyubiquitin chains from RIP2. In response to MDP, A20-deficient cells display enhanced RIP2 ubiquitination, NF-κB activation, and production of proinflammatory cytokines. *In vivo*, A20-deficient mice exhibit stronger responses to MDP challenge than control mice, as evidenced by the increased serum levels of IL-6 (Hitotsumatsu et al., 2008).

A20 exerts its inhibitory functions towards NF-κB signaling with the help of other proteins, including Tax1 binding protein 1 (TAX1BP1), Itch, Ring finger protein 11 (RNF11), A20 binding and inhibitor of NF-κB (ABIN-1), and YMER (Fig. 9). Together, these proteins form a complex termed A20 ubiquitin-editing complex.

TAX1BP1 was indentified as an A20-interacting protein with yeast two-hybrid screen and it was found to inhibit TNF induced apoptosis (De et al., 1999). Similar to *Tnfaip3*^{-/-} mice, *Tax1bp1*^{-/-} mice are born normal, but die prematurely due to inflammation, and are

hypersensitive to TNF and IL-1 (Iha et al., 2008). Both *Tnfaip3*$^{-/-}$ and *Tax1bp1*$^{-/-}$ MEFs exhibit enhanced and prolonged NF-κB activation in response to TNF or IL-1. Given that TAX1BP1 lacks a DUB domain and has a UBD in its C-terminus, it is possible that TAX1BP1 inhibits NF-κB through A20. Indeed, TAX1BP1 serves as an adaptor to bridge A20 with TRAF6 or RIP1, resulting in reduced ubiquitination of the substrates (Iha et al., 2008). In the absence of TAX1BP1, the interaction of A20 with TRAF6 or RIP1 is compromised.

Upon TNF stimulation, TAX1BP1 interacts with Itch, which is also important for recruiting A20 to RIP1 and the concomitant RIP1 deubiquitination (Shembade et al., 2008). Downregulating Itch with siRNA substantially impaired A20-mediated degradation of RIP1. Similar to *Tnfaip3*$^{-/-}$ and *Tax1bp1*$^{-/-}$ MEFs, *Itch*$^{-/-}$ MEFs display enhanced and prolonged NF-κB signaling induced by TNF or IL-1. *Itch*$^{-/-}$ mice have severe immunological defects, including lymphoid hyperplasia in peripheral lymphoid organs and spontaneous inflammation in skin and lungs, and die by 35 weeks after birth. However, unlike *Tnfaip3*$^{-/-}$ mice, in which the lethal inflammation is independent of the adaptive immune response, *Itch*$^{-/-}$ mice are protected from the deleterious inflammation by crossing with *Rag1*$^{-/-}$ mice, indicating that lymphocytes are required for the autoimmunity of *Itch*$^{-/-}$ mice (Shembade et al., 2008).

In response to TNF, TAX1BP1 and Itch inducibly interact with RNF11 (Colland et al., 2004; Shembade et al., 2009). Upon TNF stimulation, downregulation of RNF11 enhances NF-κB signaling whereas overexpression of RNF11 inhibits NF-κB activation, indicating that RNF11 is a negative regulator of NF-κB signaling. Consistently, knockdown of RNF11 with siRNA increases levels of RIP1 and TRAF6 ubiquitination upon TNF or LPS stimulation, respectively. Importantly, RNF11 is required for A20 to bind and degrade RIP1. In addition, RNF11 interacts with RIP1 and their interaction is impaired in the absence of TAX1BP1 or Itch suggesting that RNF11 is a component of the A20 ubiquitin-editing protein complex consisting of A20, TAX1BP1, and Itch (Shembade et al., 2009).

ABIN-1 and YMER are also characterized as A20 interacting proteins (Heyninck et al., 1999; Bohgaki et al., 2008). Overexpression of either ABIN-1 or YMER inhibits NF-κB signaling. Serving as an adaptor molecule, ABIN-1 is required for A20 to bind and deubiquitinate NEMO (Mauro et al., 2006). YMER also inhibits NF-κB signaling in collaboration with A20. YMER interacts with RIP1 and, as a scaffold, links A20 with K63-linked polyubiquitin chains for deubiquitination.
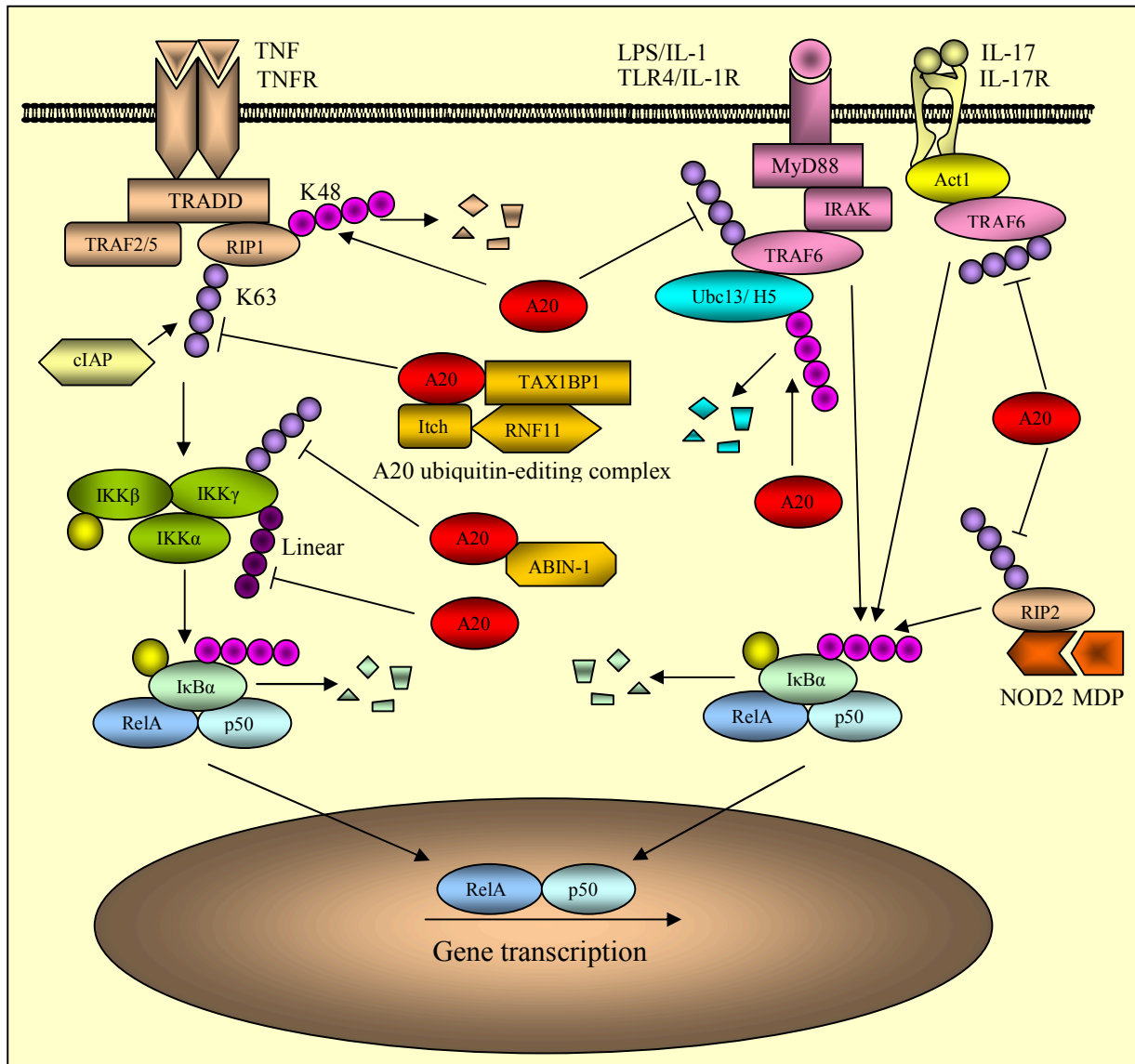
Figure 9. Regulation of the canonical NF-κB pathway by A20

A20 inhibits the canonical NF-κB pathway by removing K63-linked ubiquitin molecules from RIP1, RIP2, TRAF6 and/or NEMO under different stimuli. A20 also induces proteasome-dependent degradation of RIP1 by adding K48-linked polyubiquitin chains. In addition, A20 can also excert its inhibitory function by disrupting E2/E3 interaction and mediating degradation of E2 enzymes.

1.5.3 Function of A20 in different cell populations

Tnfaip3⁻/⁻ mice succumb prematurely due to unrestricted inflammation in multiple organs and cachexia as a result of uncontrolled NF-κB activation (Lee et al., 2000). The spontaneous inflammation and premature lethality of *Tnfaip3⁻/⁻* mice precludes the use of them for

experimentally induced disease models. In order to overcome these drawbacks, conditional gene targeting was applied to specifically ablate A20 in certain kinds of tissues.

Intestinal epithelial cell (IEC)-specific A20-deficient mice

To study IEC-specific function of A20, A20 was selectively deleted in IECs of the A20^{IEC-KO} mice, which were generated by breeding of A20$^{fl/fl}$ mice with Villin-Cre transgenic mice (Vereecke et al., 2010). Unlike *Tnfaip3$^{-/-}$* mice, A20^{IEC-KO} mice develop normally and do not show spontaneous colitis. However, A20^{IEC-KO} mice are susceptible to dextran sulphate sodium (DSS) induced colitis, which is triggered by enhanced IEC apoptosis mediated by TNF. Apoptosis of IECs further leads to the breakdown of intestinal barrier, infiltration of commensal intestinal bacteria, and ultimately, systemic inflammation and lethality. These findings are confirmed by another study with mice overexpressing A20 specifically in IECs (Kolodziej et al., 2011). Collectively, in this study, A20 is identified as an anti-apoptotic protein in IECs and is important for epithelial barrier integrity.

B cell-specific A20-deficient mice

Inactive A20 mutations are frequently discovered in B-cell lymphomas (Kato et al., 2009). To study the function of A20 in B cells, three strains of A20^{BC-KO} mice, in which A20 was specifically deleted in B lymphocytes, were generated by crossing A20$^{fl/fl}$ mice with CD19-Cre transgenic mice by three independent groups. A20^{BC-KO} mice develop symptoms of autoimmunity, including the production of autoantibodies, due to the accumulation of immature and germinal center B cells. In contrast to the well-known anti-apoptotic function of A20, A20 deficient B cells are resistant to FasL-mediated cell death, probably due to increased expression of anti-apoptotic Bcl-x (Tavares et al., 2010). Another A20^{BC-KO} mouse strain also displays autoimmune syndrome, although only in aged mice (Chu et al., 2011). Consistently, we also reported that B cell-specific A20-deficient mice, which were generated independently by us, produced autoantibodies and A20-deficient B cells were hyperactive illustrated by enhanced proliferation upon activation (Hovelmeyer et al., 2011).

Myeloid cell-specific A20-deficient mice

A20 was specifically deleted in cells of myeloid origin, including macrophages and granulocytes, in LysM-Cre A20$^{fl/fl}$ (A20$^{myel-KO}$) mice (Matmati et al., 2011). These mice develop human rheumatoid arthritis-like spontaneous polyarthritis that is associated with the presence of

collagen-specific autoantibodies and proinflammatory cytokines in serum. The phenotype is TNF independent and is IL-6 and TLR4-MyD88 dependent. A20-deficient macrophages display sustained NF-κB activation and produce more proinflammatory cytokines upon LPS stimulation. The destructive polyarthritis in A20$^{myel-KO}$ mice is ameliorated by treatment with IL-6-neutralizing antibodies and is almost completely abolished by crossing to a MyD88-deficient background. In addition, myeloid A20-deficiency also enhances osteoclast differentiation and activation (Matmati et al., 2011).

In contrast to its susceptibility to autoimmunity, A20$^{myel-KO}$ mice are protected from lethal influenza A virus infection due to increased cytokine and chemokine production (Maelfait et al., 2012).

Dendritic cell (DC)-specific A20-deficient mice

Three DC-specific A20 deficient mouse strains were generated independently by crossing A20$^{fl/fl}$ mice with CD11c-Cre transgenic mice by three groups (Hammer et al., 2011; Kool et al., 2011). In contrast to the premature lethality of globally A20-deficient mice, A20^{DC-KO} mice do not show defects in survival. However, A20^{DC-KO} mice develop splenomegaly and lymphadenopathy. A20-deficient DCs spontaneously mature and produce high levels of proinflammatory cytokines. Besides, A20-deficient DCs are resistant to apoptosis due to increased Bcl-2 and Bcl-x production (Kool et al., 2011). These A20^{DC-KO} mouse strains also show different diease phenotypes. One strain develops nephritis, antiphospholipid syndrome, and autoimmune arthritis, resembling human systemic lupus erythematosus (SLE) (Kool et al., 2011). Another strain develops lymphocyte-dependent colitis, enthesitis, and seronegative ankylosing arthritis, which are conditions typical of human inflammatory bowel disease (IBD) (Hammer et al., 2011). Our A20^{DC-KO} mice develop spontaneous hepatitis. The differences can be attributed to the different genetic backgrounds, the different gene-targeting strategies, and/or the divergent microbiota in the two strains (Honda and Littman, 2012; Hammer and Ma, 2013). Nevertheless, the three studies clearly show that A20 expression in DCs preserves immune homeostasis under steady-state conditions.

Keratinocyte-specific A20-deficient mice

Keratinocyte-specific A20 deficiency was achieved in Krt14-Cre A20$^{fl/fl}$ (A20^{K-KO}) mice (Lippens et al., 2011). A20^{K-KO} mice show no signs of spontaneous skin inflammation but

develop keratinocyte hyperproliferation and ectodermal organ abnormalities, such as disheveled hair, longer nails and sebocyte hyperplasia. These phenotypes are also present in mice with dysregulated ectodysplasin A receptor-mediated signaling. Indeed, A20 is found to be an inhibitor of EDAR-triggered NF-κB signaling (Lippens et al., 2011).

Mast cell-specific A20-deficient mice

Recently, mast cell-specific A20 deficient mice were generated by crossing A20$^{fl/fl}$ mice with Mcpt5-Cre transgenic mice (Heger et al., 2014). Although A20 inhibits TLR-, IL33R-, and IgE/FcεR1-induced NF-κB activation in mast cells, ablation of A20 in mast cells does not induce spontaneous pathology. However, mast cell-specific A20 deficient mice are more sensitive to allergic airway inflammation and collagen-induced arthritis (Heger et al., 2014).

2. Aims

Astrocytes have been shown to play diverse roles in the pathogenesis and development of EAE. To gain more insight into the role of astrocyte in EAE, we studied the function of astrocyte-derived A20 and FasL in EAE.

2.1 Function of astrocytic A20 in EAE

To study the function of astrocytic A20 in EAE, we generated mice lacking A20 in either neuroectodermal cells (Nestin-Cre A20$^{fl/fl}$ mice) or astrocytes (GFAP-Cre A20$^{fl/fl}$ mice) and challenged them with EAE. EAE severity of these mice was compared with that of A20$^{fl/fl}$ control mice, respectively, based on clinical symptoms. In addition, we also analyzed the inflammation in the spinal cord by FACS, RT-PCR, and histology. Since astrocytes play a key role in EAE pathogenesis by producing chemokines, we studied the influence of A20 on chemokine production in astrocytes. Finally, we studied the impact of A20 on signaling pathways in astrocytes.

2.2 Function of astrocytic FasL in EAE

To investigate the influence of astrocyte-derived FasL on EAE, we generated GFAP-Cre FasL$^{fl/fl}$ mice, in which FasL was specifically and efficiently ablated in astrocytes, and challenged them with EAE. EAE severity was evaluated by monitoring clinical symptoms. Further, we studied the influence of astrocyte-specific FasL deficiency on the number, composition, and apoptosis of infiltrating T cells in the spinal cord. Inflammation in the spinal cord was further studied by RT-PCR and histology. Finally, we investigated the direct impact of astrocytic FasL on T cell apoptosis using an *in vitro* co-culture system.

3.Materials and methods

3.1.Materials
3.1.1 Chemicals used for animal experiments

Embedding medium	Sakura Finetek Europe BV, Zoeterwoude Netherlands (TissueOCTTM Tek ® compound)
Freund's adjuvant, Complete	Sigma-Aldrich, Steinheim, Germany
Isoflurane (Forene ®)	Abbott, Wiesbaden, Germany
M. tuberculosis H37 RA	Difco Laboratories, Detroit, USA
Pertussis toxin	Sigma-Aldrich, Steinheim, Germany
2-methylbutane	Carl Roth, Karlsruhe, Germany
4% paraformaldehyde (PFA)	Carl Roth, Karlsruhe, Germany

3.1.2 Materials for cell culture

Cell culture was performed in a sterile environment under a laminar flow hood. The cell culture media were prewarmed in a 37 °C water bath before use. Cells were kept in an incubator at 37 °C, 5% CO_2 and 60% of water vapor. Plastic materials for cell culture were purchased from Greiner Bio-One (Frickenhausen, Germany) and Carl Roth (Karlsruhe, Germany).

Astrocyte culture medium	DMEM (PAA Laboratories GmbH, Pasching, Austria), fetal calf serum (FCS, PAA Laboratories GmbH, Pasching, Austria), 100 U Penicillin / streptomycin (PAA Laboratories GmbH, Pasching, Austria)
Hank's medium	PAA Laboratories, Pasching, Austria
Neuron culture medium	Neurobasal Medium (Gibco, Grand island, USA), B-27 Supplements (Gibco, Grand island, USA), L-Glutamine (Gibco, Grand island, USA), 100 U Penicillin / streptomycin (PAA Laboratories GmbH, Pasching, Austria)
Opti-MEM	Gibco, Grand island, USA

PBS	PAA Laboratories GmbH, Pasching, Austria
Poly-D-lysine	Sigma-Aldrich, Steinheim, Germany
poly-L-lysine	Sigma-Aldrich, Steinheim, Germany
Trypan blue	Sigma-Aldrich, Steinheim, Germany
Trypsin	PAA Laboratories GmbH, Pasching, Austria

3.1.3 Materials for molecular biology

β-mercaptoethanol	Carl Roth, Karlsruhe, Germany
DNeasy Blood and Tissue Kit	Qiagen, Hilden, Germany
dNTP	Invitrogen, Karlsruhe, Germany
DTT	Invitrogen, Karlsruhe, Germany
EasyDNA kit	Invitrogen, Karlsruhe, Germany
Ethanol (95%, 100%)	Pharmacy of the University Hospital Magdeburg
HotStar Taq	Qiagen, Hilden, Germany
Oligo-dT	Invitrogen, Karlsruhe, Germany
PCR Buffer, 10x	Qiagen, Hilden, Germany
RNeasy Mini Kit	Qiagen, Hilden, Germany
Primers for PCR	Eurofins MWG Operon, Ebersberg, Germany
Primers for qRT-PCR	Applied Biosystems, Darmstadt, Germany
siRNAs	Invitrogen, Karlsruhe, Germany
RNAiMAX Transfection Reagent	Invitrogen, Karlsruhe, Germany
Sterile distilled water	Berlin Chemie AG, Berlin, Germany
Superscript II Reverse Transcriptase	Invitrogen, Karlsruhe, Germany
TaqMan Universal PCR master mix	Applied Biosystems, Darmstadt, Germany
5x First Strand Buffer	Invitrogen, Karlsruhe, Germany

Table 1 Genotyping primers

Mouse strain	primer sequence (5 '→ 3')	amplicon size
GFAP-Cre FasL^{fl/fl} mice		

GFAP-Cre FasL$^{fl/fl}$ mice

GFAP-Cre Sense	5'-GACACCAGACCAACTGGTAATGGTAGCGAC-3'	850bp
Antisense	5'-GCATCGAGCTGGGTAATAAGCGTTGGCAAT-3'	
Del-FasL Sense	5'- GGAGTTGAACGAGTAGCCTC -3'	500bp
Antisense	5'- GTACTTCTTCTGATAAGGACC -3'	
FasL Sense	5'-ATTAATTACAGTGAAGAGATGG-3'	660bp
Antisense	5'- GTACTTCTTCTGATAAGGACC -3'	

FasL$^{wt/wt}$ mice amplicon size = 660 bp, FasL$^{fl/fl}$ mice amplicon size = 700 bp

GFAP-Cre A20$^{fl/fl}$ mice

GFAP-Cre Sense	5'-GACACCAGACCAACTGGTAATGGTAGCGAC-3'	850bp
Antisense	5'-GCATCGAGCTGGGTAATAAGCGTTGGCAAT-3'	
A20 Sense	5'-AGTCTGGGACTGGATGTAGC-3'	300bp
Antisense	5'-CTGGCTAAGGCCTTGATACC-3'	

A20$^{wt/wt}$ mice amplicon size = 300 bp, A20$^{fl/fl}$ mice amplicon size = 419 bp

Nestin-Cre A20$^{fl/fl}$ mice

Nestin-Cre Sense	5'-TCCCTTCTCTAGTGCTCCACGTCC-3'	650bp
Antisense	5'-TCCATGAGTGAACGAACCTGGTCG-3'	
A20 Sense	5'-AGTCTGGGACTGGATGTAGC-3'	300bp

      Antisense   5'-CTGGCTAAGGCCTTGATACC-3'

A20$^{wt/wt}$ mice amplicon size = 300 bp, A20$^{fl/fl}$ mice amplicon size = 419 bp

Synapsin-Cre A20$^{fl/fl}$ mice

      Synapsin-Cre Sense   5'-CCAGCACCAAAGGCGGG-3'   450bp

      Antisense   5'-TGCATCGACCGGTAATGCAG-3'

      A20 Sense   5'-AGTCTGGGACTGGATGTAGC-3'   300bp

      Antisense   5'-CTGGCTAAGGCCTTGATACC-3'

A20$^{wt/wt}$ mice amplicon size = 300 bp, A20$^{fl/fl}$ mice amplicon size = 419 bp

3.1.4 Materials for proteomics

Blotting grade milk powder	Carl Roth, Karlsruhe, Germany
Bradford reagent	Bio-Rad, Munich, Germany
BSA	Sigma-Aldrich, Steinheim, Germany
Filter paper	Carl Roth, Karlsruhe, Germany
Gel running buffer pH 8.3	25 mM Tris, 0.1% sodium dodecyl sulfate (both from Carl Roth, Karlsruhe, Germany), 250 mM glycine (Sigma Aldrich, Steinheim, Germany)
Polyvinylidene fluoride (PVDF) Membrane Immobilon P	Millipore, Schwalbach, Germany
Protein marker	Fermentas, St. Leon-Rot, Germany
5 × lane marker reducing sample buffer	Thermo scientific, MA, USA

RIPA buffer	50 mM Tris / HCl pH 7.5, 100 mM NaCl, 5 mM EDTA, 10 mM H_2PO4 (all from Carl Roth, Karlsruhe, Germany), 1% Triton X-100, 0.25% deoxycholic acid, Protease inhibitor cocktail, 20 mM sodium fluoride, 0.2 Mm phenyl methyl sulfonyl fluoride, 1mM Sodium molybdate, 20 mM glycerol-2-phosphate, 1 mM sodium phosphate buffer (all from Sigma-Aldrich, Steinheim,Germany), 10% glycerol (Calbiochem, Darmstadt, Germany), PhosStop (Roche, Mannheim, Germany) RIPA buffer
SDS-polyacrylamide separating gel	Distilled water, 8 to 10% acrylamide 30% (Applichem, Darmstadt, Germany), 0.4 M Tris, 0.1% Sodium dodecyl sulfate (both from Carl Roth, Karlsruhe, Germany), 0.1% ammonium persulfate, 0.1% TEMED (both from Sigma-Aldrich, Steinheim, Germany)
SDS-polyacrylamide stacking gel	Distilled water, 5% acrylamide 30% (Applichem, Darmstadt, Germany), 0.17 M Tris, 0.1% Sodium dodecyl sulfate (both from Carl Roth, Karlsruhe, Germany), 0.1% ammonium persulfate, 0.1% TEMED (both from Sigma-Aldrich, Steinheim, Germany)
TBS-Tween 20, pH 7.4	20 mM Tris, 140 mM NaCl (both from Carl Roth, Karlsruhe, Germany), 0.1% (v / v) Tween 20 (Sigma - Aldrich, Steinheim, Germany)
Transfer buffer pH 8.4	25 mM Tris, 0.1% sodium dodecyl sulphate (both from Carl Roth, Karlsruhe, Germany), 500 mM glycine (Sigma-Aldrich, Steinheim, Germany), 20% Methanol (J.T. Baker, Deventer, Netherlands)

Table 2. Antibodies for Western blotting and Immunoprecipitation (IP)

Primary antibody	Blocking solution	Antibody dilution
All antibodies were obtained from (Cell Signaling Technology Danvers, MA, USA) unless stated otherwise.		
Anti-A20 (# sc-166692) (Santa Cruz biotechnology, Heidelberg, Germany)	1% BSA 1% milk powder	1:500

Anti-ERK1/2 (# 4370)	5% BSA	1:1000
Anti-GAPDH (# 5174)	1% BSA 1% milk powder	1:1000
Anti-HDAC (# 5356)	1% BSA 1% milk powder	1:1000
Anti-IκBα (# 9242)	5% BSA	1:1000
Anti-JNK (# 9258)	5% BSA	1:1000
Anti-p38 (# 9212)	5% BSA	1:1000
Anti-phospho-ERK1/2 (# 4377)	5% BSA	1:1000
Anti-phospho-IκBα (# 9246)	5% BSA	1:1000
Anti-phospho-JNK (# 4668)	5% BSA	1:1000
Anti-phospho-p38 (# 9211)	5% BSA	1:1000
Anti-phospho-STAT1 (# 8826)	5% BSA	1:1000
Anti-phospho-STAT1 (# 9167)	5% BSA	1:1000
Anti-STAT1 (# 9172)	5% BSA	1:1000
Anti-tubulin (# 2148)	5% BSA	1:1000

Secondary antibodies for Western Blotting

Polyclonal Rabbit Anti-Mouse Immunoglobulins/HRP (# P 0260) Dako, Glostrup, Denmark
Polyclonal Swine Anti-Rabbit Immunoglobulins/HRP (# P 0399) Dako, Glostrup, Denmark

Table 3. Antibodies for flow cytometric analysis

Antibody	Clone
APC-anti-mouse CD4 (rat)	(RM4-5)
APC-rat-IgG isotype control	(R35-95)
FITC-anti-mouse B220 (rat)	(RA3-6B2)
FITC-anti-mouse CD3 (rat)	(G4.18)
FITC-anti-mouse CD11b (rat)	(M1/70)
FITC-anti-mouse CD11c (hamster)	(V418)

FITC-anti-mouse CD25 (rat)   (7D4)

FITC-anti-mouse CD62L (rat)   (MEL-14)

FITC-anti-mouse F4/80 (rat)   (BM8)

FITC-anti-mouse Ly6G (rat)   (RB6-8C5)

FITC-hamster-IgG isotype control   (HTK888)

FITC-rat-IgG isotype control   (A95-1)

PE-anti-mouse CD11b (rat)   (M1/70)

PE-anti-mouse CD19 (rat)   (1D3)

PE-anti-mouse CD44 (rat)   (IM7)

PE-anti-mouse CD69 (rat)   (H1.2F3)

PE-anti-mouse CD95 (hamster)   (Jo2)

PE-anti-mouse CD178.1 (mouse)   (KAY-10)

PE-anti-mouse Foxp3 (rat)   (R16-715)

PE-anti-mouse GM-CSF (rat)   (MP1-22E9)

PE-anti-mouse IFN-γ (rat)   (XMG1.2)

PE-anti-mouse IL-17A (rat)   (TC11-18H10)

PE-anti-mouse Ly6C (rat)   (AL-21)

PE-anti-mouse NK1.1 (rat)   (PK136)

PE-hamster-IgG isotype control   (G235-2356)

PE-rat-IgG isotype control   (A95-1)

PECy5-anti-mouse CD8α (rat)   (53-6.7)

PECy5-rat-IgG isotype control   (A95-1)

V450-anti-mouse CD45 (rat)   (30-F11)

V450-rat-IgG isotype control   (MOPC-21)

PE-anti-mouse Annexin V

7 AAD

(All antibodies obtained from BD Biosciences, Heidelberg, Germany and used at a concentration

of 1µg/ 1x10^6 cells)

Peptides

(MOG)$_{35-55}$ peptide   JPT, Berlin, Germany

Kits

Active Caspase-3 mAb Apoptosis kit   BD Biosciences, Heidelberg, Germany

Anti-O4 MicroBeads   Miltenyi Biotec, Bergisch Gladbach, Germany

CD4 T cell isolation kits, mouse   Miltenyi Biotec, Bergisch Gladbach, Germany

NE-PER Nuclear and Cytoplasmic   Thermo scientific, MA, USA
Extraction Reagents

Neuronal Tissue Dissociation Kit   Miltenyi Biotec, Bergisch Gladbach, Germany

Pierce ECL Plus Western Blotting substrate   Thermo scientific, MA, USA

Vybrant Apoptosis Assay   Invitrogen, Karlsruhe, Germany

3.1.5 Instruments

Bio-Rad Mini protein system   Bio-Rad, California, USA

Centrifuge 5415R   Eppendorf, Hamburg, Germany

Chemo Cam Luminescent Image Analysis system   INTAS, Göttingen, Germany

Coverslip (for Neubauer counting chamber)   Carl Roth, Karlsruhe, Germany

Documentation station   Herolab GmbH, Wiesloch, Germany

FACS Canto II   BD Biosciences, Heidelberg, Germany

FACSVantage cell sorter   BD Biosciences, Heidelberg, Germany

Incubator   Heraeus, Hanau, Germany

Laboratory balance   Sartorius, Göttingen, Germany

Laminar flow hood   Heraeus, Hanau, Germany

LightCycler 480 instrument   Roche, Mannheim, Germany

Microscope   Nikon, Tokyo, Japan

PCR machine   Peq lab, Erlangen, Germany

pH meter   SHOTT, Mainz, Germany

Pipette   Eppendorf, Hamburg, Germany

Pipette boy   INTEGRA, Fernwald, Germany

Power PAC 200	Bio-Rad, California, USA
Semi Dry blotter	Peq lab, Erlangen, Germany
Shaker	IKA-Werke, Staufen, Germany
Thermomixer compact	Eppendorf, Hamburg, Germany
Vortex Mixer	IKA-Werke, Staufen, Germany

3.1.6 Animals

Nestin-Cre$^{+/-}$ A20$^{fl/fl}$, glial fibrillary acidic protein (GFAP)-Cre$^{+/-}$ A20$^{fl/fl}$, and Synapsin-Cre$^{+/-}$ A20$^{fl/fl}$ mice were generated by crossing C57BL/6 Nestin-Cre, GFAP-Cre, and Synapsin-Cre mice, respectively, with C57BL/6 A20$^{fl/fl}$ mice in our animal facility. GFAP-Cre$^{+/-}$ FasL$^{fl/fl}$ mice were generated by crossing C57BL/6 GFAP-Cre transgenic mice with C57BL/6 FasL$^{fl/fl}$ mice (Karray et al., 2004) and the colony was maintained by breeding of GFAP-Cre$^{+/-}$ FasL$^{fl/fl}$ mice with GFAP-Cre$^{-/-}$ FasL$^{fl/fl}$ mice. C57BL/6 WT mice were obtained from Harlan (Borchen, Germany). Animal care and experimental procedures were performed according to European regulations and approved by state authorities (Landesverwaltungsamt Halle, Germany).

3.2 Methods

3.2.1 Genotyping of the mouse strains

For genotyping of mice, a tissue sample of the tail tip was cut and transferred to a 2 ml Eppendorf tube. Genomic DNA was isolated from mouse tail using easyDNA kit (Invitrogen, Karlsruhe, Germany) according to instructions of the manufacturer. PCR was performed using primers targeting Nestin-Cre, GFAP-Cre, Synapsin-Cre, FasL$^{fl/fl}$ and A20$^{fl/fl}$ respectively, as indicated in Table 1.

3.2.2 Induction of EAE

4 mg of MOG$_{35-55}$ (MEVGWYRSPFSRVVHLYRNGK) peptide dissolved in 2 ml of PBS was emulsified with 2 ml of complete Freund's adjuvant supplemented with 20 mg of killed Mycobacterium tuberculosis. Active EAE was induced in 8-12 weeks old mice by subcutaneous (s.c.) immunization with 200 μl of emulsified MOG$_{35-55}$ peptide. In addition, mice also received two intraperitoneal (i.p.) injections of 200 ng pertussis toxin dissolved in 200 μl PBS, at the time of immunization as well as 48 h thereafter.

3.2.3 Assessment of EAE

Clinical signs of EAE were monitored daily and scored according to a scale of severity from 0 to 5 as follows: 0, no sign; 0.5, partial tail weakness; 1, limp tail; 1.5, limp tail and slowing of righting; 2, marked slowing of righting and partial hind limb weakness; 2.5, dragging of hind limb(s) without complete paralysis; 3, complete paralysis of at least one hind limb; 3.5, hind limb paralysis and slight weakness of forelimbs; 4, forelimb weakness; 5, moribund or dead. The scoring of EAE mice was double blind. Daily clinical scores were calculated as the average of all individual disease scores within each group.

3.2.4 Isolation of leukocytes from spinal cord

Animals were anesthetized with isoflurane (Baxter, Deerfield, IL). Spinal cord was isolated and subject to Percoll gradient centrifugation (GE Healthcare, Freiburg, Germany) for leukocyte separation. Cell pellet was resuspended with 9 ml Percoll at a density of 1.098 g. Then, 5 ml Percoll at a density of 1.22 g was carefully loaded at the bottom. A density gradient was created by overlaying Percoll densities of 1.07 g, 1.05 g, 1.03 g and 1.00 g successively. The Percoll gradient was centrifuged at 1,200 g for 20 min with rapid start and slow stop. The upper layers of

densities 1.00 g and 1.03 g were carefully removed and discarded. The upperlayers of densities 1.05, 1.07, and 1.098 were carefully harvested and transferred to a new 50 ml Falcon tube. Cells were washed with cell culture medium containing 3% FCS by centrifugation. Cell pellet of leukocytes was resuspended in cell culture medium. Number of cells was counted using a hemocytometer.

3.2.5 Flow Cytometry

For staining of extracellular markers, 1×10^6 cells were transferred to a FACS tube containing 3 ml PBS (4 °C) and centrifuged at 1,200 rpm for 6 min at 4 °C. After discarding the supernatant, 1 µg CD16/32 antibody diluted in 50 µl PBS was added and incubated at 4 °C for 10 min to block non-specific binding sites. Subsequently, specific antibodies (as indicated in Table 3) were added to cells and incubated in the dark for 30 min at 4 °C. After staining, the cells were washed by centrifugation in 3 ml PBS (4 °C). The cell pellet was resuspended in 200 µl PBS (4 °C) and measured with a flow cytometer within 4 h. For detection of intracellular proteins, cells were stimulated with phorbol 12-myristate 13-acetate (PMA, 50 ng / ml) and Ionomycin (500 ng / ml) and incubated at 37 °C for 3 h to increase cytokine production. Then, 1 µl / ml GolgiPlug was added to block intracellular protein transport and enrich protein concentration in the Golgi complex. After an incubation period of 12 hours, cells were washed twice with 3 ml PBS (4 °C). Then, cells were incubated with CD16/32 to block non-specific binding for 10 min at 4 °C. Thereafter, extracellular proteins were stained with specific antibodies for 20 minutes at 4 °C. After washing twice with 3 ml PBS (4 °C), intracellular staining was performed. The cells were fixed in 250 µl of Cytofix / Cytoperm for 20 minutes at 4 °C and permeabilized with 1 ml of $1 \times$ Perm/Wash. The cells were then stained with specific antibodies (as indicated in Table 3) diluted in $1 \times$ Perm/Wash and incubated for 30 min at 4 °C. After 2 washes with $1 \times$ Perm/Wash, the cells were centrifuged and resuspended in 200 µl PBS (4 °C). Stained cells were measured with a FACSCanto II (BD Biosciences) flow cytometer and the analysis was performed with the FACSDiva 6 software (BD Biosciences).

3.2.6 Astrocyte culture

1- to 2-day-old new born mice were sterilized with 70% ethanol. Then, heads of mice were cut and put in astrocyte culture medium (DMEM supplemented with 10% FCS and 1% penicillin/streptomycin), and tails were cut for genotyping. Brains were removed and

mechanically dissociated with 70 μm cell strainers to generate single cell suspension. Cells were then cultured for 9 days in a cell incubator. Medium was changed every 3 days. On day 9, cells were shaken on a shaker to remove contaminating microglia and then washed intensively with PBS. Thereafter, adherent cells were harvested by trypsinization, and subcultured in new flasks. To eliminate microglia from astrocyte cultures, cells were harvested from astrocyte cultures and stained with rat anti-mouse CD11b-PE. Astrocytes ($CD11b^-$) were separated from $CD11b^+$ microglia with a FACSVantage cell sorter (BD). For the detection of FasL expressed on the surface of astrocytes, mixed astrocyte/microglia cultures were stained with mouse anti-mouse FasL-PE and CD11b-FITC. Controls were stained with isotype-matched control antibodies.

3.2.7 Neuron culture

Pregnant female mice were sacrificed by cervical dislocation at gestational day 18.5, and brains of pups were isolated. After carefully removing meninges under a macroscope, cortices were excised into small pieces and then incubated with 400 μl trypsin for 20 minutes at 37 °C. Trypsinization was stopped by adding 400 μl of trypsin inhibitor. The tissue was washed twice with 800 μl neurobasal medium to remove remaining trypsin and trypsin inhibitor and then mechanically dissociated with syringes to generate single cell suspension. Cells of each embryonic brain were counted and seeded in flasks coated with poly-D-lysine in Neurobasal medium supplemented with 2% B27, 500 μM L-glutamine, and 1% penicillin/streptomycin. Every 4 days, half of the medium was replaced with fresh neuron culture medium. The purity of cultures for neurons was ≥ 98%, as determined by immunofluorescence staining for neuron-specific class III β-tubulin.

3.2.8 Magnetic-activated cell sorting (MACS) of $CD4^+$ T cells

$CD4^+$ T cells were isolated with MACS isolation kits (Miltenyi). Spleens and/or lymph nodes were mechanically dissociated with 70 μm cell strainers to generate single cell suspension. Cells were pelleted by centrifugation at 1,200 rpm for 6 min. The cell pellet was resuspended in 40 μl of MACS buffer (PBS supplemented with 0.5% bovine serum albumin (BSA) and 2 mM EDTA, pH 7.2) per 10^7 cells. 10 μl of the biotin-antibody cocktail per 10^7 cells was added and incubated for 10 min at 4 °C. Then, 30 μl of MACS buffer and 20 μl of anti-biotin MicroBeads per 10^7 total cells were added and incubated for 15 min at 4 °C. After incubation, the cells were washed by adding 2 ml of MACS buffer per 10^7 cells and centrifuged at 1,200 rpm for 10 min. The pellet

was resuspended in 500 µl MACS buffer up to 10^8 cells. LS columns were placed in the magnetic field of the MACS separator and rinsed with 3 ml of MACS buffer as preparation. The cell suspension was applied onto the column and the flow-through containing enriched $CD4^+$ T cells was collected. The column was further washed 3 times with 3 ml MACS buffer and the flow through was collected. Enriched $CD4^+$ T cells in the flow through were centrifuged at 1,200 rpm for 10 minutes and then the cells were resuspended in 500 µl of PBS. The purity of $CD4^+$ T cells was 90-95% as determined by FACS staining.

3.2.9 Transfection of astrocytes

Cultured astrocytes were subcultured one day before transfection. Cells were washed twice with 2 ml PBS to remove remaining FCS. After that, cells were detached by incubating with trypsin at 37 °C. Trypsinazation was stopped by adding fresh astrocyte culture medium. Cells were then pelleted by centrifugation at 1,200 rpm for 5 min. Cell pellet was resuspended with fresh culture medium and seeded in 6 well plates. On the day of tranfection, astrocytes were approximately 80% confluent. Astrocytes were transfected with small interfering RNA (siRNA) targeting A20 or STAT1 (pre-designed siRNA, Applied Biosystems) with the help of Lipofectamine RNAiMAX Reagent (Invitrogen) according to the manufacturer's instructions. 30 pmol RNAi duplex was diluted in 250 µl of Opti-MEM medium (gibco) in a 15 ml falcon tube for each well and 5 µl of Lipofectamine RNAiMAX Reagent was diluted in 250 µl of Opti-MEM medium in another 15 ml falcon tube for each well. Then the diluted RNAi duplex and Lipofectamine RNAiMAX Reagent was combined and mixed. The mixture was incubated at room temperature for 20 min. After incubation, the mixture was added to each well and incubated in a cell incubator. Medium containing transfection reagent was replaced with fresh astrocyte culture medium after 6 hours of incubation. Sixty hours posttransfection, cells were used for experiments.

3.2.10 Quantitative real time-PCR (qRT-PCR)

Isolation of mRNA from the spinal cord of untreated and EAE mice was performed with an RNAeasy kit (Qiagen, Hilden, Germany). Isolated mRNA was transcribed into DNA with the SuperScript reverse transcriptase kit with oligo (dT) primers (Invitrogen) as described by the manufacturer. Quantitative RT-PCR for A20, IL-23, IL27, IL-17, IFN-γ, interleukin 6 (IL-6), GM-CSF, iNOS, TNF, chemokine (C-X-C motif) ligand 1 (CXCL1), chemokine (C-C motif)

ligand 2 (CCL2), C-X-C motif chemokine 10 (CXCL10), STAT1, and hypoxanthine phosphoribosyltransferase (HPRT) was performed with individual Taqman® gene expression assay primers (Applied Biosystems, Darmstadt, Germany). Amplification was performed on the Lightcycler 480 system (Roche). The ratio between the respective gene and corresponding HPRT was calculated per mouse according to the $\Delta\Delta$ cycle threshold method (Livak and Schmittgen, 2001), and data were expressed as the increase of mRNA expression in immunized mice over non-immunized controls of the respective mouse strain. All primers and probes were obtained from Applied Biosystems.

3.2.11 Protein isolation and Western blot

Mouse spinal cord tissue, cultured astrocytes and neurons, and FACS-sorted microglia were lysed in cold RIPA cell lysis buffer on ice for 30 min. Cytoplasmic and nuclear protein was separated using NE-Per Nuclear and Cytoplasmic Extraction Kit (Thermo Scientific). Lysates were cleared by centrifugation at 14,000 rpm for 15 min at 4 °C. The protein-containing supernatant was carefully transferred into a new 1.5 ml tube. Protein concentration was measured photometrically using the Bradford reagent (Bio-Rad) according to instructions of the manufacturer. After protein quantification, 5 × lane marker reducing sample buffer (Thermo Scientific) was added to protein and incubated at 99 °C for 5 min to denature protein. Equal amounts of protein were separated with 10% SDS-polyacrylamide gels, transferred to polyvinylidene difluoride (PVDF) membranes, and incubated with primary antibodies overnight at 4 °C followed by incubation with secondary antibodies. Blots were developed with an ECL Plus kit (GE Healthcare, Freiburg, Germany). Images were captured using the Intas Chemo Cam Luminescent Image Analysis system (INTAS Science Imaging Instruments) and analyzed with the LabImage 1D software (Kapelan Bio-Imaging Solutions, Leipzig, Germany).

3.2.12 Immunoprecipitation

Unstimulated and IFN-γ (10 ng/ml)-stimulated mouse astrocytes were lysed in RIPA cell lysis buffer as described before. 100 μl of sepharose G beads (GE Healthcare Europe GmbH, Munich, Germany) were added to 1 ml of cell lysate and incubated at 4 °C for 30 min on a rocker to pre-clear the cell lysate. The beads were removed by centrifugation at 10,000 rpm for 10 min and supernatant was transferred to a new tube. Protein concentration of pre-cleared lysates was determined and adjusted to 1 μg/μl. Equal amounts of lysates were then incubated with anti-

STAT1 and anti-A20 antibodies, respectively, at 4 °C overnight. The immunocomplex was captured with Sepharose G beads by overnight incubation at 4 °C. The beads were then washed 4 times with PBS by centrifugation at 10,000 rpm for 5 sec. The pellet was resuspended in $2 \times$ lane marker reducing sample buffer and incubated at 99°C for 5 min. The beads were collected by centrifugation and SDS-PAGE was performed with the supernatant. WB was applied to detect STAT1 and A20, respectively.

3.2.13 Detection of apoptosis of astrocytes

Apoptosis was detected with Vybrant Apoptosis Assay Kit (Invitrogen). Apoptosis was induced in cultured astrocytes by adding 20 or 100 ng / ml TNF, respectively, for 24 hr. Then, cells were harvested by trypsinization and washed with PBS (4 °C). The cell pellet was resuspended with $1 \times$ Annexin-binding buffer to the concentration of 1×10^6 cells / ml. Then, 5 µl of FITC annexin V and 1 µl of 100 µg / ml PI working solution was added to each 100 µl of cell suspension and incubated at room temperature for 15 min. After incubation, 400 µl of $1 \times$ Annexin-binding buffer was added to the cells. Apoptosis was then measured with a FACSCanto II flow cytometer.

3.2.14 Coculture of CD4$^+$ T cells with astrocytes

CD4$^+$ T cells were isolated from spleens and lymph nodes of C57BL/6 mice by MACS (Miltenyi Biotec) as described before. Purified CD4$^+$ T cells were activated for 48 h by culturing in anti-CD3 (BD, 5 µg/ml) and anti-CD28 (eBiosciences, 2 µg/ml)-coated 96-well plates at 1-2 $\times 10^5$ cells/well in 200 µl of RPMI-1640 (Gibco) supplemented with 10% FCS (Gibco), 1% L-glutamine (Gibco), 100 U/ml penicillin (Sigma), and 0.1 mg/ml streptomycin (Sigma). For coculture, 1×10^5 activated T cells were inoculated in six-well plates either alone as a background control or on the astrocytic monolayers. After 24 h incubation, T cells were collected and apoptosis was detected by flow cytometry.

3.2.15 Measurement of apoptosis of T cells

Leukocytes isolated from spinal cord were stained with CD45-Pacific Blue, CD3-FITC, CD4-APC, and 7-amino actinomycin D (7-AAD). Apoptosis of cocultured CD4$^+$ T cells was detected by measuring active caspase 3 and phosphatidylserine residues exposed on the external cell membrane. Co-cultured CD4$^+$ T cells were stained with Annexin-APC, Caspase 3-PE (Active Caspase-3 PE Mab Apoptosis kit, BD Bioscience), and CD4-Pacific Blue. For caspase-3

staining, cocultured CD4$^+$ T cells were washed twice with PBS (4 °C) and then resuspended in BD Cytofix/Cytoperm solution at the concentration of 1×10^6 cells / 0.5 ml and incubated on ice for 20 min. Cells were then pelleted and washed twice with BD Perm/Wash buffer at a volume of 0.5 ml buffer per 1×10^6 cells at room temperature. After washing, cells were incubated with Caspase 3-PE diluted in BD Perm/Wash buffer for 30 min at room temperature. Each test was washed with 1 ml BD Perm/Wash buffer and resuspended with 0.5 ml BD Perm/Wash buffer. Apoptotic CD4$^+$ T cells were then analyzed by flow cytometry.

3.2.16 Migration assay

CD4$^+$ T cells were isolated from lymph nodes of C57BL/6 mice by MACS as described before. Astrocytes were stimulated with or without IFN-γ (10 ng/ml) for 48 hr. Thereafter, medium was collected from astrocyte cultures and centrifuged at 10000 rpm for 3 min to get rid of cells and cell debris. The 24-well Transwell chambers (5 μm pore, Costar) were prepared by coating the upper part with 100 μl of 0.01% poly-l-lysine (Sigma) for 1.5 h at 37 °C. Chambers were then washed twice with 100 μl PBS. Conditioned astrocyte medium was added to the lower part of Transwell chambers and purified CD4$^+$ T cells were placed in the upper part. After two hours of incubation at 37 °C, 50 μl of 0.1M EDTA was added to stop migration. Plates were shaked on a shaker for 10 min at room temperature. Number of CD4$^+$ T cells in the lower chambers was counted microscopically.

3.2.17 Immunohistochemistry

Immunohistochemistry was performed in collaboration with Prof. Dr. Martina Deckert (Department of Neuropathology, University Hospital Cologne, Germany). Animals were anesthetized with isoflurane and then perfused intracardially with 0.9% NaCl for immunohistochemistry on frozen sections. For histology on paraffin sections, anesthetized mice were perfused with 0.9% NaCl followed by perfusion with 4% paraformaldehyde. Spinal cords were removed and fixed with 4% paraformaldehyde for 24 h at 4 °C. Spinal cords were processed and stained with hemalum & eosin, cresyl violet and luxol fast blue. For macrophage and neurofilament staining, spinal cords were stained with rat anti-mouse Mac-3 (BD), anti-mouse CD3 (Serotec, Düsseldorf, Germany), and rabbit anti-neurofilament light (NF-L, Chemicon, Limburg, Germany) in an ABC protocol with 3,3'-diaminobenzidine (Sigma) and

H_2O_2 (Merck). Images were acquired with a Zeiss Axiophot using Zeiss Axioplan objective lenses, a Zeiss Axicam camera and Zeiss Axiovision software (Zeiss, Oberkochen, Germany).

3.2.18 Statistics

To test for statistical differences, the two-tailed Student's t-test was used. P values < 0.05 were accepted as significant. All experiments were performed at least twice.

4. Results

4.1 Function of astrocytic A20 in EAE

4.1.1 Upregulation of A20 in the spinal cord during EAE

To explore a possible role of A20 in EAE, C57BL/6 mice were actively immunized with myelin oligodendrocyte glycoprotein $(MOG)_{35-55}$ peptide and A20 mRNA expression was analyzed by quantitative real-time PCR in spinal cord at day 15 and day 22 post immunization (p.i.), respectively. A20 mRNA expression was significantly upregulated in the spinal cord at both day 15 and day 22 p.i. (Fig. 10) suggesting a possible function of CNS-derived A20 during EAE.
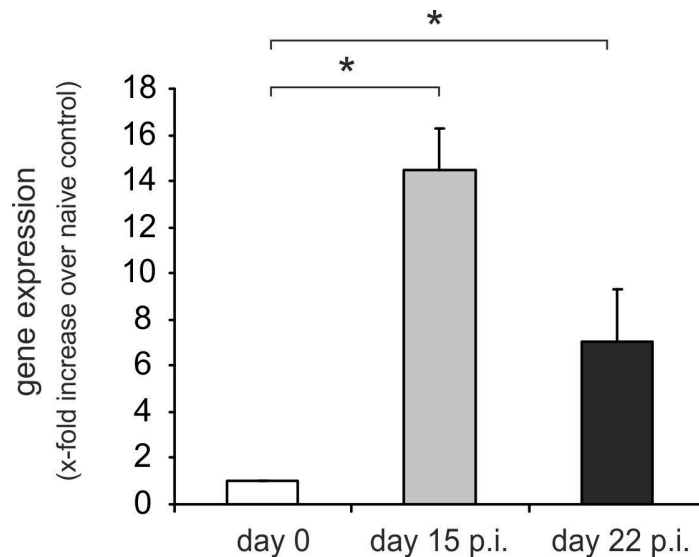
Figure 10. Upregulation of A20 in the spinal cord during EAE. mRNA transcription of A20 in the spinal cord was evaluated by quantitative RT-PCR in untreated and MOG_{35-55}-immunized C57BL/6 mice at day 15 and 22 p.i (n = 3). Data are expressed as the increase of A20 mRNA of immunized over unimmunized mice normalized to HPRT (mean + SEM * $p < 0.05$)

4.1.2 Aggravated EAE of Nestin-Cre A20^fl/fl mice

To study the contribution of A20 derived from CNS-resident cells to EAE, we generated Nestin-Cre A20^fl/fl mice, in which A20 was specifically deleted in all neuroectodermal cells including astrocytes, neurons, and oligodendrocytes (Graus-Porta et al., 2001). Spinal cord was isolated from Nestin-Cre A20^fl/fl mice and control littermates and then Western blot (WB) was performed with spinal cord samples to confirm A20 deletion. WB analysis revealed that A20 expression was deleted in spinal cord of Nestin-Cre A20^fl/fl mice (Fig. 11A). In addition, deletion of A20 in

spinal cord of Nestin-Cre A20$^{fl/fl}$ mice was also confirmed by quantitative real-time PCR (Fig. 11B). To study the susceptibility of Nestin-Cre A20$^{fl/fl}$ mice to EAE, Nestin-Cre A20$^{fl/fl}$ mice and control mice were actively immunized with MOG$_{35-55}$ peptide. Nestin-Cre A20$^{fl/fl}$ mice displayed significantly stronger EAE clinical symptoms as compared to the control A20$^{fl/fl}$ mice (Fig. 11C). The genotoxicity of Nestin-Cre transgene might also contributed to the increased susceptibility of Nestin-Cre A20$^{fl/fl}$ mice to EAE. To rule out this possibility, EAE was induced in Nestin-Cre A20$^{wt/wt}$ mice and A20$^{wt/wt}$ mice. Nestin-Cre A20$^{wt/wt}$ mice developed the same course of disease as A20$^{wt/wt}$ mice (Fig. 11D), showing that the aggravated EAE of Nestin-Cre A20$^{fl/fl}$ mice cannot be attributed to the Nestin-Cre transgene.
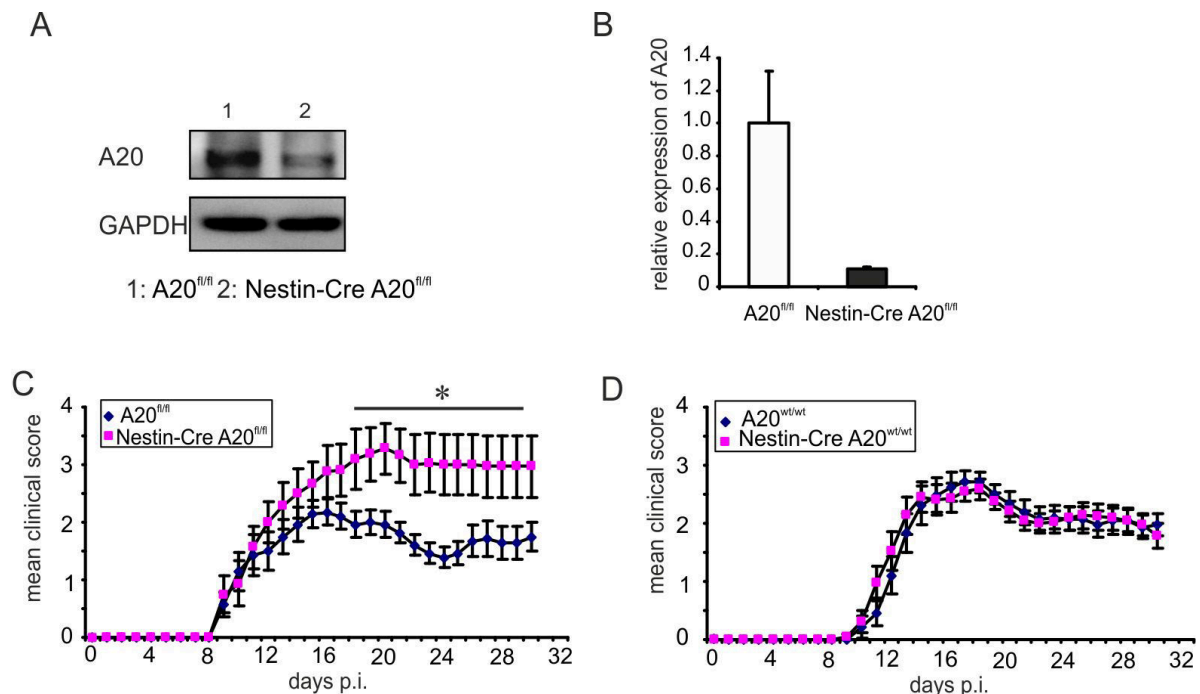

Figure 11. Nestin-Cre A20$^{fl/fl}$ mice developed more severe EAE as compared with control mice. (A) WB analysis for A20 in the spinal cord of Nestin-Cre A20$^{fl/fl}$ and A20$^{fl/fl}$ control mice. (B) RT-PCR analysis for A20 mRNA expression in the spinal cord of Nestin-Cre A20$^{fl/fl}$ and A20$^{fl/fl}$ control mice ($n = 3$ for both groups). Data show the mean + SEM. (C) Clinical scores of EAE in Nestin-Cre A20$^{fl/fl}$ ($n = 7$) and A20$^{fl/fl}$ ($n = 8$) mice induced by MOG$_{35-55}$-immunization. Data show the mean clinical scores $\pm$ SEM (* $p < 0.05$). (D) Clinical scores of EAE in Nestin-Cre A20$^{wt/wt}$ ($n = 12$) and A20$^{wt/wt}$ ($n = 11$) mice induced by MOG$_{35-55}$-immunization. Data show the mean clinical scores $\pm$ SEM.

4.1.3 Enhanced inflammation in the spinal cord of Nestin-Cre A20$^{fl/fl}$ mice

A20$^{fl/fl}$ and Nestin-cre A20$^{fl/fl}$ mice developed EAE characterized by inflammation of the spinal cord, which was, however, more prominent and widespread in Nestin-Cre A20$^{fl/fl}$ mice (Fig.

12A). While in A20$^{fl/fl}$ mice inflammation was mainly confined to the dorsal columns of the spinal cord, leukocytes had also infiltrated the anterior and posterior spinocerebellar tracts, even reaching the spino-olivary fibers, the olivospinal, and the vestibulospinal tracts in Nestin-Cre A20$^{fl/fl}$ mice. In addition, demyelination and axonal damage were also more prominent in Nestin-Cre A20$^{fl/fl}$ mice as compared to A20$^{fl/fl}$ mice. Whereas in A20$^{fl/fl}$ mice EAE regressed beyond day 15 p.i. with only small residual inflammatory infiltrates, Nestin-Cre A20$^{fl/fl}$ mice still had prominent autoimmune inflammation with accompanying widespread demyelination and axonal damage in the spinal cord (Fig. 12A).

At day 15 p.i., a higher percentage of CD4$^+$ T cells infiltrating the spinal cord was detected in Nestin-Cre A20$^{fl/fl}$ mice as compared to A20$^{fl/fl}$ mice (Fig. 12B). At day 22 p.i., the time point when Nestin-Cre A20$^{fl/fl}$ mice showed significantly more severe clinical symptoms than control mice, both the percentage and number of invading CD4$^+$ T cells was significantly increased in the spinal cord of Nestin-Cre A20$^{fl/fl}$ mice (Fig. 12B, C). The percentage and number of infiltrating CD4$^+$ T cells did not differ between unimmunized animals of the two mouse strains (day 0) showing that Nestin-Cre A20$^{fl/fl}$ mice did not develop spontaneous inflammation in the CNS (Fig. 12B, C). Correspondingly, at day 22 p.i., higher levels of proinflammatory IFN-γ, IL-17, TNF, GM-CSF, IL-6, CXCL1, CCL2, and CXCL10 mRNA were detected in the spinal cord of Nestin-Cre A20$^{fl/fl}$ mice (Fig. 12D). Noteworthy, in the CNS, astrocytes are a major inducible source of the chemokines CXCL1, CCL2, and CXCL10 (Le et al., 2010; Miljkovic et al., 2011) and chemokine production by astrocytes is critical for EAE pathogenesis, implying that the aggravated EAE in Nestin-Cre A20$^{fl/fl}$ mice might be attributed to the deletion of A20 in astrocytes.
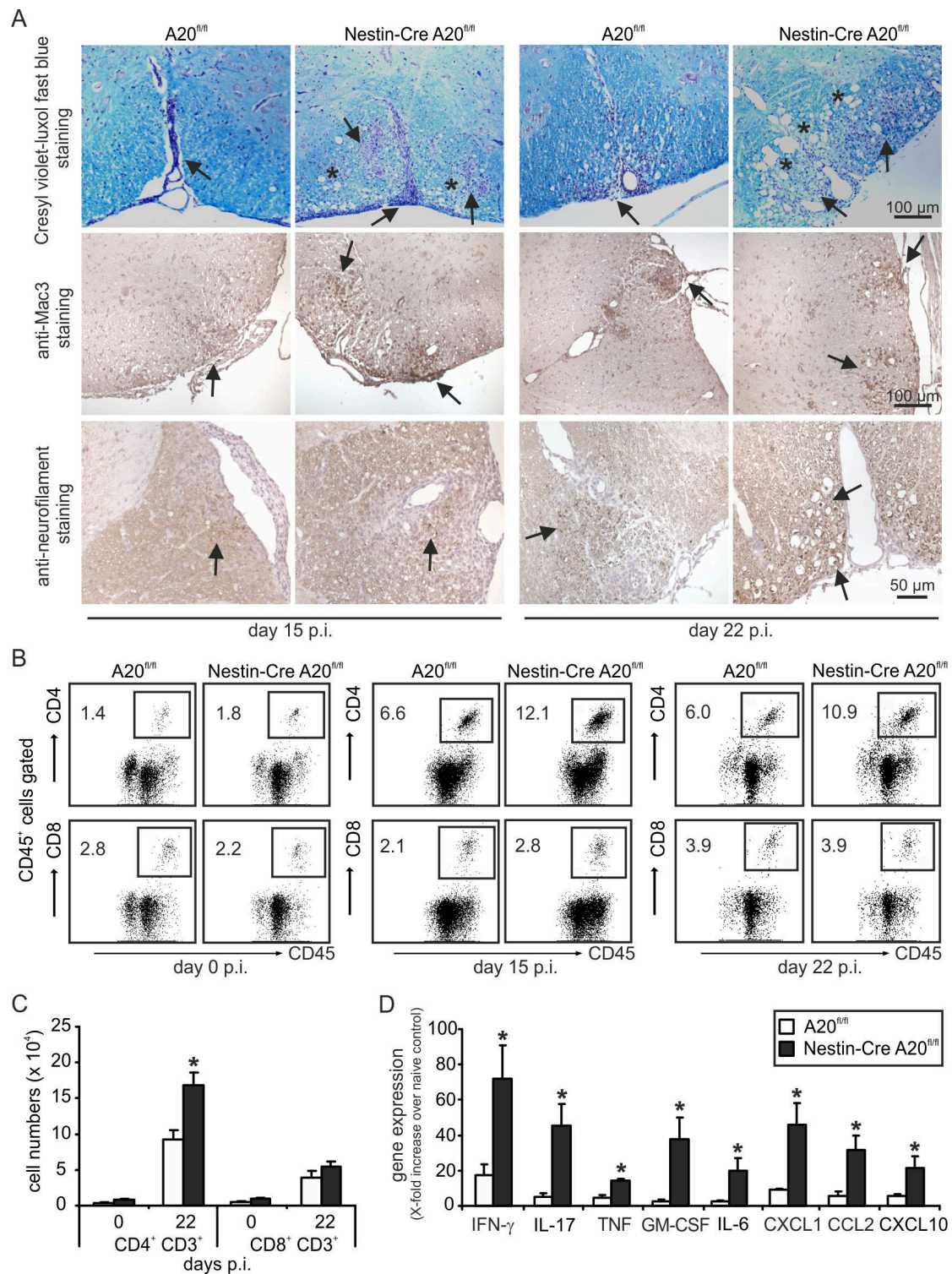
Figure 12. Exacerbated inflammation in the spinal cord of Nestin-Cre A20$^{fl/fl}$ mice. (A) At day 15 p.i., a prominent inflammatory infiltrate is associated with edema and focal loss of myelin in the posterior dorsal spinocerebellar tract of an A20$^{fl/fl}$ mouse. In a Nestin-Cre A20$^{fl/fl}$ mouse, highly cellular infiltrates are disseminated throughout the posterior columns bilaterally, also extending into the posterior dorsal spinocerebellar tracts.

Accordingly, edema and loss of myelin are much more pronounced as compared to A20$^{fl/fl}$ mice. At day 22 p.i., inflammation has regressed in an A20$^{fl/fl}$ mouse, in which only a perivascular lymphocytic infiltrate slightly extending into the neighbored parenchyma of the posterior column of the spinal cord is detectable. In contrast, inflammation and demyelination are progressive in a Nestin-Cre A20$^{fl/fl}$ mouse. The white matter of the posterior columns and the posterior as well as the anterior spinocerebellar tracts are heavily infiltrated by leukcoytes. In addition to pronounced edema, myelophages are present indicating ongoing demyelination. Cresyl violet and luxol fast blue staining. Original magnification ×200. (B) CD4$^+$ and CD8$^+$ T cells infiltrating the spinal cords of MOG$_{35-55}$-immunized Nestin-Cre A20$^{fl/fl}$ and A20$^{fl/fl}$ mice was analyzed by flow cytometry at day 0, 15 and 22 p.i. Representative dot plots are shown. (C) Absolute number of CD4$^+$ and CD8$^+$ T cells in the spinal cords of MOG$_{35-55}$-immunized Nestin-Cre A20$^{fl/fl}$ and A20$^{fl/fl}$ mice at day 0 (n = 4 for both groups) and 22 p.i. (n = 6 for both groups) (mean + SEM * p < 0.05). (D) RT-PCR analysis of relative expression of inflammatory genes as indicated in spinal cords of MOG$_{35-55}$-immunized Nestin-Cre A20$^{fl/fl}$ and A20$^{fl/fl}$ mice (n = 3 for both groups) at day 22 p.i. Data represent the mean + SEM as relative increase over unimmunized mice

4.1.4 A20-deficiency in astrocytes aggravates EAE

In order to precisely elucidate the function of A20 derived from astrocytes in EAE, we generated GFAP-Cre A20$^{fl/fl}$ mice, which lacked A20 electively in astrocytes, and challenged them with EAE. Primary astrocytes and neurons were isolated from new born mice or E18.5 fetus, respectively, and cultured *in vitro*. Microglia was harvested from astrocyte cultures by FACS sorting. WB was performed with astrocyte, neuron, and microglia samples to confirm A20 deletion. WB analysis showed that efficient A20 deletion was achieved in astrocytes (Fig. 13A), and no obvious A20 deletion was detected in microglia and neurons of GFAP-Cre A20$^{fl/fl}$ mice (Fig. 13B). EAE was induced in GFAP-Cre A20$^{fl/fl}$ mice by active immunization with MOG$_{35-55}$ peptide. Similar to Nestin-Cre A20$^{fl/fl}$ mice, GFAP-Cre A20$^{fl/fl}$ mice showed significantly more severe clinical symptoms than control mice (Fig. 13C), demonstrating that A20 in astrocytes is important for the amelioration of EAE. EAE symptoms of GFAP-Cre A20$^{wt/wt}$ mice were similar to that of A20$^{wt/wt}$ mice (Fig. 13D), showing that the more severe EAE of GFAP-Cre A20$^{fl/fl}$ mice was not due to the GFAP-Cre transgene. Histology showed that GFAP-Cre A20$^{fl/fl}$ mice displayed more pronounced demyelination in the spinal cord than control mice at day 15 p.i. (Fig. 13E). Up to day 22 p.i., demyelination and axonal damage had regressed in A20$^{fl/fl}$ mice, but persisted in GFAP-Cre A20$^{fl/fl}$ mice.
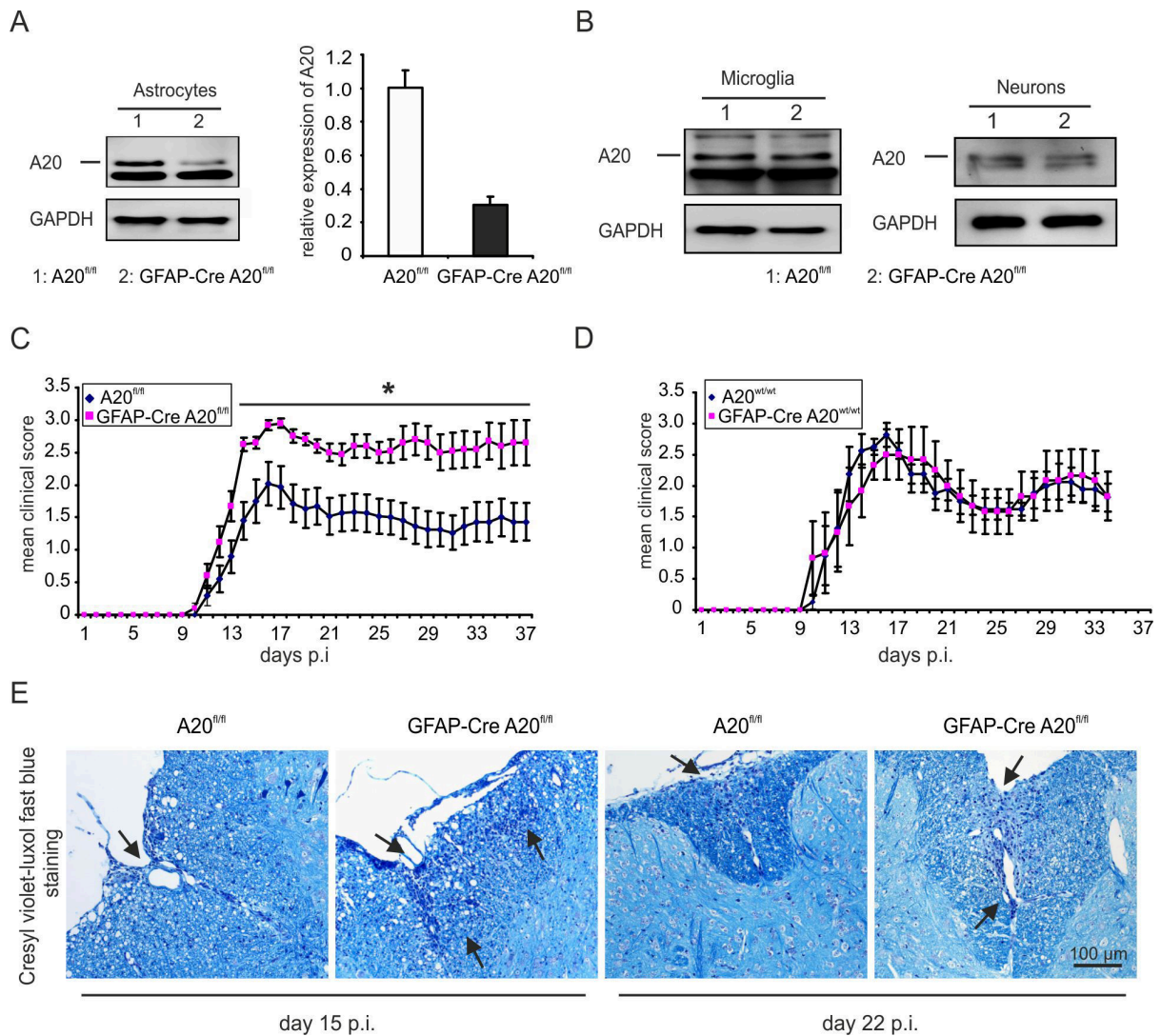
Figure 13. EAE was aggravated in GFAP-Cre A20$^{fl/fl}$ mice. (A) WB analysis for A20 expression in cultured astrocytes isolated from GFAP-Cre A20$^{fl/fl}$ and A20$^{fl/fl}$ control mice (left). The right panel shows the relative quantification of A20 normalized to GAPDH. Data show the mean + SEM. (B) WB analysis for A20 expression in FACS-sorted microglia and cultured neurons from GFAP-Cre A20$^{fl/fl}$ and A20$^{fl/fl}$ mice. (C) Clinical scores of EAE in GFAP-Cre A20$^{fl/fl}$ ($n = 10$) and A20$^{fl/fl}$ ($n = 15$) mice induced by MOG$_{35-55}$-immunization. Data show the mean clinical scores $\pm$ SEM (* $p < 0.05$). (D) Clinical scores of EAE in GFAP-Cre A20$^{wt/wt}$ ($n = 5$) and A20$^{wt/wt}$ ($n = 5$) mice induced by MOG$_{35-55}$-immunization. Data show the mean clinical scores $\pm$ SEM. (E) At day 15 p.i., a GFAP-Cre A20$^{fl/fl}$ mouse shows widespread inflammation, edema, and focal loss of myelin in the posterior colums and the spinocerebellar tracts. In contrast, inflammation and demyelination are much milder in an A20$^{fl/fl}$ mouse. At day 22 p.i., inflammation and demyelination are still active in the posterior columns of a GFAP-Cre A20$^{fl/fl}$ mouse, whereas they have declined in an A20$^{fl/fl}$ mouse. Cresyl violet and luxol fast blue staining. Original magnification ×200

4.1.5 A20 deletion in neurons does not aggravate EAE

Although we did not observe A20 deletion in cultured neurons of GFAP-Cre A20$^{fl/fl}$ mice, it has been shown that low levels of gene deletion can occur in neurons of GFAP-Cre expressing mice.

To consolidate the contention that EAE development was not influenced by A20 deletion in neurons, we generated Synapsin-Cre A20$^{fl/fl}$ mice, in which A20 was efficiently and specifically deleted in neurons (Fig. 14A). Synapsin-Cre A20$^{fl/fl}$ mice developed comparable clinical symptoms as A20$^{fl/fl}$ mice (Fig. 14B) illustrating that neuronal A20 deletion does not cause aggravation of EAE.
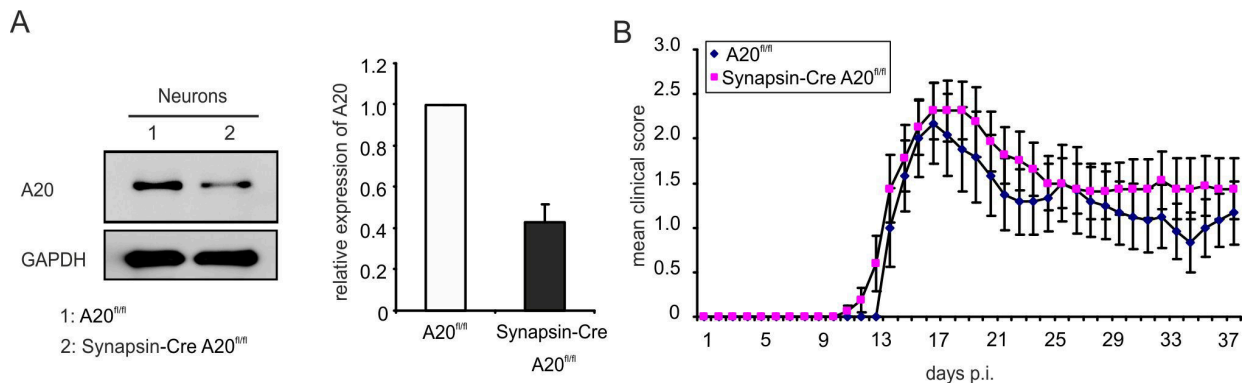

Figure 14. EAE was not aggravated in Synapsin-Cre A20$^{fl/fl}$ mice. (A) WB analysis for A20 expression in cultured neurons from neuron-restricted A20 deficient (Synapsin-Cre A20$^{fl/fl}$) and control (A20$^{fl/fl}$) mice. The right panel shows the relative quantification of A20 normalized to GAPDH. Data show the mean + SEM. (B) Clinical scores of EAE in Synapsin-Cre A20$^{fl/fl}$ ($n = 8$) and A20$^{fl/fl}$ ($n = 6$) mice induced by MOG$_{35-55}$-immunization. Data show the mean clinical scores $\pm$ SEM

4.1.6 Increased infiltration of inflammatory cells in the spinal cord of GFAP-Cre A20$^{fl/fl}$ mice

In accordance with the histopathological results, the number of leukocytes infiltrating the spinal cord of GFAP-Cre A20$^{fl/fl}$ was increased with a higher percentage of CD4$^+$ T lymphocytes at both early (day 15 p.i.) and late (day 22 p.i) stages of EAE (Fig. 15A, B). The number of infiltrating leukocytes and the percentage of infiltrating CD4$^+$ T cells did not differ between unimmunized animals of both mouse strains (day 0) showing that GFAP-Cre A20$^{fl/fl}$ mice did not develop spontaneous inflammation in the CNS (Fig. 15A, B). In addition to CD4$^+$ T cells, absolute numbers of infiltrating CD8$^+$ T cells, Ly6C^{hi} CD11b$^+$ inflammatory monocytes, and F4/80$^+$ CD68$^+$ macrophages were also significantly increased in the spinal cord of GFAP-Cre A20$^{fl/fl}$ mice at both day 15 and 22 p.i. (Fig. 15C).
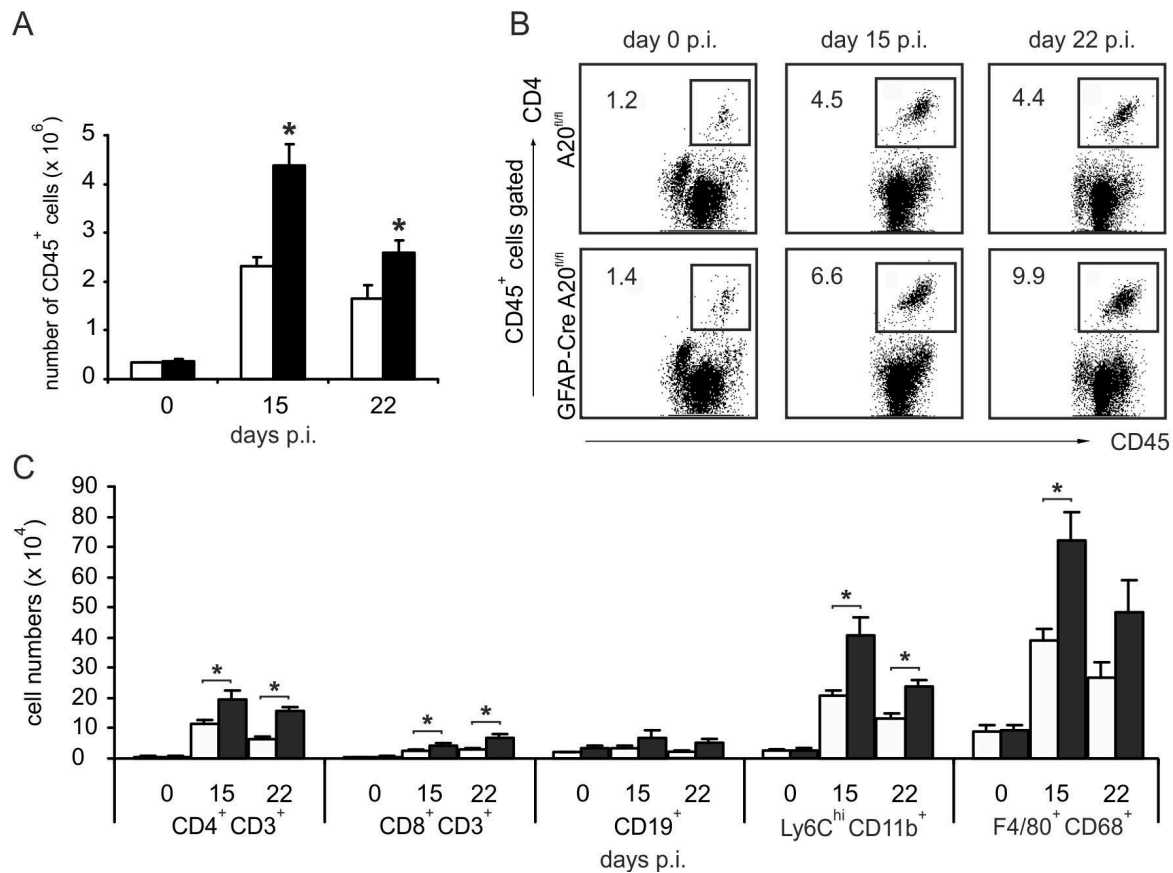
Figure 15. Increased immune cell infiltration in the spinal cords of GFAP-Cre A20$^{fl/fl}$ mice during EAE. (A) Absolute number of infiltrating CD45$^+$ cells in the spinal cords of unimmunized or MOG$_{35-55}$-immunized GFAP-Cre A20$^{fl/fl}$ and A20$^{fl/fl}$ mice ($n = 6$ for both groups) (mean + SEM * p < 0.05). (B) Percentage of infiltrating CD4$^+$ T cells in the spinal cords of MOG$_{35-55}$-immunized GFAP-Cre A20$^{fl/fl}$ and A20$^{fl/fl}$ mice was analyzed by flow cytometry. Representative dot plots are shown. (C) Absolute number of infiltrating immune cells in the spinal cords of GFAP-Cre A20$^{fl/fl}$ and A20$^{fl/fl}$ mice at day 0 ($n = 6$ for both groups), 15 ($n = 6$ for GFAP-Cre A20$^{fl/fl}$ group; $n = 5$ for A20$^{fl/fl}$ group), and 22 ($n = 6$ for both groups) p.i. (mean + SEM * p < 0.05).

4.1.7 GM-CSF, IL-17, and IFN-γ-producing T cells are increased in the spinal cord of GFAP-Cre A20$^{fl/fl}$ mice

Given that GM-CSF, IL-17, and IFN-γ-producing T cells can all induce EAE (Brustle et al., 2012; Codarri et al., 2011; Domingues et al., 2010) while regulatory Foxp3$^+$ CD4$^+$ T cells suppress the disease (Anderton and Liblau, 2008; McGeachy et al., 2005), we studied these subpopulations of invading CD4$^+$ T cells. At both days 15 and 22 p.i., numbers of activated CD69$^+$ CD4$^+$ T cells were increased in the spinal cord of GFAP-Cre A20$^{fl/fl}$ mice (Fig. 16A). In contrast, the percentage of Foxp3$^+$ regulatory CD4$^+$ T cells was significantly decreased in the spinal cord of GFAP-Cre A20$^{fl/fl}$ mice at day 22 p.i. (Fig. 16B). Flow cytometry showed that

only the percentage of IL-17 but not of IFN-γ and GM-CSF producing CD4$^+$ T cells was increased in GFAP-Cre A20$^{fl/fl}$ mice. However, the total number of all three T cell populations was significantly increased in the spinal cord of GFAP-Cre A20$^{fl/fl}$ mice as compared to A20$^{fl/fl}$ mice (Fig. 16C) explaining the more severe EAE in GFAP-Cre A20$^{fl/fl}$ mice.
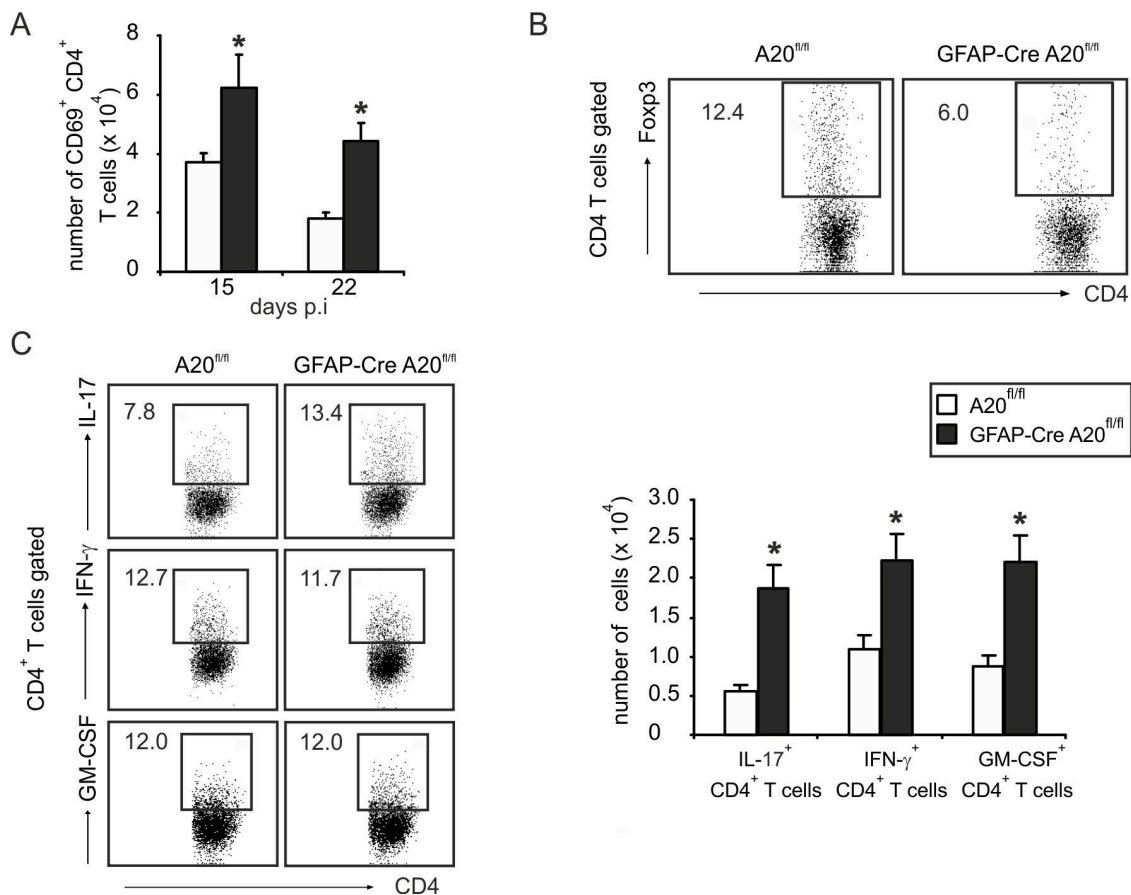

Figure 16. Increased activated T cells in the spinal cords of GFAP-Cre A20$^{fl/fl}$ mice during EAE. (A) Absolute number of CD69$^+$ CD4$^+$ T cells was calculated based on flow cytometry results at day 15 (n = 6 for GFAP-Cre A20$^{fl/fl}$ group; n = 5 for A20$^{fl/fl}$ group) and 22 (n = 6 for both groups) p.i. (mean + SEM * p < 0.05). (B) Representative dot plots show Foxp3$^+$ CD4$^+$ T cells in the spinal cords of MOG$_{35-55}$-immunized GFAP-Cre A20$^{fl/fl}$ and A20$^{fl/fl}$ mice at day 22 p.i. (C) The relative (left panel) and absolute (right panel) number of IL-17$^+$ CD4$^+$, IFN-γ$^+$ CD4$^+$, and GM-CSF$^+$ CD4$^+$ T cells in the spinal cords of MOG$_{35-55}$-immunized GFAP-Cre A20$^{fl/fl}$ and A20$^{fl/fl}$ mice (n = 6 for both groups) at day 22 p.i. was analyzed by flow cytometry (mean + SEM * p < 0.05)

4.1.8 Increased proinflammatory gene transcription in the spinal cord of GFAP-Cre A20$^{fl/fl}$ mice

To examine the impact of astrocytic A20 on the expression of proinflammatory genes in the spinal cord during EAE, quantitative real-time PCR for cytokine and chemokine mRNA

transcripts was performed on spinal cord tissue at days 15 and 22 p.i., respectively. Already at day 15 p.i., GFAP-Cre A20$^{fl/fl}$ mice had significantly increased transcription of IFN-γ, TNF, IL-6, CXCL1, and CCL2 mRNA (Fig. 17A-H). At day 22 p.i., TNF and CXCL10 mRNA was still significantly elevated in GFAP-Cre A20$^{fl/fl}$ mice as compared to control mice (Fig. 17A-H). The significantly higher levels of chemoattractant IL-6, CXCL1, CCL2, and CXCL10 mRNA in spinal cords of GFAP-Cre A20$^{fl/fl}$ mice during EAE implied that the more severe EAE in GFAP-Cre A20$^{fl/fl}$ mice might be attributed to the enhanced chemokine production by A20-deficient astrocytes.
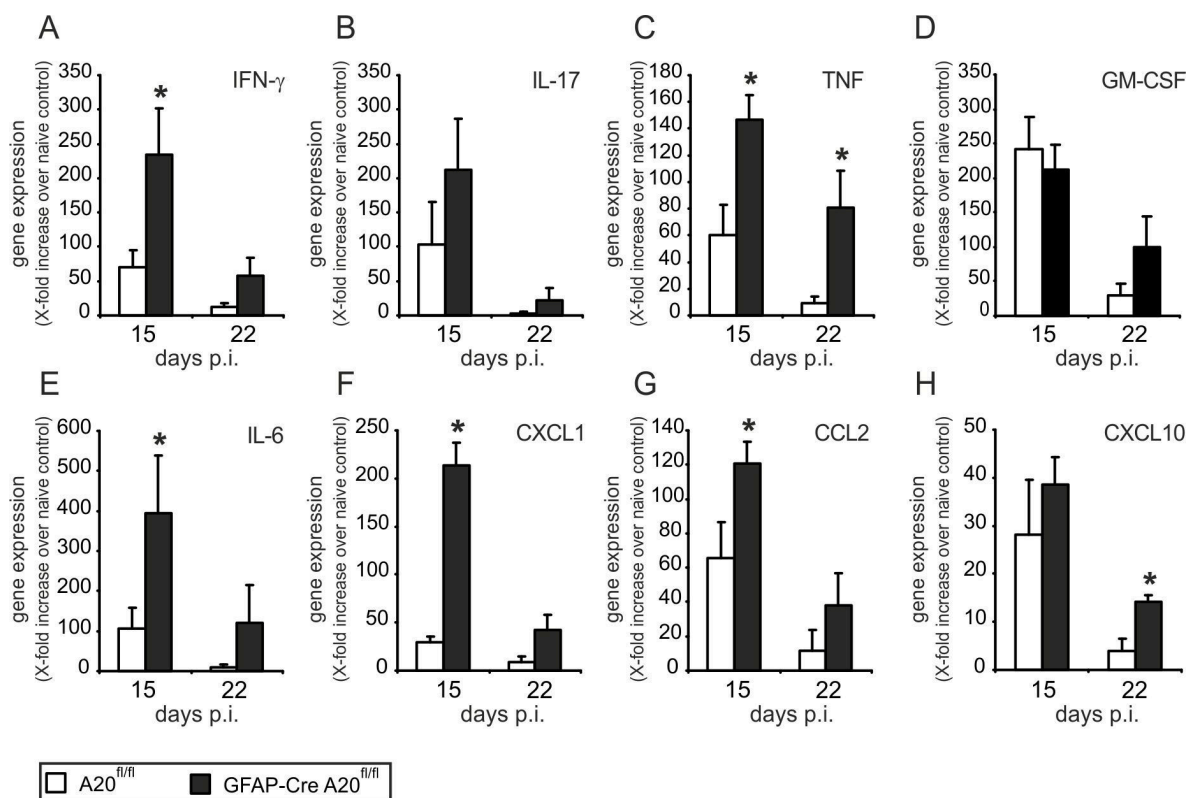

Figure 17. Increased pro-inflammatory gene expression in the spinal cords of GFAP-Cre A20$^{fl/fl}$ mice. (A-H) Expression of (A) IFN-γ, (B) IL-17, (C) TNF, (D) GM-CSF, (E) IL-6, (F) CXCL1, (G) CCL2, and (H) CXCL10 mRNA was determined by quantitative RT-PCR in GFAP-Cre A20$^{fl/fl}$ and A20$^{fl/fl}$ mice at days 15 and 22 p.i. Spinal cords of three mice per group were analyzed. Data represent the mean + SEM as relative increase over unimmunized mice (* $p < 0.05$)

4.1.9 Enhanced production of chemokines by A20-deficient astrocytes *in vitro*

Astrocytes are a major producer of proinflammatory cytokines and chemokines in the CNS during EAE upon stimulation with TNF, IFN-γ, and IL-17 (Dong and Benveniste, 2001; Zepp et al., 2011). Therefore, we studied the regulation of chemokine production by A20 in cytokine-stimulated astrocytes *in vitro*. A20-deficient astrocytes expressed more CXCL10, CCL2, and CXCL1 mRNA in response to IL-17, IFN-γ, TNF, IL-17 + TNF, and IFN-γ + TNF, respectively (Fig. 18A-D). In addition, A20-deficient astrocytes expressed more IL-6 mRNA in response to IFN-γ and IFN-γ + TNF, respectively (Fig. 18C).

Although GM-CSF has been shown to play a pivotal role in EAE (Petermann and Korn, 2011), the function of GM-CSF on astrocytes is largely unknown. A20-sufficient astrocytes expressed only low levels of CXCL10, CCL2, CXCL1, and IL-6 mRNA upon GM-CSF stimulation, but the level of all these mRNAs increased dramatically in the absence of A20 (Fig. 18E). These data suggest that GM-CSF contributes to the aggravated EAE in GFAP-Cre A20$^{fl/fl}$ mice at least partially by inducing chemokine production in astrocytes. Taken together, these results show that in response to proinflammatory cytokines produced by encephalitogenic T cells, A20-deficient astrocytes in GFAP-Cre A20$^{fl/fl}$ mice exhibited an elevated production of chemoattractant cytokines and chemokines, which was also observed *in vivo* (Fig. 17) and paralleled by increased recruitment of encephalitogenic CD4^{+} T cells and more severe EAE.
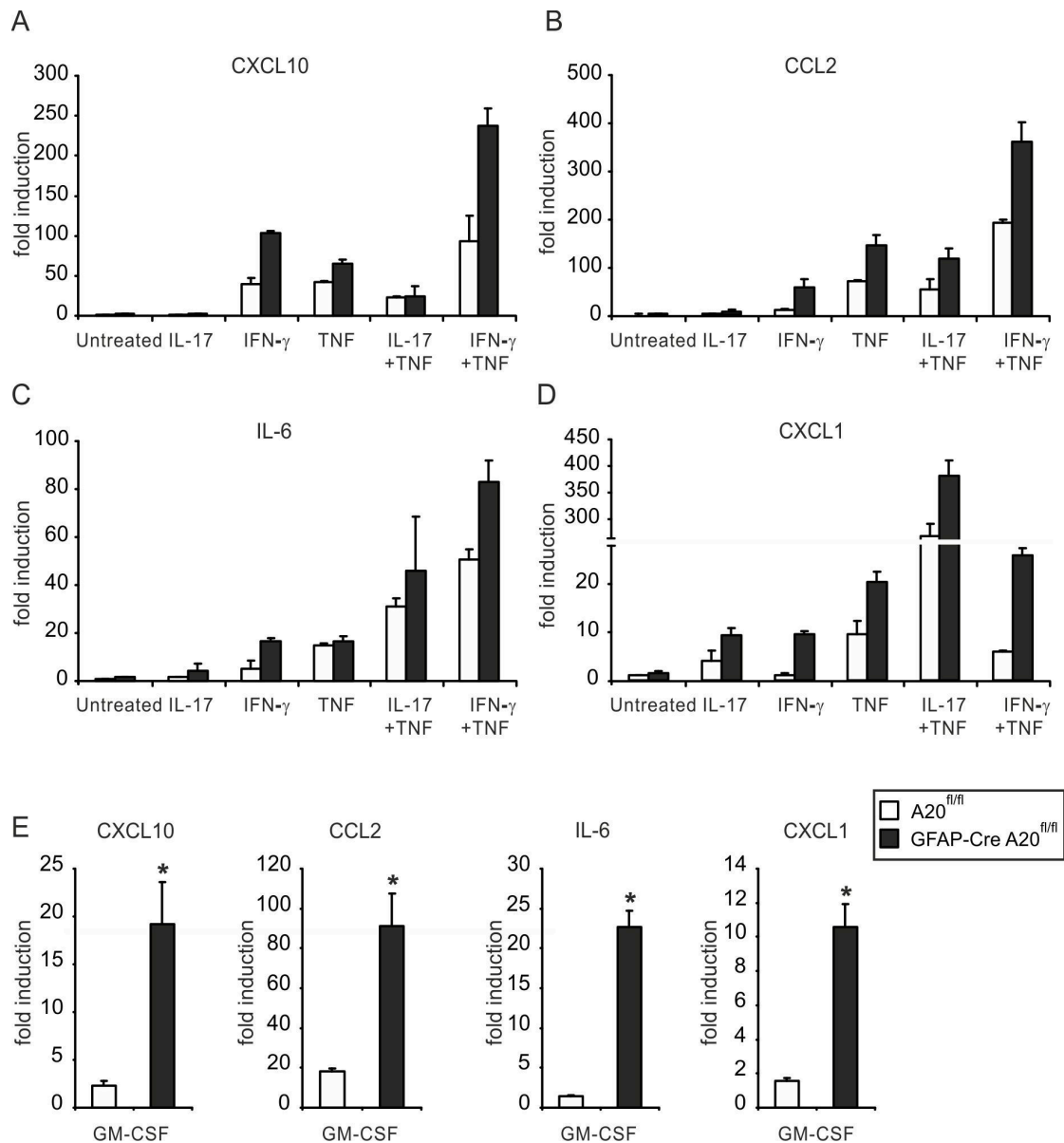
Figure 18. Increased *in vitro* pro-inflammatory gene transcription in A20-deficient astrocytes. (A-D) RT-PCR analysis of (A) CXCL10, (B) CCL2, (C) IL-6, and (D) CXCL1 in control ($n = 2$) and A20-deficient ($n = 2$) astrocytes left untreated or treated with IL-17 (50 ng/ml), IFN-γ (10 ng/ml) or TNF (10 ng/ml) alone or with IL-17 + TNF or IFN-γ + TNF for 16 hr. Data represent the mean + SEM as relative increase over untreated control samples. (E) RT-PCR analysis of CXCL10, CCL2, IL-6 and CXCL1 in control ($n = 3$) and A20-deficient ($n = 3$) astrocytes stimulated with GM-CSF (20 ng/ml) for 16 hr. Data represent the mean + SEM as relative increase over untreated control samples (* $p < 0.05$)

4.1.10 A20-deletion does increase apoptosis of astrocytes

Since (i) astrocyte loss is found in the center of the demyelinated lesions in patients suffering from acute MS (Ozawa et al., 1994), (ii) astrocyte survival is important for the control of EAE (Haroon et al., 2011; Voskuhl et al., 2009), and (iii) A20 can regulate apoptosis (Lee et al., 2000; Tavares et al., 2010; Vucic et al., 2011), we investigated whether the exacerbated EAE in GFAP-Cre A20$^{fl/fl}$ mice was due to enhanced astrocyte apoptosis. A20-deficient astrocytes stimulated *in vitro* with increasing concentrations of TNF did not undergo enhanced apoptosis as compared to A20-sufficient astrocytes (Fig. 19) suggesting that A20 does not critically regulate apoptosis of astrocytes in EAE. Therefore, the exacerbated EAE in GFAP-Cre A20$^{fl/fl}$ mice should be attributed to the enhanced chemokine production by astrocytes.
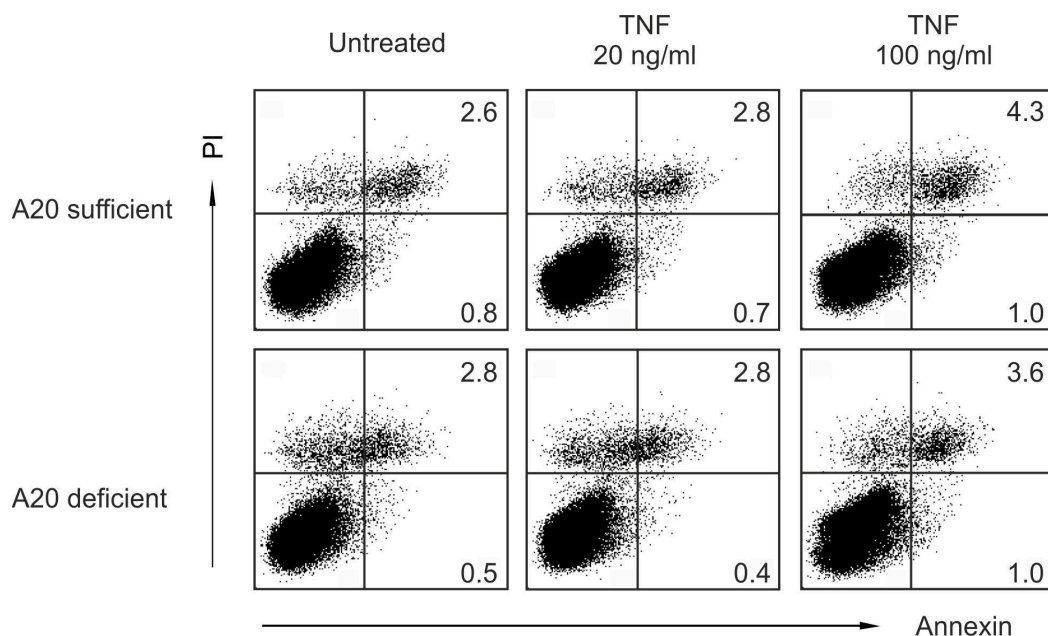

Figure 19. Normal apoptosis of A20-deficient and -sufficient astrocytes after TNF stimulation. Astrocytes isolated from GFAP-Cre A20$^{fl/fl}$ and A20$^{fl/fl}$ mice were treated with 20 or 100 ng/ml TNF, respectively, for 24 hr. Apoptosis was detected by PI and Annexin staining

4.1.11 A20 negatively regulates NF-κB, MAP kinase, and STAT1 pathways induced by fingerprint cytokines of autoreactive T cells

To understand how A20 suppresses chemokine production, we studied signaling pathways induced by TNF, IL-17, IFN-γ, and GM-CSF. Consistent with previous reports of A20 as a negative regulator of the canonical NF-κB pathway (Skaug et al., 2011) and that NF-κB pathway

is activated in response to TNF, IL-17, and GM-CSF (Bulek et al., 2011; Meads et al., 2010), enhanced phosphorylation of IκBα was detected in A20-deficient astrocytes in response to all three cytokines (Fig. 20A-C). In addition, A20 deficiency also enhanced p38 and JNK phosphorylation upon stimulation with TNF, IL-17, and GM-CSF (Fig. 20A-C).

A20-deficient astrocytes produced significantly more chemokines in response to IFN-γ (Fig. 18) implying that A20 might also negatively regulate IFN-γ-induced signaling. Although phosphorylation of STAT1 at tyrosine 701 was only slightly increased in the absence of A20, phosphorylation of serine 727 was dramatically increased in A20-deficient astrocytes (Fig. 20D). An analysis of cytosolic and nuclear extracts of IFN-γ-stimulated astrocytes showed that the increased phosphorylation of serine 727 occurred in both cytoplasm and nucleus (Fig. 20E). Strikingly, the protein level of STAT1 was also increased in A20-deficient astrocytes (Fig. 20D, E).
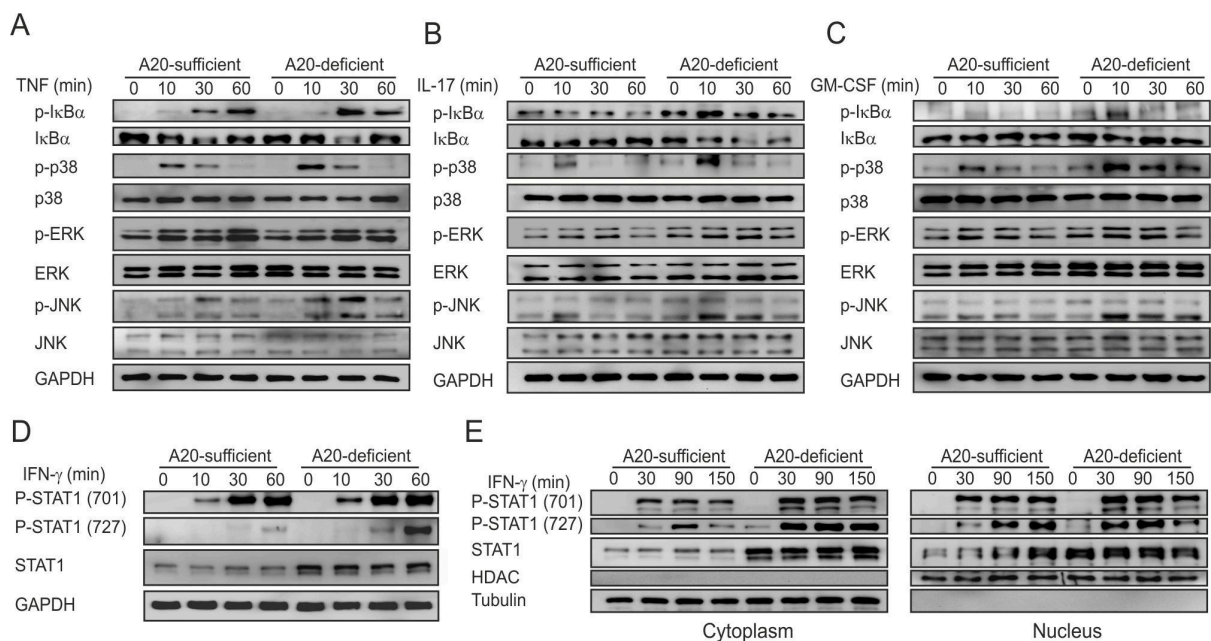

Figure 20. A20 negatively regulates multiple signaling pathways in astrocytes. (A-D) Western blot of whole cell lysates stimulated for the indicated time points with (A) TNF (10 ng/ml), (B) IL-17 (50 ng/ml), (C) GM-CSF (20 ng/ml), and (D) IFN-γ (10 ng/ml). (E) Western blot of cytoplasmic and nuclear extracts after stimulation with IFN-γ (10 ng/ml) for the indicated time points

4.1.12 A20 inhibits STAT1 expression in astrocytes

To rule out the possibility that STAT1 protein level was increased due to a genotoxic effect of the GFAP-Cre transgene, we studied the correlation between STAT1 expression and A20 expression by RNA interference (RNAi). Compared with control siRNA, A20 knockdown significantly enhanced expression of STAT1 (Fig. 21) confirming that A20 negatively regulates the protein level of STAT1.
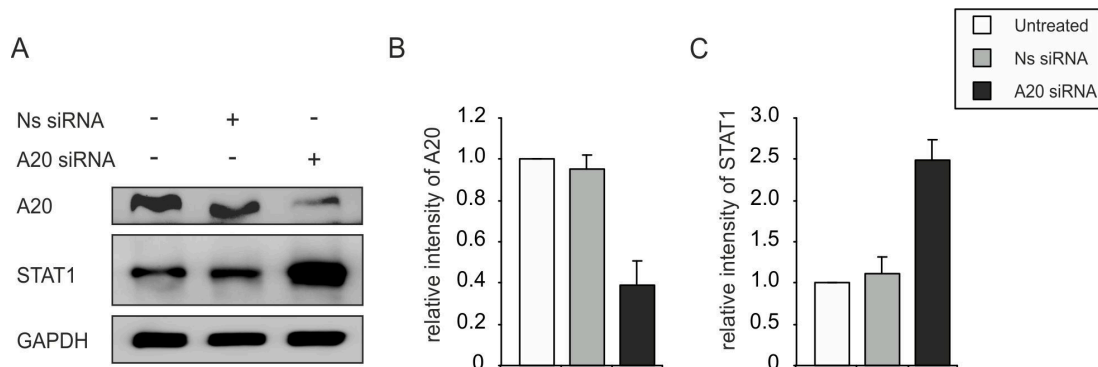

Figure 21. STAT1 expression was upregulated in astrocytes after A20 siRNA treatment. (A) Astrocytes derived from C57BL/6 mice were transfected with siRNA targeting A20 or nonsense siRNA. Sixty hours later, WB analysis was performed on total cell lysates for A20, STAT1 and GAPDH. (B) Relative quantification of A20 normalized to GAPDH. Data show the mean + SEM. (C) Relative quantification of STAT1 normalized to GAPDH. Data show the mean + SEM

4.1.13 A20 inhibits IFN-γ-induced STAT1-dependent chemokine production and T cell migration

The increased STAT1 protein levels of A20-deficient astrocytes were likely caused by an elevated STAT1 mRNA production as compared to A20-sufficient astrocytes (Fig. 22A). Interestingly, inhibition of NF-κB abolished the upregulated STAT1 mRNA production of A20-deficient astrocytes indicating that A20 indirectly modulated STAT1 function via controlling NF-κB activation (Fig. 22B). Knockdown of STAT1 by siRNA (Fig. 22C) revealed that in IFN-γ-stimulated astrocytes the increased CXCL10 and CCL2 mRNA production was largely dependent on STAT1 (Fig. 22D).

Since A20 strongly suppressed IFN-γ-induced STAT1-dependent chemokine production of astrocytes, we next studied the impact of A20 on astrocyte-induced T cell migration. In accordance with the *in vitro* chemokine production data, IFN-γ-conditioned medium of A20-

deficient astrocytes induced recruitment of an increased number of CD4^{+} T cells as demonstrated by an *in vitro* CD4^{+} T cell migration assay (Fig. 22E).
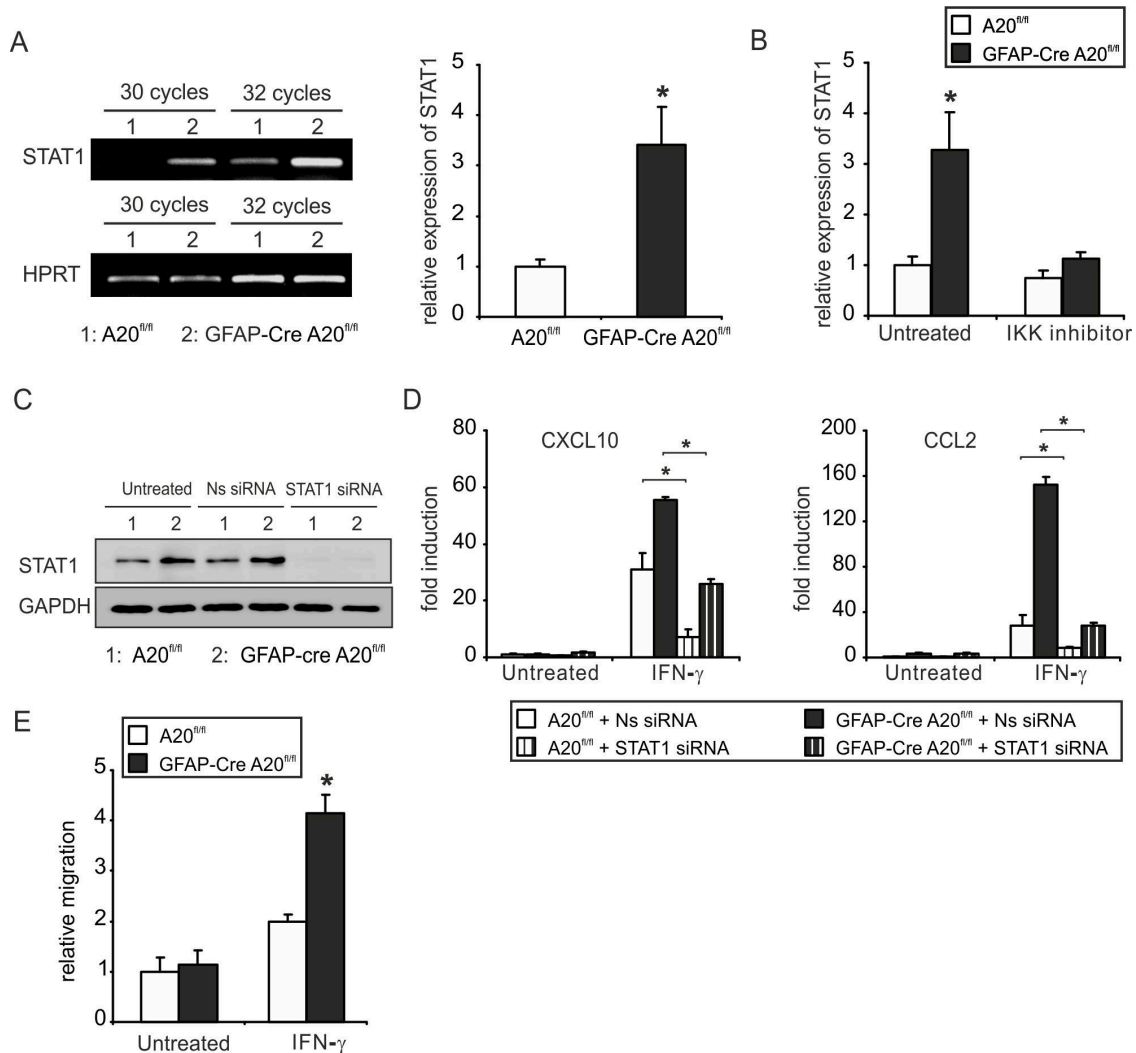

Figure 22. A20 negatively regulates STAT1 expression on the transcriptional level in a NF-κB-dependent fashion. (A) RT-PCR analysis of STAT1 mRNA expression in cultured astrocytes derived from GFAP-Cre A20^{fl/fl} and A20^{fl/fl} mice (left). The right panel shows the relative quantification of STAT1 normalized to HPRT (mean + SEM * p < 0.05). (B) RT-PCR analysis for the STAT1 mRNA expression after IKK inhibitor (1 μM) treatment for 48 hr (mean + SEM * p < 0.05). (C) Astrocytes derived from GFAP-Cre A20^{fl/fl} and A20^{fl/fl} mice were transfected with siRNA targeting STAT1 or nonsense (Ns) siRNA. Sixty hours later, WB analysis was performed on total cell lysates for STAT1 and GAPDH. (D) Sixty hours after siRNA transfection, astrocytes were left untreated or treated with IFN-γ (10 ng/ml) for 16 hr. CXCL10 and CCL2 mRNA levels were determined by RT-PCR. Data represent the mean + SEM as relative increase over untreated control samples (* p < 0.05). (E) Purified CD4^{+} T cells were placed into the upper part of transwell chambers with untreated or IFN-γ-conditioned medium (48 hr stimulation) of cultured astrocytes isolated from GFAP-Cre A20^{fl/fl} and A20^{fl/fl} mice in the lower part. After two hours of incubation, migrated T cells in the lower chambers were counted. T cell migration was calculated as relative increase over untreated controls (mean + SEM * p < 0.05)

Based on these findings, we conclude that A20 prevents the hyperactivation of multiple signaling pathways in astrocytes in response to cytokines produced by autoimmune T cells. Therefore, A20 suppresses the production of chemoattractant cytokines and chemokines by astrocytes, resulting in diminished recruitment of inflammatory leukocytes to the CNS and amelioration of EAE.

4.2 Function of astrocytic FasL in EAE

In order to determine whether FasL$^+$ astrocytes are inducers of CD4$^+$ T-cell apoptosis in EAE, we generated GFAP-Cre FasL$^{fl/fl}$ mice that are deficient of FasL selectively in astrocytes. We show in the present study that astrocytic FasL is crucial to terminate the autoimmune T-cell response in the CNS, which allows clinical recovery from EAE.

4.2.1 Selective deletion of FasL in astrocytes of GFAP-Cre FasL$^{fl/fl}$ mice

We generated GFAP-Cre FasL$^{fl/fl}$ mice with selective FasL deletion in the CNS (Fig. 23A). Further PCR analysis of cultivated cells showed FasL deletion in astrocytes and to a minor extent in neurons (Fig. 23B). In contrast, microglia of GFAP-Cre FasL$^{fl/fl}$ as well as astrocytes, neurons, and microglia of FasL$^{fl/fl}$ control mice did not show deletion of FasL (Fig. 23B). To confirm astrocytic FasL deletion at the protein level, cell surface expression of FasL protein was analysed by flow cytometry from cultivated astrocytes of GFAP-Cre FasL$^{fl/fl}$ and FasL$^{fl/fl}$ mice. As shown in Fig. 23C, FasL expression was reduced on the surface of astrocytes from GFAP-Cre FasL$^{fl/fl}$ as compared with those from FasL$^{fl/fl}$ mice. Both GFAP-Cre FasL$^{fl/fl}$ mice and FasL$^{fl/fl}$ (control) mice were born in a normal Mendelian ratio and reached adulthood without any CNS defects.

Collectively, these findings show that astrocyte-specific deletion of FasL was achieved in our newly generated GFAP-Cre FasL$^{fl/fl}$ mice, which did not show abnormalities under physiological conditions, thereby providing a useful tool for studying the function of astrocyte-specific FasL in experimentally induced models of CNS disorders.
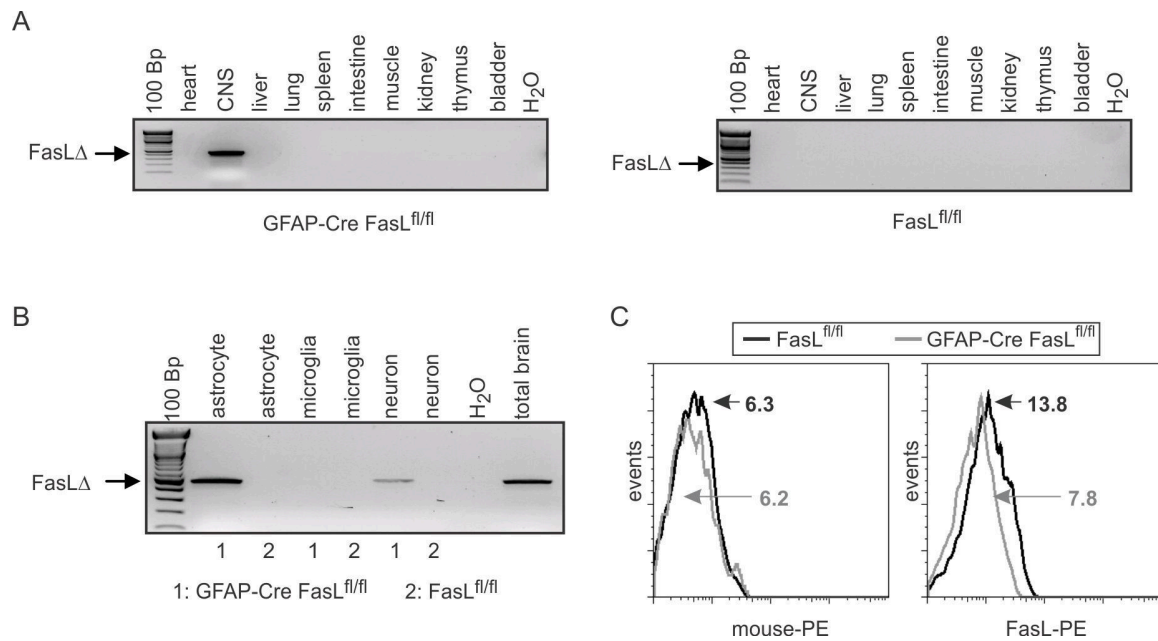
Figure 23. Organ and cell-type-specific deletion of FasL in GFAP-Cre FasL$^{fl/fl}$ mice. (A) Deletion of FasL in various organs of non-immunized GFAP-Cre FasL$^{fl/fl}$ and FasL$^{fl/fl}$ mice was analysed by PCR. The FasLΔ product has a size of 500 bp. Representative data from one of two experiments with three mice each are shown. (B) Deletion of FasL from cultivated and FACS-sorted astrocytes, microglia, and cultivated neurons of GFAP-Cre FasL$^{fl/fl}$ (lanes labelled 1) and FasL$^{fl/fl}$ (lanes labelled 2) mice. Total brain (positive control) was from a GFAP-Cre FasL$^{fl/fl}$ mouse. (C) Cell surface expression of the FasL protein (right) was analysed by flow cytometry from cultivated astrocytes of GFAP-Cre FasL$^{fl/fl}$ and FasL$^{fl/fl}$ mice. Staining with control mouse antibody is shown (left). Representative data from one of two experiments are shown and the mean fluorescence intensity of FasL expression is given in each histogram.

4.2.2 Aggravated EAE of GFAP-Cre FasL$^{fl/fl}$ mice with increased inflammation and demyelination

To gain insight into the astrocyte-specific function of FasL in the pathogenesis of EAE, we actively immunized GFAP-Cre FasL$^{fl/fl}$ mice and control mice with MOG$_{35-55}$ peptide emulsified in complete Freund's adjuvant (CFA) and assessed clinical disease activity daily. Both GFAP-Cre FasL$^{fl/fl}$ mice and FasL$^{fl/fl}$ control mice developed EAE starting at around day 9 p.i. and reaching peak disease at day 15 p.i.; over this period of time they developed similar clinical symptoms (Fig. 24A). However, beyond the maximum of disease, i.e. day 15 p.i., FasL$^{fl/fl}$ mice recovered gradually while EAE progressed in GFAP-Cre FasL$^{fl/fl}$ mice indicating a significantly more severe course of EAE in the later group of mice (Fig. 24A). Already at day 15 p.i., inflammation of GFAP-Cre FasL$^{fl/fl}$ mice was more severe and more widespread as compared with that in control animals, leading to more severe demyelination. While inflammatory foci consisting of CD3$^+$ T cells and macrophages were confined to the dorsal columns of the spinal

cord in FasL$^{fl/fl}$ mice, they also infiltrated the spinocerebellar tracts in GFAP-Cre FasL$^{fl/fl}$ mice. Differences between the two mouse strains were more prominent at day 22 p.i. as compared with those at day 15 p.i. Inflammation and demyelination were mild in FasL$^{fl/fl}$ mice (Fig. 24B, D) as compared with that in GFAP-Cre FasL$^{fl/fl}$ mice, with widespread inflammatory foci consisting of CD3$^+$ T cells and Mac3$^+$ macrophages (Fig. 24C, E). In GFAP-Cre FasL$^{fl/fl}$ mice, demyelination was prominent in the posterior columns as well as in spinocerebellar tracts (Fig. 24C), which also showed evidence of a disturbed axonal transport as evidenced by axonal bulbs. Inflammation was also prominent in the dorsal horn of the spinal cord, where many infiltrates resided (Fig. 24E).
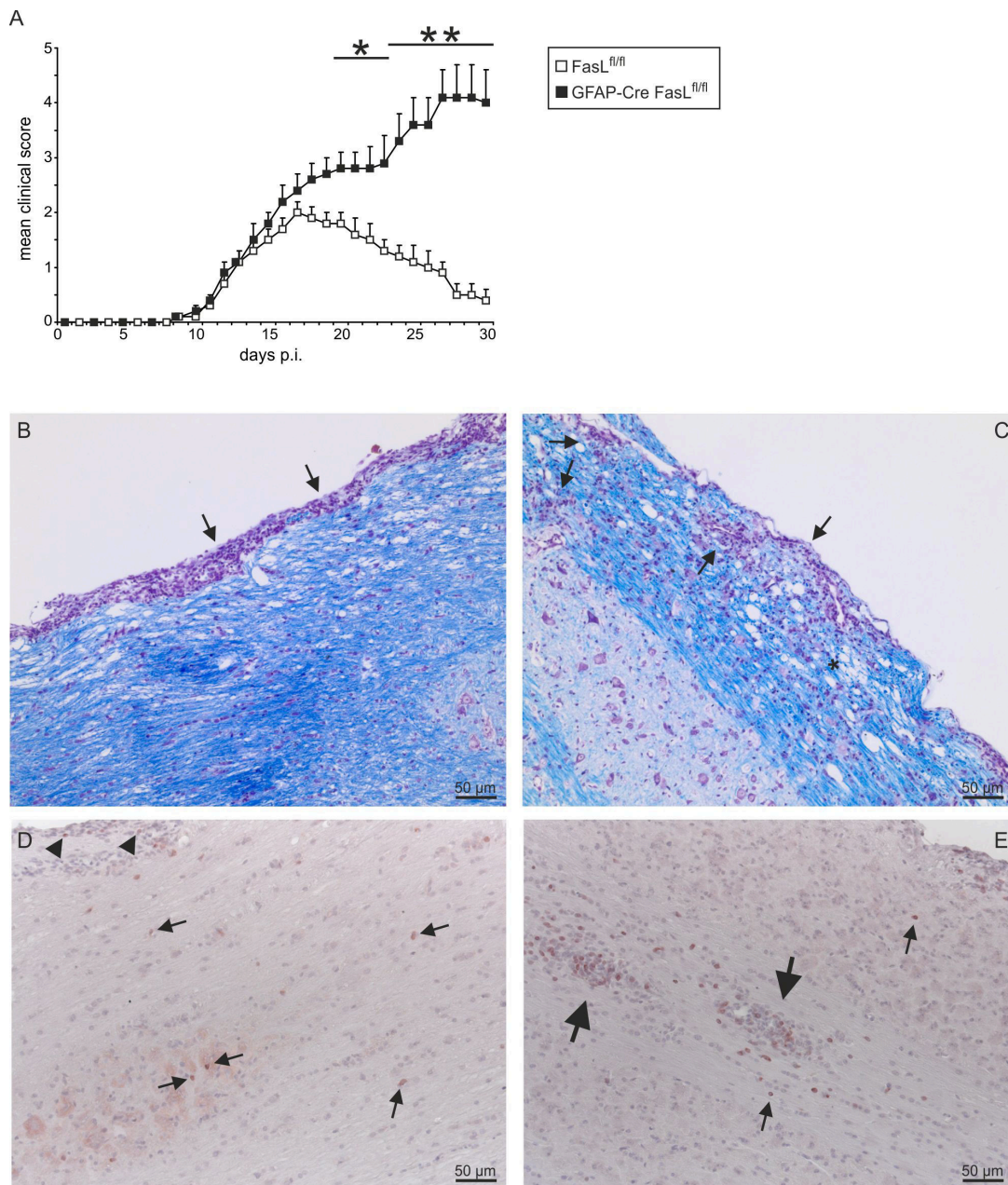
Figure 24. Aggravated EAE with increased demyelination and inflammation in GFAP-Cre FasL$^{fl/fl}$ mice. (A) Clinical symptoms of GFAP-Cre FasL$^{fl/fl}$ and FasL$^{fl/fl}$ mice were scored daily after immunization with MOG$_{35-55}$ peptide in CFA, and data are displayed as the mean + SEM of 8-10 mice per group, from one experiment representative of four performed. * p < 0.05, ** p < 0.01, t-tests. (B) Lack of ongoing demyelination in the posterior column of the spinal cord in a FasL$^{fl/fl}$ mouse, although myelin sheaths are reduced. Inflammatory infiltrates are confined to the leptomeninges (arrows), but do not infiltrate the spinal cord parenchyma. Cresyl violet - luxol fast blue staining. (C) Severe inflammation with leptomeningeal and spinal cord parenchymal infiltrates (arrows) with pronounced demyelination (*) in the posterior column of the spinal cord in a GFAP-Cre FasL$^{fl/fl}$ mouse. Note numerous myelin fragments and pronounced edema. Cresyl violet - luxol fast blue staining. (D) Some CD3$^+$ T cells contributed to leptomeningeal infiltrates (arrowheads) and only single CD3$^+$ T cells are still present in parenchyma of the spinal cord of a FasL$^{fl/fl}$ mouse (small arrows). Anti-CD3 immunostaining, slight counterstaining with hemalum. (E) Many CD3$^+$ T cells form inflammatory cuffs in the posterior colums and around blood vessels in the

posterior horn (large arrows) and are also scattered throughout the spinal cord (small arrows) in a GFAP-Cre FasL$^{fl/fl}$ mouse. Anti-CD3 immunostaining, slight counterstaining with hemalum. (B-E) Histological findings of representative mice (day 22 p.i.) from one of two independent experiments with three mice each are shown, bar 50 µm.

4.2.3 Increased numbers of infiltrating T cells in the spinal cord of GFAP-Cre FasL$^{fl/fl}$ mice

Since autoimmune T cells are the key mediator of EAE, we analysed T cells infiltrating the spinal cord. At day 15 p.i., flow cytometry revealed that numbers of infiltrating CD4$^+$ and CD8$^+$ T cells were slightly but not significantly increased in the spinal cord of GFAP-Cre FasL$^{fl/fl}$ mice as compared with those in FasL$^{fl/fl}$ mice (Fig. 25A, B), which corresponds to the similar clinical scores at this time point (Fig. 24). At day 22 p.i., significantly more CD4$^+$ and CD8$^+$ T cells were detected in the spinal cord of GFAP-Cre FasL$^{fl/fl}$ mice than in FasL$^{fl/fl}$ mice (Fig. 25A, B; $p <$ 0.01 for CD4$^+$ and CD8$^+$ T cells).

As GM-CSF-producing CD4$^+$ T cells are essential for the induction of EAE (Codarri et al., 2011), we determined the percentage and number of GM-CSF-producing CD4$^+$ T cells in the spinal cord of both mouse strains. Flow cytometry revealed that GM-CSF-producing CD4$^+$ T cells accounted for approximately 15% of CD4$^+$ T cells in both mouse strains; however, the absolute number of GM-CSF-producing CD4$^+$ T cells was significantly increased in GFAP-Cre FasL$^{fl/fl}$ mice as compared with those in control animals at day 22 p.i. (Fig. 25C). In addition, we compared the phenotypic composition of CD4$^+$ T cells between the two genotypes to determine whether astrocyte-specific deletion of FasL influenced the activation state of infiltrating CD4$^+$ T cells in EAE. At day 15 p.i., the percentage of Foxp3$^-$ CD25$^+$ activated CD4$^+$ T cells (Fig. 25D) and Foxp3$^+$ regulatory CD4$^+$ T cells (Fig. 25E) was similar in both strains of mice, whereas at day 22 p.i., as compared with FasL$^{fl/fl}$ mice, the percentage of Foxp3$^-$ CD25$^+$ activated CD4$^+$ T cells was increased while the percentage of Foxp3$^+$ regulatory CD4$^+$ T cells was reduced in GFAP-Cre FasL$^{fl/fl}$ mice respectively (Fig. 25D, E). Intraspinal CD4$^+$ T cells from both mouse strains expressed Fas, as detected by flow cytometry (Fig. 25F), and, thus, they might be regulated by FasL$^+$ cells. At d 22 p.i., the percentage of 7-aminoactinomycin (7-AAD)$^+$ CD4$^+$ T cells was significantly reduced in GFAP-Cre FasL$^{fl/fl}$ mice as compared with that in FasL$^{fl/fl}$ mice (Fig. 25G, * $p <$ 0.05) suggesting that elimination of infiltrating T cells by apoptosis was impaired in GFAP-Cre FasL$^{fl/fl}$ mice in late stages of EAE. Annexin V staining was not used to detect CD4$^+$ T-cell apoptosis *in vivo* because previous reports showed that annexin V did not

selectively detect apoptotic T cells, since it also stained activated CD4$^+$ T cells (Elliott et al., 2005).
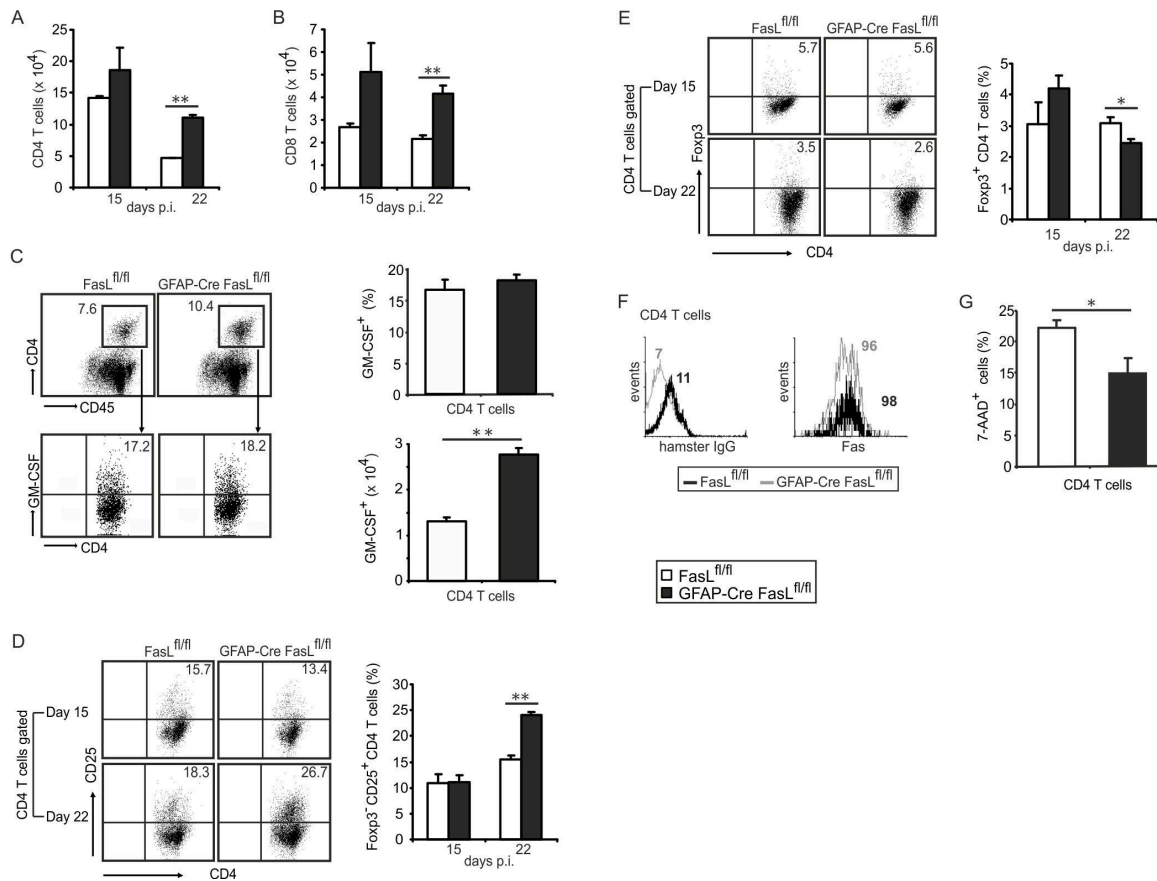

Figure 25. Increased numbers of activated and reduced numbers of regulatory T cells in the CNS of GFAP-Cre FasL$^{fl/fl}$ mice. (A, B) Leukocytes were isolated from the spinal cord of GFAP-Cre FasL$^{fl/fl}$ and FasL$^{fl/fl}$ mice and numbers of (A) CD4$^+$ and (B) CD8$^+$ T cells were determined by flow cytometry. (C) Leukocytes isolated from the spinal cord were stained for extracellular CD4 and CD45 and intracellular GM-CSF. Dot plots (left) show the percentage of CD4$^+$ CD45$^+$ cells (upper left) and GM-CSF$^+$ CD4$^+$ cells (lower left) at day 22 p.i., as well as the gating strategy for CD4$^+$ cells. The relative (upper right) and absolute number (lower right) of GM-CSF$^+$ CD4$^+$ cells is shown. (D, E) The percentage of (D) CD25$^+$ CD4$^+$ T cells and (E) Foxp3$^+$ regulatory CD4$^+$ T cells was analysed by flow cytometry. (F) Cell surface expression of Fas on CD4$^+$ T cells from both GFAP-Cre FasL$^{fl/fl}$ and FasL$^{fl/fl}$ mice was analysed by flow cytometry at day 15 p.i. and representative histograms are shown (right). Control staining was performed with hamster IgG (left). The mean fluorescence intensity is shown in each histogram. (G) The percentage of 7-AAD$^+$ CD4$^+$ T cells was determined by flow cytometry at day 22 p.i., and the mean + SD is shown. (A-G) Data are shown as representative dot plots as well as the mean + SD of 6-9 mice per experimental group from one of two independent experiments. * $p < 0.05$, ** $p < 0.01$, t-tests.

4.2.4 Increased proinflammatory gene transcription in the spinal cord of GFAP-Cre FasL$^{fl/fl}$ mice

To examine the impact of astrocyte-specific FasL deletion on the expression of proinflammatory genes during EAE, quantitative real time PCR for cytokines and chemokines was performed on

spinal cord tissue at day 15 p.i. and day 22 p.i. of EAE respectively. At day 15 p.i., IFN-γ and IL-27 mRNA was significantly elevated in GFAP-Cre FasL$^{fl/fl}$ mice as compared to FasL$^{fl/fl}$ mice while mRNA levels of IL-17, TNF, IL-23, and GM-CSF did not differ between the two mouse strains (Fig. 26). In contrast, at day 22 p.i., mRNA levels of all mediators, except for IL-23, were significantly upregulated in GFAP-Cre FasL$^{fl/fl}$ mice as compared with levels in FasL$^{fl/fl}$ mice, indicating an increased pro-inflammatory response in the spinal cord of GFAP-Cre FasL$^{fl/fl}$ mice at this late time point (Fig. 26). Interestingly, mRNA of IL-17, a main mediator of EAE, persisted at high levels in the spinal cord of GFAP-Cre FasL$^{fl/fl}$ mice up to day 22 p.i. Taken together, these results show that astrocytic deletion of FasL resulted in an increased transcription of important pro-inflammatory genes in the spinal cord which induce and contribute to severity of EAE.
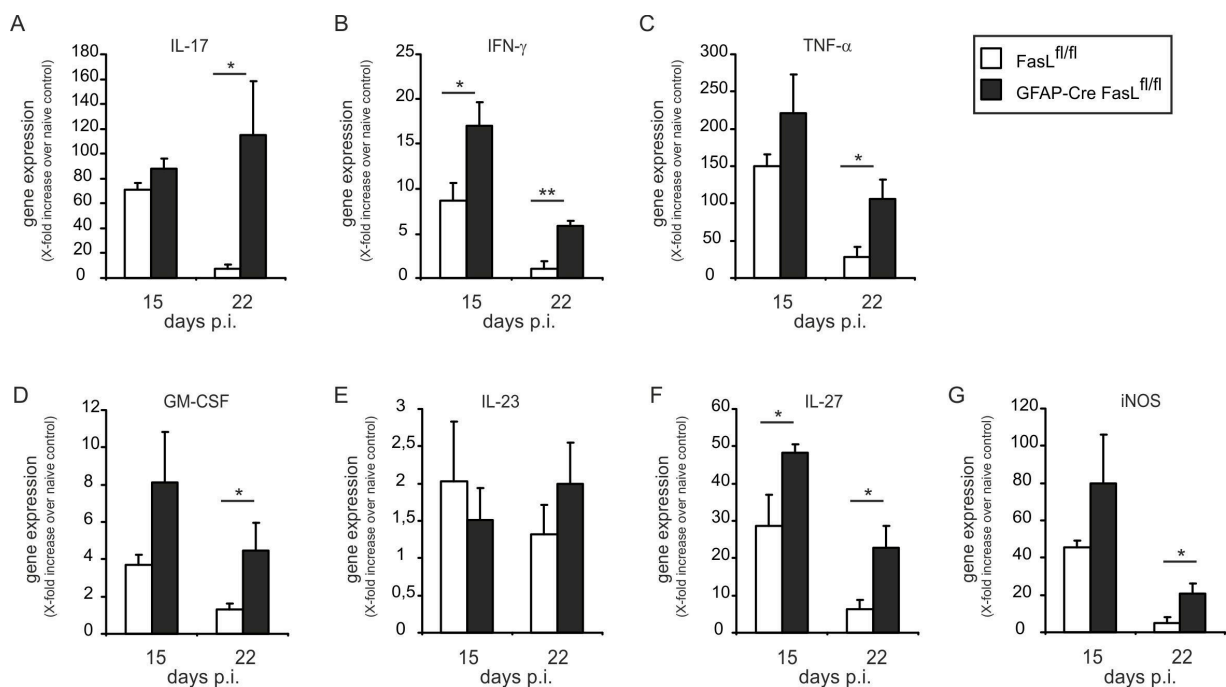

Figure 26. Increased pro-inflammatory gene expression in the spinal cords of GFAP-Cre FasL$^{fl/fl}$ mice. (A-G) Expression of (A) IL-17, (B) IFN-γ, (C) TNF-α, (D) GM-CSF, (E) IL-23, (F) IL-27, and (G) iNOS mRNA was determined by quantitative RT-PCR in GFAP-Cre FasL$^{fl/fl}$ and FasL$^{fl/fl}$ mice at days 15 and 22 p.i. Spinal cords of three mice per group were analysed. Data represent the mean + SEM as relative increase over non-immunized mice. * p < 0.05, ** p < 0.01, t-tests. One of two independent experiments with three mice each is shown.

4.2.5 Reduced apoptosis of CD4$^+$ T cells in co-culture with FasL-deficient astrocytes

Twenty-four hours after co-culture of FasL$^{fl/fl}$ CD4$^+$ T cells with primary astrocytes isolated from the CNS of FasL$^{fl/fl}$ or GFAP-Cre FasL$^{fl/fl}$ mice, T cell apoptosis induced by FasL-deficient

astrocytes was compared to that induced by control astrocytes. In accordance with a previous report of Bechmann et al. (Bechmann et al., 2002), significantly lower numbers of T cells cocultured with FasL-deficient astrocytes underwent apoptosis as demonstrated by both annexin V binding and caspase-3 staining (Fig. 27). Based on these findings, we conclude that, during EAE, astrocytic FasL-induced apoptotic elimination of T cells in the CNS of GFAP-Cre FasL^{fl/fl} mice is significantly compromised as compared with that of control animals, resulting in a significantly enhanced disease activity.

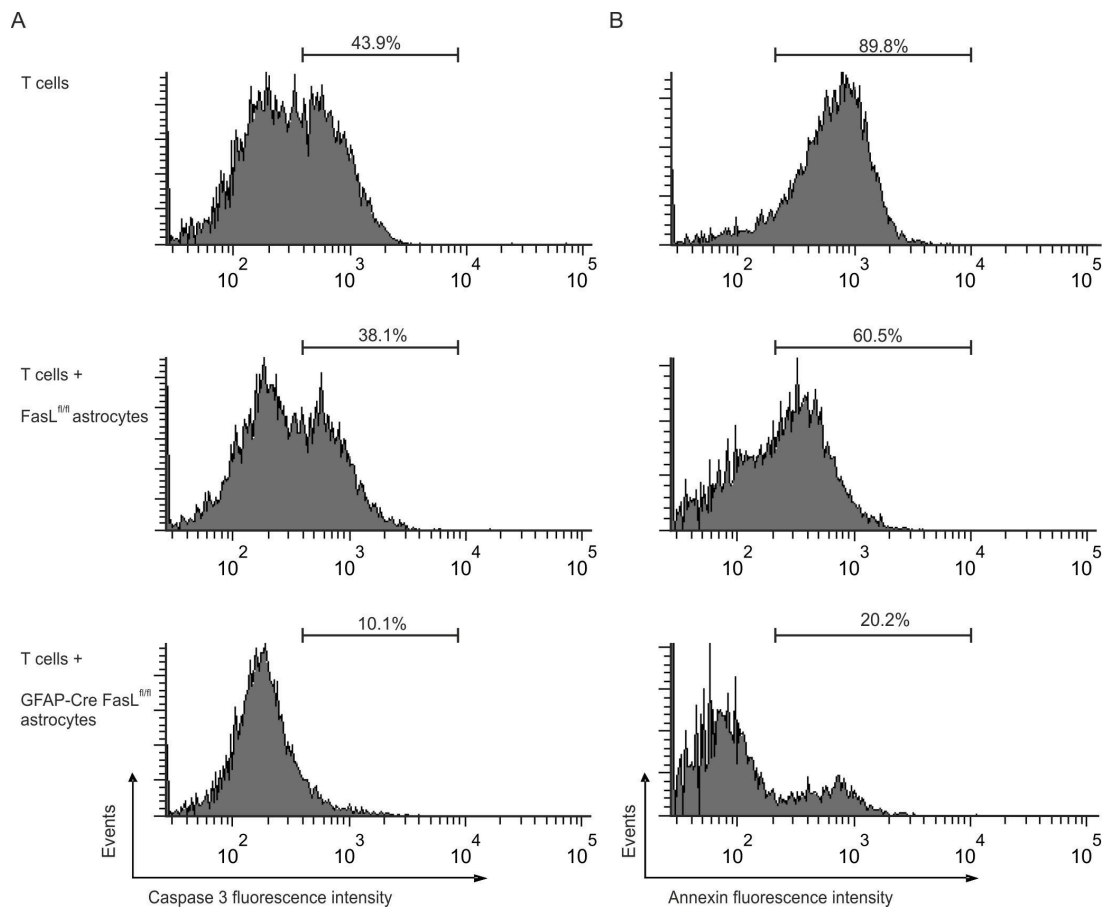**Figure 27. Astrocytes induce apoptosis of activated T cells via FasL *in vitro*.** (A, B) After monoculture or coculture with astrocytes from FasL^{fl/fl} or GFAP-Cre FasL^{fl/fl} mice for 24 hours, apoptosis of T cells was detected by (A) caspase 3 and (B) annexin V staining. No difference was observed in the corresponding control stainings with isotype-matched IgG (data not shown). One of two independent experiments is shown.

5. Discussion

In this study, we show that in the early stage of EAE astrocytes were deactivated by A20 to prevent T-cell recruitment. If A20 is not active, such as in MS patients with inactive A20 muations, astrocytes may contribute to the initiation of CNS pathology. In the late stage of EAE, astrocytes are protective by inducing the apoptosis of autoreactive CD4$^+$ T cells. Therefore, astrocytes can protect the CNS from the autoimmune CD4$^+$ T cell attack by A20 and FasL expression.

Role of astrocytic A20 in EAE

The first part of study demonstrates that targeted deletion of A20 in neuroectodermal cells increased severity of the autoimmune demyelinating disease EAE. Consistently, previous reports showed that blocking NF-κB in neuroectodermal cells by deleting NEMO, IKK2, and Act1, respectively, ameliorated EAE (Kang et al., 2010; van et al., 2006). Although these reports point to an important function of astrocytic NF-κB in EAE, direct *in vivo* evidence using astrocyte-specific gene-deficient mice was still missing. Here, we extend these findings and newly show that A20 deletion in astrocytes, but not in neurons, caused an aggravated EAE by augmenting NF-κB and STAT1 activity.

Chemokine production of astrocytes is important in the effector stage of EAE that is associated with clinical disease onset (Miljkovic et al., 2011; Zepp et al., 2011). After priming in lymph nodes, antigen-specific T cells traffic through the choroid plexus to the subarachnoid space (Wave 1) where they are reactivated by meningeal APCs (Engelhardt and Sorokin, 2009; Kebir et al., 2007; Reboldi et al., 2009). Consequently, T cells expand and produce inflammatory cytokines, which stimulate adjacent CNS resident cells, mainly astrocytes, to produce leukocyte-recruiting chemokines and cytokines, leading to the further recruitment of leukocytes into the CNS (Wave 2). We observed that IL-17, IFN-γ, TNF, and GM-CSF, which are signature cytokines of encephalitogenic T cells, induced significantly higher levels of CXCL1, CXCL10, CCL2, and IL-6 in A20-deficient astrocytes *in vitro*. In line with this, increased CXCL1, CXCL10, CCL2, and IL-6 mRNA was also detected in spinal cords of Nestin-Cre and GFAP-Cre A20$^{fl/fl}$ mice, respectively, as compared to control mice, suggesting that astrocytic A20 ameliorates EAE by inhibiting the progression of Wave 1 to Wave 2 of T cell recruitment. A20 plays divergent roles in regulating apoptosis in different cell types (Lee et al., 2000; Tavares et al., 2010; Vucic et al., 2011) and astrocyte survival is critical for EAE suppression (Haroon et al.,

2011; Voskuhl et al., 2009). Importantly, we did not obtain any evidence that A20 deficiency rendered astrocytes more sensitive to apoptosis. Thus, the more severe EAE of Nestin-Cre and GFAP-Cre A20$^{fl/fl}$ mice was not due to the enhanced apoptosis of astrocytes.

TNF, IL-17, and GM-CSF are produced by Th1 cells, Th17 cells, and GM-CSF-producing CD4^{+} T cells, respectively, and all of them can activate the NF-κB pathway (Bulek et al., 2011; Meads et al., 2010), which drives chemokine and cytokine production in astrocytes (Bruck et al., 2012; van et al., 2006). In the absence of A20, activation of NF-κB was enhanced in astrocytes upon stimulation with IL-17, TNF, and GM-CSF, respectively, explaining the increased expression of leukocyte attracting genes in A20-deficient astrocytes. Besides, A20 also inhibited activation of p38 and JNK pathway illustrating that the inhibitory function of A20 was not restricted to NF-κB.

We observed that IFN-γ induced a dramatic increase in chemokine production in A20-deficient astrocytes implying that A20 might interfere with IFN-γ-mediated signaling. IFN-γ mediated STAT1 activation was stronger in the absence of A20 as shown by increased STAT1 phosphorylation at serine 727, which is required for the full activation of STAT1 (Decker and Kovarik, 2000; Varinou et al., 2003). Interestingly, STAT1 protein was also increased in unstimulated and IFN-γ-stimulated A20-deficient astrocytes, which was caused by an enhanced NF-κB-dependent STAT1 mRNA production in the absence of A20, showing that STAT1 signaling pathway was also negatively regulated by A20. Therefore, it is possible that NF-κB-activating cytokines such as IL17, TNF, and GM-CSF induce increased chemokine production in A20-deficient astrocytes by cooperation with IFN-γ-dependent STAT1 activation. In fact, treatment with TNF + IFN-γ resulted in an augmented production of chemokines and cytokines in A20-deficient astrocytes.

STAT1 protein levels can be regulated by K48 ubiquitin-dependent proteasomal degradation that is induced by the E3 ligase Smurf1 (Yuan et al., 2012). As an ubiquitin E3 ligase, A20 is involved in the proteasomal degradation of several signaling molecules including RIP1 (Wertz et al., 2004). However, no direct interaction between A20 and STAT1 was detected by immunoprecipitation ruling out the possibility that A20 promoted the degradation of STAT1 by K48-ubiquitination or inhibited its function by K63-deubiquitination. Instead, we observed higher STAT1 mRNA expression in A20-deficient astrocytes than in control cells, indicating that the increased STAT1 protein level in A20-deficient astrocytes should be attributed to increased

production but not to reduced degradation. Although numerous reports mentioned phosphorylation of STAT1, barely any of them elucidated STAT1 production. We showed that A20 negatively regulated STAT1 production indirectly by inhibiting the NF-κB signaling cascade that is responsible for STAT1 mRNA synthesis. Our novel observation that A20 inhibited STAT1 at both expression and phosphorylation levels explains why IFN-γ stimulated A20-deficient astrocytes produced more chemokines as compared to A20-sufficient astrocytes. The enhanced migration of wildtype CD4^{+} T cells in response to IFN-γ conditioned medium of A20-deficient astrocytes also provided direct evidence that the enhanced production of chemoattractant molecules by A20-deficient astrocytes induced CD4^{+} T cell recruitment.

Single nucleotide polymorphisms (SNPs) in or close to the human tumor necrosis factor, alpha-induced protein 3 (TNFAIP3) gene are associated with several human autoimmune diseases including psoriasis, rheumatoid arthritis, type 1 diabetes, and systemic lupus erythematosus (SLE) (Fung et al., 2009; Musone et al., 2008; Musone et al., 2011; Nair et al., 2009). Recent genome wide association study (GWAS) identified OLIG3/TNFAIP3 as a susceptibility locus for MS (De Jager et al., 2009). In addition, TNFAIP3 expression was found to be tightly correlated with clinical features of MS (Gilli et al., 2011). Compared with healthy controls, a lower mRNA expression of TNFAIP3 was observed in untreated patients with MS and its baseline levels were lower in patients with a more malignant disease course than in patients with a more benign course. Accordingly, treatment of MS patients with glatiramer acetate reverted TNFAIP3 expression to levels displayed by healthy controls. A recent study showed that SNPs in the OLIG3/TNFAIP3 gene correlated significantly with increased cerebrospinal fluid (CSF) levels of the chemokine CXCL13, a prognostic marker for MS (Linden et al., 2013). Given that our study shows that astrocytic A20 suppresses EAE by inhibiting chemokine production in astrocytes, it therefore provides a biological rationale for the clinical observation that SNPs in or close to TNFAIP3 gene influences the development of MS. Thus, therapeutical augmentation of A20 in astrocytes might be beneficial for the treatment of MS.

Role of astrocytic FasL in EAE

The second part of study demonstrates that elimination of infiltrating encephalitogenic T lymphocytes is a key mechanism for EAE resolution and that FasL[+] astrocytes are crucial to induce T-cell apoptosis and elimination from the CNS in this autoimmune disease. In agreement

with Bechmann et al (Bechmann et al., 2002), who demonstrated that astrocytes induced apoptosis of activated T cells in a FasL-dependent way *in vitro*, we observed that FasL$^+$ astrocytes induced apoptosis of activated Fas$^+$ CD4$^+$ T cells *in vitro*. Since astrocytes are also FasL$^+$ in multiple sclerosis, our data suggest a similar role of astrocytes for the elimination of inflammatory leukocytes in this severe human autoimmune disease.

Astrocytic FasL was protective for mice during EAE, since MOG$_{35-55}$-immunized mice lacking astrocyte-specific FasL suffered from a clinically more severe EAE compared with their control littermates. The onset of clinical symptoms was similar in both GFAP-Cre FasL$^{fl/fl}$ and control FasL$^{fl/fl}$ mice at day 9 p.i. indicating that homing of myelin-specific leucocytes was not regulated by astrocytic FasL expression. In addition, the clinical score of GFAP-Cre FasL$^{fl/fl}$ and FasL$^{fl/fl}$ mice increased with the same kinetics until the peak of disease in FasL$^{fl/fl}$ mice at day 15 p.i. In accordance, numbers of CD4$^+$ T cells were not significantly increased in GFAP-Cre FasL$^{fl/fl}$ mice at day 15 p.i. However, during the clinical recovery phase of FasL$^{fl/fl}$ mice (day 22 p.i.), numbers of CD4$^+$ T cells were significantly increased in the spinal cord of GFAP-Cre FasL$^{fl/fl}$ mice as shown by both flow cytometry and histology at day 22 p.i. The reduced number of CD4$^+$ T cells positive for 7-AAD, which identifies late apoptotic and dead cells, illustrates the compromised ability of FasL-deficient astrocytes to induce apoptosis and elimination of infiltrating autoimmune T cells. The kinetics of disease and intraspinal CD4$^+$ T-cell numbers indicate that FasL-dependent elimination of CD4$^+$ T cells in EAE plays a particularly protective role in the recovery phase. Noteworthy, the more severe EAE of GFAP-Cre FasL$^{fl/fl}$ mice cannot be attributed to the GFAP-Cre transgene, since C57BL/6 GFAP-Cre mice without a loxP-flanked gene develop the same course of EAE as compared to wild-type mice (Haroon et al., 2011).

We also observed a significantly higher number of activated CD25$^+$ CD4$^+$ T cells and a significantly reduced number of Foxp3$^+$ regulatory CD4$^+$ T cells in the spinal cord of GFAP-Cre FasL$^{fl/fl}$ as compared with FasL$^{fl/fl}$ mice at day 22 p.i. Lack of astrocytic FasL expression altered the ratio of activated CD25$^+$ versus regulatory Foxp3$^+$ CD4$^+$ T cells in the spinal cord from 5:1 in FasL$^{fl/fl}$ mice to 10:1 in GFAP-Cre FasL$^{fl/fl}$ mice. These data suggest that astrocytic FasL expression predominantly contributes to elimination of activated disease-promoting CD25$^+$ CD4$^+$ T cells but not of protective regulatory Foxp3$^+$ CD4$^+$ T cells in order to recover from EAE and to achieve a restitutio ad integrum. These data are in line with previous reports illustrating that astrocytes induce a regulatory phenotype in autoimmune CD4$^+$ T cells (Trajkovic et al., 2004),

which play an important protective role in EAE (Gultner et al., 2010; Tsakiri et al., 2012). In agreement, the number of GM-CSF-producing CD4^{+} T cells, i.e. the essential EAE-inducing CD4^{+} T-cell subset (Codarri et al., 2011), was significantly increased in the spinal cord of GFAP-Cre FasL^{fl/fl} mice at day 22 p.i.

The increased number of infiltrating activated autoreactive CD4^{+} T cells in GFAP-Cre FasL^{fl/fl} mice was associated with an enhanced production of proinflammatory cytokines. At day 15 p.i., IFN-γ, TNF, GM-CSF, IL-27 and iNOS but not IL17 mRNA was increased in GFAP-Cre FasL^{fl/fl} mice as compared with that in FasL^{fl/fl} mice. IFN-γ, TNF, and GM-CSF have been reported to contribute to disease progression and demyelination in EAE (Codarri et al., 2011; Petermann and Korn, 2011). GM-CSF and IFN-γ are mainly produced by encephalitogenic T cells. GM-CSF sustains neuroinflammation via myeloid cells that infiltrate the spinal cord. In addition to its pro-inflammatory function, IFN-γ is also a potent stimulator of IL-27 production by astrocytes (Fitzgerald et al., 2007), which might explain the increased production of this immunosuppressive and protective cytokine in the spinal cord of GFAP-Cre FasL^{fl/fl} mice at day 15 p.i. IL-27 can suppress IL-17 production of primed Th17 cells (Fitzgerald et al., 2007), which might explain that GFAP-Cre FasL^{fl/fl} mice did not show elevated IL-17 mRNA expression in the spinal cord as compared to FasL^{fl/fl} mice. IL-17 is an important cytokine contributing to demyelination and progression of EAE (Komiyama et al., 2006). Comparable levels of IL-17 mRNA transcription in GFAP-Cre FasL^{fl/fl} and FasL^{fl/fl} mice at day 15 p.i. might, therefore, explain similar clinical scores in the two mouse strains at this stage of disease. However at day 22 p.i., when numbers of activated CD25^{+} and GM-CSF-producing CD4^{+} T cells were significantly increased and numbers of Foxp3^{+} regulatory CD4^{+} T cells decreased in GFAP-Cre FasL^{fl/fl} mice, IL-17 mRNA was very prominently increased in addition to IFN-γ, TNF, GM-CSF, and iNOS mRNA. Thus, aggravation of clinical symptoms in GFAP-Cre FasL^{fl/fl} mice correlated with an increased IL-17 mRNA transcription, indicating that this cytokine was decisive for the more severe and persisting EAE in these mice. IL-23, which drives IL-17 polarisation of CD4^{+} T cells was not increased in the CNS of GFAP-Cre FasL^{fl/fl} mice, which fits to the important role of IL-23 for Th17 polarisation in lymphatic organs (Kobayashi et al., 2008). The second part of study illustrates that astrocytes confer protection against EAE by the FasL-dependent apoptotic elimination of activated CD25^{+} Foxp3^{-} and GM-CSF-producing CD4^{+} T cells and the concomitant inhibition of proinflammatory cytokine production. Thus,

augmentation of astrocytic FasL may provide a favourable strategy for treatment of clinically active MS.
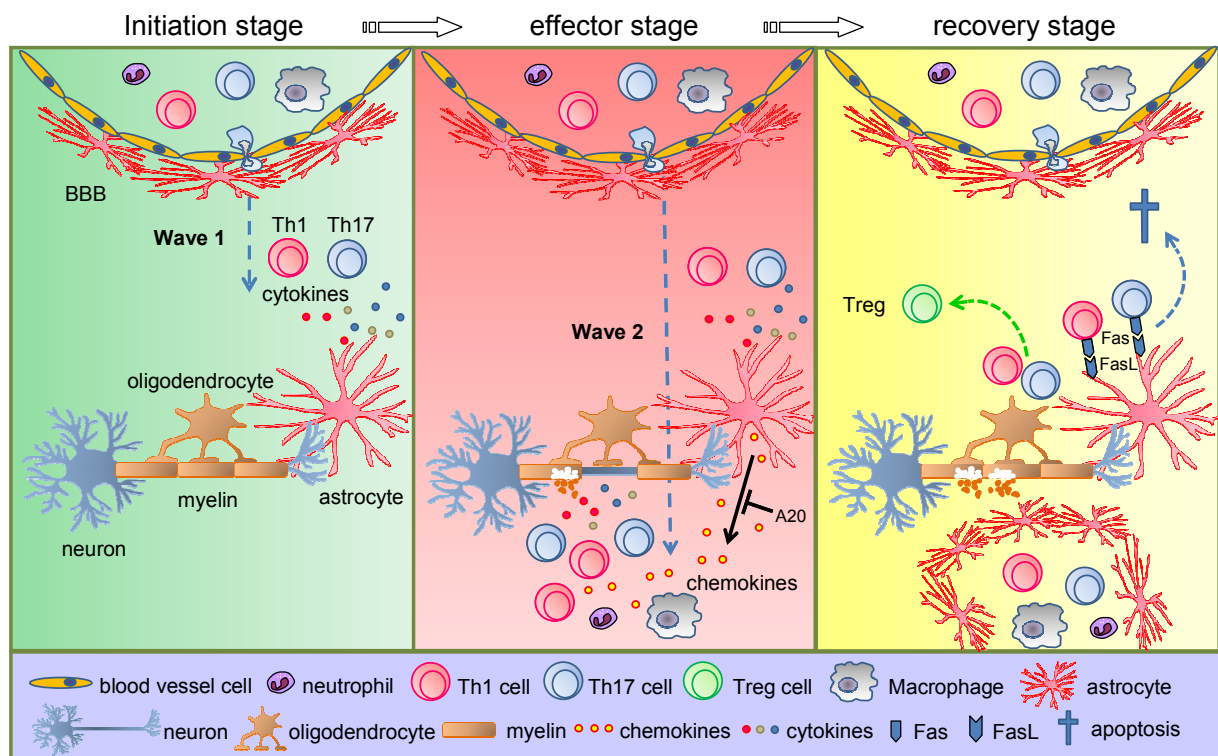
Summary of the study

Figure 28. Graphic summary of the present study.

Collectively, in the present study, we extend the *in vivo* function of astrocytes in EAE. In the effector stage, astrocytes contribute to the development of EAE by producing leukocyte-attracting chemokines, which is negatively regulated by A20. In contrast, in the recovery stage, astrocytes are also helpful for EAE recovery by inducing apoptotic elimination of infiltrating T cells via FasL (Fig. 28).

Reference List

Adhikari,A., Xu,M., and Chen,Z.J. (2007). Ubiquitin-mediated activation of TAK1 and IKK. Oncogene *26*, 3214-3226.

Anderton,S.M. and Liblau,R.S. (2008). Regulatory T cells in the control of inflammatory demyelinating diseases of the central nervous system. Curr. Opin. Neurol. *21*, 248-254.

Antony,J.M., van,M.G., Opii,W., Butterfield,D.A., Mallet,F., Yong,V.W., Wallace,J.L., Deacon,R.M., Warren,K., and Power,C. (2004). Human endogenous retrovirus glycoprotein-mediated induction of redox reactants causes oligodendrocyte death and demyelination. Nat. Neurosci. *7*, 1088-1095.

Ascherio,A. and Munger,K.L. (2007a). Environmental risk factors for multiple sclerosis. Part I: the role of infection. Ann. Neurol. *61*, 288-299.

Ascherio,A. and Munger,K.L. (2007b). Environmental risk factors for multiple sclerosis. Part II: Noninfectious factors. Ann. Neurol. *61*, 504-513.

Banker,G.A. (1980). Trophic interactions between astroglial cells and hippocampal neurons in culture. Science *209*, 809-810.

Bannerman,P., Hahn,A., Soulika,A., Gallo,V., and Pleasure,D. (2007). Astrogliosis in EAE spinal cord: derivation from radial glia, and relationships to oligodendroglia. Glia *55*, 57-64.

Barnhart,B.C., Alappat,E.C., and Peter,M.E. (2003). The CD95 type I/type II model. Semin. Immunol. *15*, 185-193.

Barres,B.A. (2008). The mystery and magic of glia: a perspective on their roles in health and disease. Neuron *60*, 430-440.

Baxter,A.G. (2007). The origin and application of experimental autoimmune encephalomyelitis. Nat. Rev. Immunol. *7*, 904-912.

Bechmann,I., Galea,I., and Perry,V.H. (2007). What is the blood-brain barrier (not)? Trends Immunol. *28*, 5-11.

Bechmann,I., Mor,G., Nilsen,J., Eliza,M., Nitsch,R., and Naftolin,F. (1999). FasL (CD95L, Apo1L) is expressed in the normal rat and human brain: evidence for the existence of an immunological brain barrier. Glia *27*, 62-74.

Bechmann,I., Steiner,B., Gimsa,U., Mor,G., Wolf,S., Beyer,M., Nitsch,R., and Zipp,F. (2002). Astrocyte-induced T cell elimination is CD95 ligand dependent. J. Neuroimmunol. *132*, 60-65.

Bellail,A.C., Olson,J.J., Yang,X., Chen,Z.J., and Hao,C. (2012). A20 ubiquitin ligase-mediated polyubiquitination of RIP1 inhibits caspase-8 cleavage and TRAIL-induced apoptosis in glioblastoma. Cancer Discov. *2*, 140-155.

Bellgrau,D., Gold,D., Selawry,H., Moore,J., Franzusoff,A., and Duke,R.C. (1995). A role for CD95 ligand in preventing graft rejection. Nature *377*, 630-632.

Bertrand,M.J., Milutinovic,S., Dickson,K.M., Ho,W.C., Boudreault,A., Durkin,J., Gillard,J.W., Jaquith,J.B., Morris,S.J., and Barker,P.A. (2008). cIAP1 and cIAP2 facilitate cancer cell survival by functioning as E3 ligases that promote RIP1 ubiquitination. Mol. Cell *30*, 689-700.

Beyaert,R., Heyninck,K., and Van,H.S. (2000). A20 and A20-binding proteins as cellular inhibitors of nuclear factor-kappa B-dependent gene expression and apoptosis. Biochem. Pharmacol. *60*, 1143-1151.

Boatright,K.M., Renatus,M., Scott,F.L., Sperandio,S., Shin,H., Pedersen,I.M., Ricci,J.E., Edris,W.A., Sutherlin,D.P., Green,D.R., and Salvesen,G.S. (2003). A unified model for apical caspase activation. Mol. Cell *11*, 529-541.

Bodmer,J.L., Schneider,P., and Tschopp,J. (2002). The molecular architecture of the TNF superfamily. Trends Biochem. Sci. *27*, 19-26.

Bohgaki,M., Tsukiyama,T., Nakajima,A., Maruyama,S., Watanabe,M., Koike,T., and Hatakeyama,S. (2008). Involvement of Ymer in suppression of NF-kappaB activation by regulated interaction with lysine-63-linked polyubiquitin chain. Biochim. Biophys. Acta *1783*, 826-837.

Boldin,M.P., Goncharov,T.M., Goltsev,Y.V., and Wallach,D. (1996). Involvement of MACH, a novel MORT1/FADD-interacting protease, in Fas/APO-1- and TNF receptor-induced cell death. Cell *85*, 803-815.

Boldin,M.P., Varfolomeev,E.E., Pancer,Z., Mett,I.L., Camonis,J.H., and Wallach,D. (1995). A novel protein that interacts with the death domain of Fas/APO1 contains a sequence motif related to the death domain. J. Biol. Chem. *270*, 7795-7798.

Bonetti,B., Pohl,J., Gao,Y.L., and Raine,C.S. (1997). Cell death during autoimmune demyelination: effector but not target cells are eliminated by apoptosis. J. Immunol. *159*, 5733-5741.

Boone,D.L., Turer,E.E., Lee,E.G., Ahmad,R.C., Wheeler,M.T., Tsui,C., Hurley,P., Chien,M., Chai,S., Hitotsumatsu,O., McNally,E., Pickart,C., and Ma,A. (2004). The ubiquitin-modifying enzyme A20 is required for termination of Toll-like receptor responses. Nat. Immunol. *5*, 1052-1060.

Brambilla,R., Bracchi-Ricard,V., Hu,W.H., Frydel,B., Bramwell,A., Karmally,S., Green,E.J., and Bethea,J.R. (2005). Inhibition of astroglial nuclear factor kappaB reduces inflammation and improves functional recovery after spinal cord injury. J. Exp. Med. *202*, 145-156.

Brambilla,R., Persaud,T., Hu,X., Karmally,S., Shestopalov,V.I., Dvoriantchikova,G., Ivanov,D., Nathanson,L., Barnum,S.R., and Bethea,J.R. (2009). Transgenic inhibition of astroglial NF-kappa B improves functional outcome in experimental autoimmune encephalomyelitis by suppressing chronic central nervous system inflammation. J. Immunol. *182*, 2628-2640.

Bruck,W., Pfortner,R., Pham,T., Zhang,J., Hayardeny,L., Piryatinsky,V., Hanisch,U.K., Regen,T., Van,R.D., Brakelmann,L., Hagemeier,K., Kuhlmann,T., Stadelmann,C., John,G.R., Kramann,N., and Wegner,C. (2012). Reduced astrocytic NF-kappaB activation by laquinimod protects from cuprizone-induced demyelination. Acta Neuropathol. *124*, 411-424.

Brustle,A., Brenner,D., Knobbe,C.B., Lang,P.A., Virtanen,C., Hershenfield,B.M., Reardon,C., Lacher,S.M., Ruland,J., Ohashi,P.S., and Mak,T.W. (2012). The NF-kappaB regulator MALT1 determines the encephalitogenic potential of Th17 cells. J. Clin. Invest *122*, 4698-4709.

Bulek,K., Liu,C., Swaidani,S., Wang,L., Page,R.C., Gulen,M.F., Herjan,T., Abbadi,A., Qian,W., Sun,D., Lauer,M., Hascall,V., Misra,S., Chance,M.R., Aronica,M., Hamilton,T., and Li,X. (2011). The inducible kinase IKKi is required for IL-17-dependent signaling associated with neutrophilia and pulmonary inflammation. Nat. Immunol. *12*, 844-852.

Chinnaiyan,A.M., O'Rourke,K., Tewari,M., and Dixit,V.M. (1995). FADD, a novel death domain-containing protein, interacts with the death domain of Fas and initiates apoptosis. Cell *81*, 505-512.

Christopherson,K.S., Ullian,E.M., Stokes,C.C., Mullowney,C.E., Hell,J.W., Agah,A., Lawler,J., Mosher,D.F., Bornstein,P., and Barres,B.A. (2005). Thrombospondins are astrocyte-secreted proteins that promote CNS synaptogenesis. Cell *120*, 421-433.

Chu,Y., Vahl,J.C., Kumar,D., Heger,K., Bertossi,A., Wojtowicz,E., Soberon,V., Schenten,D., Mack,B., Reutelshofer,M., Beyaert,R., Amann,K., van,L.G., and Schmidt-Supprian,M. (2011). B cells lacking the tumor suppressor TNFAIP3/A20 display impaired differentiation and hyperactivation and cause inflammation and autoimmunity in aged mice. Blood *117*, 2227-2236.

Claudio,E., Brown,K., Park,S., Wang,H., and Siebenlist,U. (2002). BAFF-induced NEMO-independent processing of NF-kappa B2 in maturing B cells. Nat. Immunol. *3*, 958-965.

Codarri,L., Gyulveszi,G., Tosevski,V., Hesske,L., Fontana,A., Magnenat,L., Suter,T., and Becher,B. (2011). RORgammat drives production of the cytokine GM-CSF in helper T cells, which is essential for the effector phase of autoimmune neuroinflammation. Nat. Immunol. *12*, 560-567.

Colland,F., Jacq,X., Trouplin,V., Mougin,C., Groizeleau,C., Hamburger,A., Meil,A., Wojcik,J., Legrain,P., and Gauthier,J.M. (2004). Functional proteomics mapping of a human signaling pathway. Genome Res. *14*, 1324-1332.

Coope,H.J., Atkinson,P.G., Huhse,B., Belich,M., Janzen,J., Holman,M.J., Klaus,G.G., Johnston,L.H., and Ley,S.C. (2002). CD40 regulates the processing of NF-kappaB2 p100 to p52. EMBO J. *21*, 5375-5385.

Crocker,S.J., Whitmire,J.K., Frausto,R.F., Chertboonmuang,P., Soloway,P.D., Whitton,J.L., and Campbell,I.L. (2006). Persistent macrophage/microglial activation and myelin disruption after experimental autoimmune encephalomyelitis in tissue inhibitor of metalloproteinase-1-deficient mice. Am. J. Pathol. *169*, 2104-2116.

Dammer,E.B., Na,C.H., Xu,P., Seyfried,N.T., Duong,D.M., Cheng,D., Gearing,M., Rees,H., Lah,J.J., Levey,A.I., Rush,J., and Peng,J. (2011). Polyubiquitin linkage profiles in three models of proteolytic stress suggest the etiology of Alzheimer disease. J. Biol. Chem. *286*, 10457-10465.

Daniel,S., Arvelo,M.B., Patel,V.I., Longo,C.R., Shrikhande,G., Shukri,T., Mahiou,J., Sun,D.W., Mottley,C., Grey,S.T., and Ferran,C. (2004). A20 protects endothelial cells from TNF-, Fas-, and NK-mediated cell death by inhibiting caspase 8 activation. Blood *104*, 2376-2384.

De Jager,P.L., Jia,X., Wang,J., de Bakker,P.I., Ottoboni,L., Aggarwal,N.T., Piccio,L., Raychaudhuri,S., Tran,D., Aubin,C., Briskin,R., Romano,S., Baranzini,S.E., McCauley,J.L., Pericak-Vance,M.A., Haines,J.L., Gibson,R.A., Naeglin,Y., Uitdehaag,B., Matthews,P.M., Kappos,L., Polman,C., McArdle,W.L., Strachan,D.P., Evans,D., Cross,A.H., Daly,M.J., Compston,A., Sawcer,S.J., Weiner,H.L., Hauser,S.L., Hafler,D.A., and Oksenberg,J.R. (2009). Meta-analysis of genome scans and replication identify CD6, IRF8 and TNFRSF1A as new multiple sclerosis susceptibility loci. Nat. Genet. *41*, 776-782.

De,V.D., Jin,D.Y., Heyninck,K., Van de,C.M., Contreras,R., Fiers,W., Jeang,K.T., and Beyaert,R. (1999). The zinc finger protein A20 interacts with a novel anti-apoptotic protein which is cleaved by specific caspases. Oncogene *18*, 4182-4190.

Decker,T. and Kovarik,P. (2000). Serine phosphorylation of STATs. Oncogene *19*, 2628-2637.

Dejardin,E. (2006). The alternative NF-kappaB pathway from biochemistry to biology: pitfalls and promises for future drug development. Biochem. Pharmacol. *72*, 1161-1179.

Dejardin,E., Droin,N.M., Delhase,M., Haas,E., Cao,Y., Makris,C., Li,Z.W., Karin,M., Ware,C.F., and Green,D.R. (2002). The lymphotoxin-beta receptor induces different patterns of gene expression via two NF-kappaB pathways. Immunity. *17*, 525-535.

Deshaies,R.J. and Joazeiro,C.A. (2009). RING domain E3 ubiquitin ligases. Annu. Rev. Biochem. *78*, 399-434.

Diniz,L.P., Almeida,J.C., Tortelli,V., Vargas,L.C., Setti-Perdigao,P., Stipursky,J., Kahn,S.A., Romao,L.F., de,M.J., ves-Leon,S.V., de Souza,J.M., Castro,N.G., Panizzutti,R., and Gomes,F.C. (2012). Astrocyte-induced synaptogenesis is mediated by transforming growth factor beta signaling through modulation of D-serine levels in cerebral cortex neurons. J. Biol. Chem. *287*, 41432-41445.

Domingues,H.S., Mues,M., Lassmann,H., Wekerle,H., and Krishnamoorthy,G. (2010). Functional and pathogenic differences of Th1 and Th17 cells in experimental autoimmune encephalomyelitis. PLoS. One. *5*, e15531.

Donepudi,M., Mac,S.A., Briand,C., and Grutter,M.G. (2003). Insights into the regulatory mechanism for caspase-8 activation. Mol. Cell *11*, 543-549.

Dong,Y. and Benveniste,E.N. (2001). Immune function of astrocytes. Glia *36*, 180-190.

Drogemuller,K., Helmuth,U., Brunn,A., Sakowicz-Burkiewicz,M., Gutmann,D.H., Mueller,W., Deckert,M., and Schluter,D. (2008). Astrocyte gp130 expression is critical for the control of Toxoplasma encephalitis. J. Immunol. *181*, 2683-2693.

Dvoriantchikova,G., Barakat,D., Brambilla,R., Agudelo,C., Hernandez,E., Bethea,J.R., Shestopalov,V.I., and Ivanov,D. (2009). Inactivation of astroglial NF-kappa B promotes survival of retinal neurons following ischemic injury. Eur. J. Neurosci. *30*, 175-185.

Egen,J.G., Kuhns,M.S., and Allison,J.P. (2002). CTLA-4: new insights into its biological function and use in tumor immunotherapy. Nat. Immunol. *3*, 611-618.

Ehrenschwender,M. and Wajant,H. (2009). The role of FasL and Fas in health and disease. Adv. Exp. Med. Biol. *647*, 64-93.

Elliott,J.I., Surprenant,A., Marelli-Berg,F.M., Cooper,J.C., Cassady-Cain,R.L., Wooding,C., Linton,K., Alexander,D.R., and Higgins,C.F. (2005). Membrane phosphatidylserine distribution as a non-apoptotic signalling mechanism in lymphocytes. Nat. Cell Biol. *7*, 808-816.

Enesa,K., Zakkar,M., Chaudhury,H., Luong,l.A., Rawlinson,L., Mason,J.C., Haskard,D.O., Dean,J.L., and Evans,P.C. (2008). NF-kappaB suppression by the deubiquitinating enzyme Cezanne: a novel negative feedback loop in pro-inflammatory signaling. J. Biol. Chem. *283*, 7036-7045.

Eng,L.F. (1985). Glial fibrillary acidic protein (GFAP): the major protein of glial intermediate filaments in differentiated astrocytes. J. Neuroimmunol. *8*, 203-214.

Engelhardt,B. and Sorokin,L. (2009). The blood-brain and the blood-cerebrospinal fluid barriers: function and dysfunction. Semin. Immunopathol. *31*, 497-511.

Evans,P.C., Ovaa,H., Hamon,M., Kilshaw,P.J., Hamm,S., Bauer,S., Ploegh,H.L., and Smith,T.S. (2004). Zinc-finger protein A20, a regulator of inflammation and cell survival, has de-ubiquitinating activity. Biochem. J. *378*, 727-734.

Fitzgerald,D.C., Ciric,B., Touil,T., Harle,H., Grammatikopolou,J., Das,S.J., Gran,B., Zhang,G.X., and Rostami,A. (2007). Suppressive effect of IL-27 on encephalitogenic Th17 cells and the effector phase of experimental autoimmune encephalomyelitis. J. Immunol. *179*, 3268-3275.

Fung,E.Y., Smyth,D.J., Howson,J.M., Cooper,J.D., Walker,N.M., Stevens,H., Wicker,L.S., and Todd,J.A. (2009). Analysis of 17 autoimmune disease-associated variants in type 1 diabetes identifies 6q23/TNFAIP3 as a susceptibility locus. Genes Immun. *10*, 188-191.

Garg,A.V., Ahmed,M., Vallejo,A.N., Ma,A., and Gaffen,S.L. (2013). The deubiquitinase A20 mediates feedback inhibition of interleukin-17 receptor signaling. Sci. Signal. *6*, ra44.

Ghosh,S., May,M.J., and Kopp,E.B. (1998). NF-kappa B and Rel proteins: evolutionarily conserved mediators of immune responses. Annu. Rev. Immunol. *16*, 225-260.

Gilli,F., Navone,N.D., Perga,S., Marnetto,F., Caldano,M., Capobianco,M., Pulizzi,A., Malucchi,S., and Bertolotto,A. (2011). Loss of braking signals during inflammation: a factor affecting the development and disease course of multiple sclerosis. Arch. Neurol. *68*, 879-888.

Gimsa,U., Oren,A., Pandiyan,P., Teichmann,D., Bechmann,I., Nitsch,R., and Brunner-Weinzierl,M.C. (2004). Astrocytes protect the CNS: antigen-specific T helper cell responses are inhibited by astrocyte-induced upregulation of CTLA-4 (CD152). J. Mol. Med. (Berl) *82*, 364-372.

Giraud,S.N., Caron,C.M., Pham-Dinh,D., Kitabgi,P., and Nicot,A.B. (2010). Estradiol inhibits ongoing autoimmune neuroinflammation and NFkappaB-dependent CCL2 expression in reactive astrocytes. Proc. Natl. Acad. Sci. U. S. A *107*, 8416-8421.

Graus-Porta,D., Blaess,S., Senften,M., Littlewood-Evans,A., Damsky,C., Huang,Z., Orban,P., Klein,R., Schittny,J.C., and Muller,U. (2001). Beta1-class integrins regulate the development of laminae and folia in the cerebral and cerebellar cortex. Neuron *31*, 367-379.

Grey,S.T., Arvelo,M.B., Hasenkamp,W., Bach,F.H., and Ferran,C. (1999). A20 inhibits cytokine-induced apoptosis and nuclear factor kappaB-dependent gene activation in islets. J. Exp. Med. *190*, 1135-1146.

Griffith,T.S., Brunner,T., Fletcher,S.M., Green,D.R., and Ferguson,T.A. (1995). Fas ligand-induced apoptosis as a mechanism of immune privilege. Science *270*, 1189-1192.

Gultner,S., Kuhlmann,T., Hesse,A., Weber,J.P., Riemer,C., Baier,M., and Hutloff,A. (2010). Reduced Treg frequency in LFA-1-deficient mice allows enhanced T effector differentiation and pathology in EAE. Eur. J. Immunol. *40*, 3403-3412.

Hammer,G.E. and Ma,A. (2013). Molecular control of steady-state dendritic cell maturation and immune homeostasis. Annu. Rev. Immunol. *31*, 743-791.

Hammer,G.E., Turer,E.E., Taylor,K.E., Fang,C.J., Advincula,R., Oshima,S., Barrera,J., Huang,E.J., Hou,B., Malynn,B.A., Reizis,B., DeFranco,A., Criswell,L.A., Nakamura,M.C., and Ma,A. (2011). Expression of A20 by dendritic cells preserves immune homeostasis and prevents colitis and spondyloarthritis. Nat. Immunol. *12*, 1184-1193.

Haroon,F., Drogemuller,K., Handel,U., Brunn,A., Reinhold,D., Nishanth,G., Mueller,W., Trautwein,C., Ernst,M., Deckert,M., and Schluter,D. (2011). Gp130-dependent astrocytic survival is critical for the control of autoimmune central nervous system inflammation. J. Immunol. *186*, 6521-6531.

Hayashi,Y., Nomura,M., Yamagishi,S., Harada,S., Yamashita,J., and Yamamoto,H. (1997). Induction of various blood-brain barrier properties in non-neural endothelial cells by close apposition to co-cultured astrocytes. Glia *19*, 13-26.

Hayden,M.S. and Ghosh,S. (2008). Shared principles in NF-kappaB signaling. Cell *132*, 344-362.

Hayden,M.S. and Ghosh,S. (2011). NF-kappaB in immunobiology. Cell Res. *21*, 223-244.

Heger,K., Fierens,K., Vahl,J.C., Aszodi,A., Peschke,K., Schenten,D., Hammad,H., Beyaert,R., Saur,D., van,L.G., Roers,A., Lambrecht,B.N., Kool,M., and Schmidt-Supprian,M. (2014). A20-deficient mast cells exacerbate inflammatory responses in vivo. PLoS. Biol. *12*, e1001762.

Hershko,A. and Ciechanover,A. (1998). The ubiquitin system. Annu. Rev. Biochem. *67*, 425-479.

Heyninck,K., De,V.D., Vanden,B.W., Van,C.W., Contreras,R., Fiers,W., Haegeman,G., and Beyaert,R. (1999). The zinc finger protein A20 inhibits TNF-induced NF-kappaB-dependent gene expression by interfering with an RIP- or TRAF2-mediated transactivation signal and directly binds to a novel NF-kappaB-inhibiting protein ABIN. J. Cell Biol. *145*, 1471-1482.

Hindinger,C., Bergmann,C.C., Hinton,D.R., Phares,T.W., Parra,G.I., Hussain,S., Savarin,C., Atkinson,R.D., and Stohlman,S.A. (2012). IFN-gamma signaling to astrocytes protects from autoimmune mediated neurological disability. PLoS. One. *7*, e42088.

Hitotsumatsu,O., Ahmad,R.C., Tavares,R., Wang,M., Philpott,D., Turer,E.E., Lee,B.L., Shiffin,N., Advincula,R., Malynn,B.A., Werts,C., and Ma,A. (2008). The ubiquitin-editing enzyme A20 restricts nucleotide-binding oligomerization domain containing 2-triggered signals. Immunity. *28*, 381-390.

Honda,K. and Littman,D.R. (2012). The microbiome in infectious disease and inflammation. Annu. Rev. Immunol. *30*, 759-795.

Hovelmeyer,N., Hao,Z., Kranidioti,K., Kassiotis,G., Buch,T., Frommer,F., von,H.L., Kramer,D., Minichiello,L., Kollias,G., Lassmann,H., and Waisman,A. (2005). Apoptosis of oligodendrocytes via Fas and TNF-R1 is a key event in the induction of experimental autoimmune encephalomyelitis. J. Immunol. *175*, 5875-5884.

Hovelmeyer,N., Reissig,S., Xuan,N.T., ms-Quack,P., Lukas,D., Nikolaev,A., Schluter,D., and Waisman,A. (2011). A20 deficiency in B cells enhances B-cell proliferation and results in the development of autoantibodies. Eur. J. Immunol. *41*, 595-601.

Hu,H., Brittain,G.C., Chang,J.H., Puebla-Osorio,N., Jin,J., Zal,A., Xiao,Y., Cheng,X., Chang,M., Fu,Y.X., Zal,T., Zhu,C., and Sun,S.C. (2013). OTUD7B controls non-canonical NF-kappaB activation through deubiquitination of TRAF3. Nature *494*, 371-374.

Hunt,J.S., Vassmer,D., Ferguson,T.A., and Miller,L. (1997). Fas ligand is positioned in mouse uterus and placenta to prevent trafficking of activated leukocytes between the mother and the conceptus. J. Immunol. *158*, 4122-4128.

Iha,H., Peloponese,J.M., Verstrepen,L., Zapart,G., Ikeda,F., Smith,C.D., Starost,M.F., Yedavalli,V., Heyninck,K., Dikic,I., Beyaert,R., and Jeang,K.T. (2008). Inflammatory cardiac valvulitis in TAX1BP1-deficient mice through selective NF-kappaB activation. EMBO J. *27*, 629-641.

Ikeda,F., Deribe,Y.L., Skanland,S.S., Stieglitz,B., Grabbe,C., Franz-Wachtel,M., van Wijk,S.J., Goswami,P., Nagy,V., Terzic,J., Tokunaga,F., Androulidaki,A., Nakagawa,T., Pasparakis,M., Iwai,K., Sundberg,J.P., Schaefer,L., Rittinger,K., Macek,B., and Dikic,I. (2011). SHARPIN forms a linear ubiquitin ligase complex regulating NF-kappaB activity and apoptosis. Nature *471*, 637-641.

Ikeda,F. and Dikic,I. (2008). Atypical ubiquitin chains: new molecular signals. 'Protein Modifications: Beyond the Usual Suspects' review series. EMBO Rep. *9*, 536-542.

Itoh,N. and Nagata,S. (1993). A novel protein domain required for apoptosis. Mutational analysis of human Fas antigen. J. Biol. Chem. *268*, 10932-10937.

Itoh,N., Yonehara,S., Ishii,A., Yonehara,M., Mizushima,S., Sameshima,M., Hase,A., Seto,Y., and Nagata,S. (1991). The polypeptide encoded by the cDNA for human cell surface antigen Fas can mediate apoptosis. Cell *66*, 233-243.

Jaattela,M., Mouritzen,H., Elling,F., and Bastholm,L. (1996). A20 zinc finger protein inhibits TNF and IL-1 signaling. J. Immunol. *156*, 1166-1173.

Janzer,R.C. and Raff,M.C. (1987). Astrocytes induce blood-brain barrier properties in endothelial cells. Nature *325*, 253-257.

Jin,L., Williamson,A., Banerjee,S., Philipp,I., and Rape,M. (2008). Mechanism of ubiquitin-chain formation by the human anaphase-promoting complex. Cell *133*, 653-665.

Jin,Z., Li,Y., Pitti,R., Lawrence,D., Pham,V.C., Lill,J.R., and Ashkenazi,A. (2009). Cullin3-based polyubiquitination and p62-dependent aggregation of caspase-8 mediate extrinsic apoptosis signaling. Cell *137*, 721-735.

Jung,S.M., Lee,J.H., Park,J., Oh,Y.S., Lee,S.K., Park,J.S., Lee,Y.S., Kim,J.H., Lee,J.Y., Bae,Y.S., Koo,S.H., Kim,S.J., and Park,S.H. (2013). Smad6 inhibits non-canonical TGF-beta1 signalling by recruiting the deubiquitinase A20 to TRAF6. Nat. Commun. *4*, 2562.

Kang,Z., Altuntas,C.Z., Gulen,M.F., Liu,C., Giltiay,N., Qin,H., Liu,L., Qian,W., Ransohoff,R.M., Bergmann,C., Stohlman,S., Tuohy,V.K., and Li,X. (2010). Astrocyte-restricted ablation of interleukin-17-induced Act1-mediated signaling ameliorates autoimmune encephalomyelitis. Immunity. *32*, 414-425.

Karin,M. and Ben-Neriah,Y. (2000). Phosphorylation meets ubiquitination: the control of NF-[kappa]B activity. Annu. Rev. Immunol. *18*, 621-663.

Karray,S., Kress,C., Cuvellier,S., Hue-Beauvais,C., Damotte,D., Babinet,C., and Levi-Strauss,M. (2004). Complete loss of Fas ligand gene causes massive lymphoproliferation and early death, indicating a residual activity of gld allele. J. Immunol. *172*, 2118-2125.

Kato,M., Sanada,M., Kato,I., Sato,Y., Takita,J., Takeuchi,K., Niwa,A., Chen,Y., Nakazaki,K., Nomoto,J., Asakura,Y., Muto,S., Tamura,A., Iio,M., Akatsuka,Y., Hayashi,Y., Mori,H., Igarashi,T., Kurokawa,M., Chiba,S., Mori,S., Ishikawa,Y., Okamoto,K., Tobinai,K.,

Nakagama,H., Nakahata,T., Yoshino,T., Kobayashi,Y., and Ogawa,S. (2009). Frequent inactivation of A20 in B-cell lymphomas. Nature *459*, 712-716.

Kebir,H., Kreymborg,K., Ifergan,I., Dodelet-Devillers,A., Cayrol,R., Bernard,M., Giuliani,F., Arbour,N., Becher,B., and Prat,A. (2007). Human TH17 lymphocytes promote blood-brain barrier disruption and central nervous system inflammation. Nat. Med. *13*, 1173-1175.

Kirkpatrick,D.S., Hathaway,N.A., Hanna,J., Elsasser,S., Rush,J., Finley,D., King,R.W., and Gygi,S.P. (2006). Quantitative analysis of in vitro ubiquitinated cyclin B1 reveals complex chain topology. Nat. Cell Biol. *8*, 700-710.

Kobayashi,T., Okamoto,S., Hisamatsu,T., Kamada,N., Chinen,H., Saito,R., Kitazume,M.T., Nakazawa,A., Sugita,A., Koganei,K., Isobe,K., and Hibi,T. (2008). IL23 differentially regulates the Th1/Th17 balance in ulcerative colitis and Crohn's disease. Gut *57*, 1682-1689.

Kohji,T. and Matsumoto,Y. (2000). Coexpression of Fas/FasL and Bax on brain and infiltrating T cells in the central nervous system is closely associated with apoptotic cell death during autoimmune encephalomyelitis. J. Neuroimmunol. *106*, 165-171.

Kolodziej,L.E., Lodolce,J.P., Chang,J.E., Schneider,J.R., Grimm,W.A., Bartulis,S.J., Zhu,X., Messer,J.S., Murphy,S.F., Reddy,N., Turner,J.R., and Boone,D.L. (2011). TNFAIP3 maintains intestinal barrier function and supports epithelial cell tight junctions. PLoS. One. *6*, e26352.

Komiyama,Y., Nakae,S., Matsuki,T., Nambu,A., Ishigame,H., Kakuta,S., Sudo,K., and Iwakura,Y. (2006). IL-17 plays an important role in the development of experimental autoimmune encephalomyelitis. J. Immunol. *177*, 566-573.

Kool,M., van,L.G., Waelput,W., De,P.S., Muskens,F., Sze,M., van,P.J., Branco-Madeira,F., Janssens,S., Reizis,B., Elewaut,D., Beyaert,R., Hammad,H., and Lambrecht,B.N. (2011). The ubiquitin-editing protein A20 prevents dendritic cell activation, recognition of apoptotic cells, and systemic autoimmunity. Immunity. *35*, 82-96.

Kort,J.J., Kawamura,K., Fugger,L., Weissert,R., and Forsthuber,T.G. (2006). Efficient presentation of myelin oligodendrocyte glycoprotein peptides but not protein by astrocytes from HLA-DR2 and HLA-DR4 transgenic mice. J. Neuroimmunol. *173*, 23-34.

Krumbholz,M., Theil,D., Derfuss,T., Rosenwald,A., Schrader,F., Monoranu,C.M., Kalled,S.L., Hess,D.M., Serafini,B., Aloisi,F., Wekerle,H., Hohlfeld,R., and Meinl,E. (2005). BAFF is produced by astrocytes and up-regulated in multiple sclerosis lesions and primary central nervous system lymphoma. J. Exp. Med. *201*, 195-200.

Kuchler-Bopp,S., Delaunoy,J.P., Artault,J.C., Zaepfel,M., and Dietrich,J.B. (1999). Astrocytes induce several blood-brain barrier properties in non-neural endothelial cells. Neuroreport *10*, 1347-1353.

Larsen,P.H., Wells,J.E., Stallcup,W.B., Opdenakker,G., and Yong,V.W. (2003). Matrix metalloproteinase-9 facilitates remyelination in part by processing the inhibitory NG2 proteoglycan. J. Neurosci. *23*, 11127-11135.

Le,D.G., Kular,L., Nicot,A.B., Calmel,C., Melik-Parsadaniantz,S., Kitabgi,P., Laurent,M., and Martinerie,C. (2010). NOV/CCN3 upregulates CCL2 and CXCL1 expression in astrocytes through beta1 and beta5 integrins. Glia *58*, 1510-1521.

Lee,E.G., Boone,D.L., Chai,S., Libby,S.L., Chien,M., Lodolce,J.P., and Ma,A. (2000). Failure to regulate TNF-induced NF-kappaB and cell death responses in A20-deficient mice. Science *289*, 2350-2354.

Lee,S.C., Moore,G.R., Golenwsky,G., and Raine,C.S. (1990). Multiple sclerosis: a role for astroglia in active demyelination suggested by class II MHC expression and ultrastructural study. J. Neuropathol. Exp. Neurol. *49*, 122-136.

Lees,J.R., Golumbek,P.T., Sim,J., Dorsey,D., and Russell,J.H. (2008). Regional CNS responses to IFN-gamma determine lesion localization patterns during EAE pathogenesis. J. Exp. Med. *205*, 2633-2642.

Li,S., Zheng,H., Mao,A.P., Zhong,B., Li,Y., Liu,Y., Gao,Y., Ran,Y., Tien,P., and Shu,H.B. (2010). Regulation of virus-triggered signaling by OTUB1- and OTUB2-mediated deubiquitination of TRAF3 and TRAF6. J. Biol. Chem. *285*, 4291-4297.

Lieberman,A.P., Pitha,P.M., Shin,H.S., and Shin,M.L. (1989). Production of tumor necrosis factor and other cytokines by astrocytes stimulated with lipopolysaccharide or a neurotropic virus. Proc. Natl. Acad. Sci. U. S. A *86*, 6348-6352.

Linden,M., Khademi,M., Lima,B., I, Piehl,F., Jagodic,M., Kockum,I., and Olsson,T. (2013). Multiple sclerosis risk genotypes correlate with an elevated cerebrospinal fluid level of the suggested prognostic marker CXCL13. Mult. Scler. *19*, 863-870.

Lippens,S., Lefebvre,S., Gilbert,B., Sze,M., Devos,M., Verhelst,K., Vereecke,L., Mc,G.C., Guerin,C., Vandenabeele,P., Pasparakis,M., Mikkola,M.L., Beyaert,R., Declercq,W., and van,L.G. (2011). Keratinocyte-specific ablation of the NF-kappaB regulatory protein A20 (TNFAIP3) reveals a role in the control of epidermal homeostasis. Cell Death. Differ. *18*, 1845-1853.

Liu,C., Qian,W., Qian,Y., Giltiay,N.V., Lu,Y., Swaidani,S., Misra,S., Deng,L., Chen,Z.J., and Li,X. (2009). Act1, a U-box E3 ubiquitin ligase for IL-17 signaling. Sci. Signal. *2*, ra63.

Liu,Y., Teige,I., Birnir,B., and Issazadeh-Navikas,S. (2006). Neuron-mediated generation of regulatory T cells from encephalitogenic T cells suppresses EAE. Nat. Med. *12*, 518-525.

Livak,K.J. and Schmittgen,T.D. (2001). Analysis of relative gene expression data using real-time quantitative PCR and the 2(-Delta Delta C(T)) Method. Methods *25*, 402-408.

Maelfait,J., Roose,K., Bogaert,P., Sze,M., Saelens,X., Pasparakis,M., Carpentier,I., van,L.G., and Beyaert,R. (2012). A20 (Tnfaip3) deficiency in myeloid cells protects against influenza A virus infection. PLoS. Pathog. *8*, e1002570.

Maher,S., Toomey,D., Condron,C., and Bouchier-Hayes,D. (2002). Activation-induced cell death: the controversial role of Fas and Fas ligand in immune privilege and tumour counterattack. Immunol. Cell Biol. *80*, 131-137.

Mason,J.L., Suzuki,K., Chaplin,D.D., and Matsushima,G.K. (2001). Interleukin-1beta promotes repair of the CNS. J. Neurosci. *21*, 7046-7052.

Matmati,M., Jacques,P., Maelfait,J., Verheugen,E., Kool,M., Sze,M., Geboes,L., Louagie,E., Mc,G.C., Vereecke,L., Chu,Y., Boon,L., Staelens,S., Matthys,P., Lambrecht,B.N., Schmidt-Supprian,M., Pasparakis,M., Elewaut,D., Beyaert,R., and van,L.G. (2011). A20 (TNFAIP3) deficiency in myeloid cells triggers erosive polyarthritis resembling rheumatoid arthritis. Nat. Genet. *43*, 908-912.

Matsumoto,M.L., Wickliffe,K.E., Dong,K.C., Yu,C., Bosanac,I., Bustos,D., Phu,L., Kirkpatrick,D.S., Hymowitz,S.G., Rape,M., Kelley,R.F., and Dixit,V.M. (2010). K11-linked polyubiquitination in cell cycle control revealed by a K11 linkage-specific antibody. Mol. Cell *39*, 477-484.

Mauro,C., Pacifico,F., Lavorgna,A., Mellone,S., Iannetti,A., Acquaviva,R., Formisano,S., Vito,P., and Leonardi,A. (2006). ABIN-1 binds to NEMO/IKKgamma and co-operates with A20 in inhibiting NF-kappaB. J. Biol. Chem. *281*, 18482-18488.

Mc,G.C., Volckaert,T., Wolke,U., Sze,M., De,R.R., Waisman,A., Prinz,M., Beyaert,R., Pasparakis,M., and van,L.G. (2010). Oligodendrocyte-specific FADD deletion protects mice from autoimmune-mediated demyelination. J. Immunol. *185*, 7646-7653.

McFarland,H.F. and Martin,R. (2007). Multiple sclerosis: a complicated picture of autoimmunity. Nat. Immunol. *8*, 913-919.

McGeachy,M.J., Stephens,L.A., and Anderton,S.M. (2005). Natural recovery and protection from autoimmune encephalomyelitis: contribution of CD4+CD25+ regulatory cells within the central nervous system. J. Immunol. *175*, 3025-3032.

Meads,M.B., Li,Z.W., and Dalton,W.S. (2010). A novel TNF receptor-associated factor 6 binding domain mediates NF-kappa B signaling by the common cytokine receptor beta subunit. J. Immunol. *185*, 1606-1615.

Meiron,M., Zohar,Y., Anunu,R., Wildbaum,G., and Karin,N. (2008). CXCL12 (SDF-1alpha) suppresses ongoing experimental autoimmune encephalomyelitis by selecting antigen-specific regulatory T cells. J. Exp. Med. *205*, 2643-2655.

Miljkovic,D., Timotijevic,G., and Mostarica,S.M. (2011). Astrocytes in the tempest of multiple sclerosis. FEBS Lett. *585*, 3781-3788.

Milo,R. and Kahana,E. (2010). Multiple sclerosis: geoepidemiology, genetics and the environment. Autoimmun. Rev. *9*, A387-A394.

Miranda,M. and Sorkin,A. (2007). Regulation of receptors and transporters by ubiquitination: new insights into surprisingly similar mechanisms. Mol. Interv. *7*, 157-167.

Musone,S.L., Taylor,K.E., Lu,T.T., Nititham,J., Ferreira,R.C., Ortmann,W., Shifrin,N., Petri,M.A., Kamboh,M.I., Manzi,S., Seldin,M.F., Gregersen,P.K., Behrens,T.W., Ma,A., Kwok,P.Y., and Criswell,L.A. (2008). Multiple polymorphisms in the TNFAIP3 region are independently associated with systemic lupus erythematosus. Nat. Genet. *40*, 1062-1064.

Musone,S.L., Taylor,K.E., Nititham,J., Chu,C., Poon,A., Liao,W., Lam,E.T., Ma,A., Kwok,P.Y., and Criswell,L.A. (2011). Sequencing of TNFAIP3 and association of variants with multiple autoimmune diseases. Genes Immun. *12*, 176-182.

Muzio,M., Chinnaiyan,A.M., Kischkel,F.C., O'Rourke,K., Shevchenko,A., Ni,J., Scaffidi,C., Bretz,J.D., Zhang,M., Gentz,R., Mann,M., Krammer,P.H., Peter,M.E., and Dixit,V.M. (1996). FLICE, a novel FADD-homologous ICE/CED-3-like protease, is recruited to the CD95 (Fas/APO-1) death--inducing signaling complex. Cell *85*, 817-827.

Nair,A., Frederick,T.J., and Miller,S.D. (2008). Astrocytes in multiple sclerosis: a product of their environment. Cell Mol. Life Sci. *65*, 2702-2720.

Nair,R.P., Duffin,K.C., Helms,C., Ding,J., Stuart,P.E., Goldgar,D., Gudjonsson,J.E., Li,Y., Tejasvi,T., Feng,B.J., Ruether,A., Schreiber,S., Weichenthal,M., Gladman,D., Rahman,P., Schrodi,S.J., Prahalad,S., Guthery,S.L., Fischer,J., Liao,W., Kwok,P.Y., Menter,A., Lathrop,G.M., Wise,C.A., Begovich,A.B., Voorhees,J.J., Elder,J.T., Krueger,G.G., Bowcock,A.M., and Abecasis,G.R. (2009). Genome-wide scan reveals association of psoriasis with IL-23 and NF-kappaB pathways. Nat. Genet. *41*, 199-204.

Novack,D.V., Yin,L., Hagen-Stapleton,A., Schreiber,R.D., Goeddel,D.V., Ross,F.P., and Teitelbaum,S.L. (2003). The IkappaB function of NF-kappaB2 p100 controls stimulated osteoclastogenesis. J. Exp. Med. *198*, 771-781.

O' Reilly,L.A., Tai,L., Lee,L., Kruse,E.A., Grabow,S., Fairlie,W.D., Haynes,N.M., Tarlinton,D.M., Zhang,J.G., Belz,G.T., Smyth,M.J., Bouillet,P., Robb,L., and Strasser,A. (2009). Membrane-bound Fas ligand only is essential for Fas-induced apoptosis. Nature *461*, 659-663.

Oeckinghaus,A., Hayden,M.S., and Ghosh,S. (2011). Crosstalk in NF-kappaB signaling pathways. Nat. Immunol. *12*, 695-708.

Opipari,A.W., Jr., Boguski,M.S., and Dixit,V.M. (1990). The A20 cDNA induced by tumor necrosis factor alpha encodes a novel type of zinc finger protein. J. Biol. Chem. *265*, 14705-14708.

Opipari,A.W., Jr., Hu,H.M., Yabkowitz,R., and Dixit,V.M. (1992). The A20 zinc finger protein protects cells from tumor necrosis factor cytotoxicity. J. Biol. Chem. *267*, 12424-12427.

Orlinick,J.R., Vaishnaw,A., Elkon,K.B., and Chao,M.V. (1997). Requirement of cysteine-rich repeats of the Fas receptor for binding by the Fas ligand. J. Biol. Chem. *272*, 28889-28894.

Ottonello,L., Tortolina,G., Amelotti,M., and Dallegri,F. (1999). Soluble Fas ligand is chemotactic for human neutrophilic polymorphonuclear leukocytes. J. Immunol. *162*, 3601-3606.

Ozawa,K., Suchanek,G., Breitschopf,H., Bruck,W., Budka,H., Jellinger,K., and Lassmann,H. (1994). Patterns of oligodendroglia pathology in multiple sclerosis. Brain *117 (Pt 6)*, 1311-1322.

Pagenstecher,A., Stalder,A.K., Kincaid,C.L., Shapiro,S.D., and Campbell,I.L. (1998). Differential expression of matrix metalloproteinase and tissue inhibitor of matrix metalloproteinase genes in the mouse central nervous system in normal and inflammatory states. Am. J. Pathol. *152*, 729-741.

Pender,M.P., Nguyen,K.B., McCombe,P.A., and Kerr,J.F. (1991). Apoptosis in the nervous system in experimental allergic encephalomyelitis. J. Neurol. Sci. *104*, 81-87.

Perrin,P.J., Maldonado,J.H., Davis,T.A., June,C.H., and Racke,M.K. (1996). CTLA-4 blockade enhances clinical disease and cytokine production during experimental allergic encephalomyelitis. J. Immunol. *157*, 1333-1336.

Peter,M.E. and Krammer,P.H. (2003). The CD95(APO-1/Fas) DISC and beyond. Cell Death. Differ. *10*, 26-35.

Petermann,F. and Korn,T. (2011). Cytokines and effector T cell subsets causing autoimmune CNS disease. FEBS Lett. *585*, 3747-3757.

Pfrieger,F.W. and Barres,B.A. (1997). Synaptic efficacy enhanced by glial cells in vitro. Science *277*, 1684-1687.

Qian,Y., Liu,C., Hartupee,J., Altuntas,C.Z., Gulen,M.F., Jane-Wit,D., Xiao,J., Lu,Y., Giltiay,N., Liu,J., Kordula,T., Zhang,Q.W., Vallance,B., Swaidani,S., Aronica,M., Tuohy,V.K., Hamilton,T., and Li,X. (2007). The adaptor Act1 is required for interleukin 17-dependent signaling associated with autoimmune and inflammatory disease. Nat. Immunol. *8*, 247-256.

Reboldi,A., Coisne,C., Baumjohann,D., Benvenuto,F., Bottinelli,D., Lira,S., Uccelli,A., Lanzavecchia,A., Engelhardt,B., and Sallusto,F. (2009). C-C chemokine receptor 6-regulated entry of TH-17 cells into the CNS through the choroid plexus is required for the initiation of EAE. Nat. Immunol. *10*, 514-523.

Reyes-Turcu,F.E., Ventii,K.H., and Wilkinson,K.D. (2009). Regulation and cellular roles of ubiquitin-specific deubiquitinating enzymes. Annu. Rev. Biochem. *78*, 363-397.

Riedl,S.J. and Salvesen,G.S. (2007). The apoptosome: signalling platform of cell death. Nat. Rev. Mol. Cell Biol. *8*, 405-413.

Sabelko-Downes,K.A., Cross,A.H., and Russell,J.H. (1999). Dual role for Fas ligand in the initiation of and recovery from experimental allergic encephalomyelitis. J. Exp. Med. *189*, 1195-1205.

Saha,R.N. and Pahan,K. (2006). Regulation of inducible nitric oxide synthase gene in glial cells. Antioxid. Redox. Signal. *8*, 929-947.

Saitoh,T., Yamamoto,M., Miyagishi,M., Taira,K., Nakanishi,M., Fujita,T., Akira,S., Yamamoto,N., and Yamaoka,S. (2005). A20 is a negative regulator of IFN regulatory factor 3 signaling. J. Immunol. *174*, 1507-1512.

Schmied,M., Breitschopf,H., Gold,R., Zischler,H., Rothe,G., Wekerle,H., and Lassmann,H. (1993). Apoptosis of T lymphocytes in experimental autoimmune encephalomyelitis. Evidence for programmed cell death as a mechanism to control inflammation in the brain. Am. J. Pathol. *143*, 446-452.

Schulman,B.A. and Harper,J.W. (2009). Ubiquitin-like protein activation by E1 enzymes: the apex for downstream signalling pathways. Nat. Rev. Mol. Cell Biol. *10*, 319-331.

Seino,K., Iwabuchi,K., Kayagaki,N., Miyata,R., Nagaoka,I., Matsuzawa,A., Fukao,K., Yagita,H., and Okumura,K. (1998). Chemotactic activity of soluble Fas ligand against phagocytes. J. Immunol. *161*, 4484-4488.

Shao,L., Oshima,S., Duong,B., Advincula,R., Barrera,J., Malynn,B.A., and Ma,A. (2013). A20 restricts wnt signaling in intestinal epithelial cells and suppresses colon carcinogenesis. PLoS. One. *8*, e62223.

Shembade,N., Harhaj,N.S., Parvatiyar,K., Copeland,N.G., Jenkins,N.A., Matesic,L.E., and Harhaj,E.W. (2008). The E3 ligase Itch negatively regulates inflammatory signaling pathways by controlling the function of the ubiquitin-editing enzyme A20. Nat. Immunol. *9*, 254-262.

Shembade,N., Ma,A., and Harhaj,E.W. (2010). Inhibition of NF-kappaB signaling by A20 through disruption of ubiquitin enzyme complexes. Science *327*, 1135-1139.

Shembade,N., Parvatiyar,K., Harhaj,N.S., and Harhaj,E.W. (2009). The ubiquitin-editing enzyme A20 requires RNF11 to downregulate NF-kappaB signalling. EMBO J. *28*, 513-522.

Skaug,B., Chen,J., Du,F., He,J., Ma,A., and Chen,Z.J. (2011). Direct, noncatalytic mechanism of IKK inhibition by A20. Mol. Cell *44*, 559-571.

Skaug,B., Jiang,X., and Chen,Z.J. (2009). The role of ubiquitin in NF-kappaB regulatory pathways. Annu. Rev. Biochem. *78*, 769-796.

Solan,N.J., Miyoshi,H., Carmona,E.M., Bren,G.D., and Paya,C.V. (2002). RelB cellular regulation and transcriptional activity are regulated by p100. J. Biol. Chem. *277*, 1405-1418.

Stromnes,I.M., Cerretti,L.M., Liggitt,D., Harris,R.A., and Goverman,J.M. (2008). Differential regulation of central nervous system autoimmunity by T(H)1 and T(H)17 cells. Nat. Med. *14*, 337-342.

Suda,T., Takahashi,T., Golstein,P., and Nagata,S. (1993). Molecular cloning and expression of the Fas ligand, a novel member of the tumor necrosis factor family. Cell *75*, 1169-1178.

Sun,S.C. (2008). Deubiquitylation and regulation of the immune response. Nat. Rev. Immunol. *8*, 501-511.

Sun,S.C. (2010). CYLD: a tumor suppressor deubiquitinase regulating NF-kappaB activation and diverse biological processes. Cell Death. Differ. *17*, 25-34.

Sun,S.C. (2011). Non-canonical NF-kappaB signaling pathway. Cell Res. *21*, 71-85.

Suvannavejh,G.C., Dal Canto,M.C., Matis,L.A., and Miller,S.D. (2000). Fas-mediated apoptosis in clinical remissions of relapsing experimental autoimmune encephalomyelitis. J. Clin. Invest *105*, 223-231.

Takahashi,T., Tanaka,M., Brannan,C.I., Jenkins,N.A., Copeland,N.G., Suda,T., and Nagata,S. (1994). Generalized lymphoproliferative disease in mice, caused by a point mutation in the Fas ligand. Cell *76*, 969-976.

Tan,L., Gordon,K.B., Mueller,J.P., Matis,L.A., and Miller,S.D. (1998). Presentation of proteolipid protein epitopes and B7-1-dependent activation of encephalitogenic T cells by IFN-gamma-activated SJL/J astrocytes. J. Immunol. *160*, 4271-4279.

Tavares,R.M., Turer,E.E., Liu,C.L., Advincula,R., Scapini,P., Rhee,L., Barrera,J., Lowell,C.A., Utz,P.J., Malynn,B.A., and Ma,A. (2010). The ubiquitin modifying enzyme A20 restricts B cell survival and prevents autoimmunity. Immunity. *33*, 181-191.

Tewari,M., Wolf,F.W., Seldin,M.F., O'Shea,K.S., Dixit,V.M., and Turka,L.A. (1995). Lymphoid expression and regulation of A20, an inhibitor of programmed cell death. J. Immunol. *154*, 1699-1706.

Tokunaga,F., Nakagawa,T., Nakahara,M., Saeki,Y., Taniguchi,M., Sakata,S., Tanaka,K., Nakano,H., and Iwai,K. (2011). SHARPIN is a component of the NF-kappaB-activating linear ubiquitin chain assembly complex. Nature *471*, 633-636.

Tokunaga,F., Nishimasu,H., Ishitani,R., Goto,E., Noguchi,T., Mio,K., Kamei,K., Ma,A., Iwai,K., and Nureki,O. (2012). Specific recognition of linear polyubiquitin by A20 zinc finger 7 is involved in NF-kappaB regulation. EMBO J. *31*, 3856-3870.

Tokunaga,F., Sakata,S., Saeki,Y., Satomi,Y., Kirisako,T., Kamei,K., Nakagawa,T., Kato,M., Murata,S., Yamaoka,S., Yamamoto,M., Akira,S., Takao,T., Tanaka,K., and Iwai,K. (2009). Involvement of linear polyubiquitylation of NEMO in NF-kappaB activation. Nat. Cell Biol. *11*, 123-132.

Trajkovic,V., Stosic-Grujicic,S., Samardzic,T., Markovic,M., Miljkovic,D., Ramic,Z., and Mostarica,S.M. (2001). Interleukin-17 stimulates inducible nitric oxide synthase activation in rodent astrocytes. J. Neuroimmunol. *119*, 183-191.

Trajkovic,V., Vuckovic,O., Stosic-Grujicic,S., Miljkovic,D., Popadic,D., Markovic,M., Bumbasirevic,V., Backovic,A., Cvetkovic,I., Harhaji,L., Ramic,Z., and Mostarica,S.M. (2004). Astrocyte-induced regulatory T cells mitigate CNS autoimmunity. Glia *47*, 168-179.

Tran,E.H., Hardin-Pouzet,H., Verge,G., and Owens,T. (1997). Astrocytes and microglia express inducible nitric oxide synthase in mice with experimental allergic encephalomyelitis. J. Neuroimmunol. *74*, 121-129.

Tran,E.H., Hoekstra,K., van,R.N., Dijkstra,C.D., and Owens,T. (1998). Immune invasion of the central nervous system parenchyma and experimental allergic encephalomyelitis, but not leukocyte extravasation from blood, are prevented in macrophage-depleted mice. J. Immunol. *161*, 3767-3775.

Tsakiri,N., Papadopoulos,D., Denis,M.C., Mitsikostas,D.D., and Kollias,G. (2012). TNFR2 on non-haematopoietic cells is required for Foxp3+ Treg-cell function and disease suppression in EAE. Eur. J. Immunol. *42*, 403-412.

Turer,E.E., Tavares,R.M., Mortier,E., Hitotsumatsu,O., Advincula,R., Lee,B., Shifrin,N., Malynn,B.A., and Ma,A. (2008). Homeostatic MyD88-dependent signals cause lethal inflamMation in the absence of A20. J. Exp. Med. *205*, 451-464.

Uhm,J.H., Dooley,N.P., Oh,L.Y., and Yong,V.W. (1998). Oligodendrocytes utilize a matrix metalloproteinase, MMP-9, to extend processes along an astrocyte extracellular matrix. Glia *22*, 53-63.

Ullian,E.M., Sapperstein,S.K., Christopherson,K.S., and Barres,B.A. (2001). Control of synapse number by glia. Science *291*, 657-661.

Vallabhapurapu,S. and Karin,M. (2009). Regulation and function of NF-kappaB transcription factors in the immune system. Annu. Rev. Immunol. *27*, 693-733.

Van Wagoner,N.J., Oh,J.W., Repovic,P., and Benveniste,E.N. (1999). Interleukin-6 (IL-6) production by astrocytes: autocrine regulation by IL-6 and the soluble IL-6 receptor. J. Neurosci. *19*, 5236-5244.

van,L.G., De,L.R., Schmidt,H., Huth,M., Mildner,A., Schmidt-Supprian,M., Lassmann,H., Prinz,M.R., and Pasparakis,M. (2006). Inhibition of transcription factor NF-kappaB in the central nervous system ameliorates autoimmune encephalomyelitis in mice. Nat. Immunol. *7*, 954-961.

Varinou,L., Ramsauer,K., Karaghiosoff,M., Kolbe,T., Pfeffer,K., Muller,M., and Decker,T. (2003). Phosphorylation of the Stat1 transactivation domain is required for full-fledged IFN-gamma-dependent innate immunity. Immunity. *19*, 793-802.

Vereecke,L., Sze,M., Mc,G.C., Rogiers,B., Chu,Y., Schmidt-Supprian,M., Pasparakis,M., Beyaert,R., and van,L.G. (2010). Enterocyte-specific A20 deficiency sensitizes to tumor necrosis factor-induced toxicity and experimental colitis. J. Exp. Med. *207*, 1513-1523.

Verhelst,K., Carpentier,I., Kreike,M., Meloni,L., Verstrepen,L., Kensche,T., Dikic,I., and Beyaert,R. (2012). A20 inhibits LUBAC-mediated NF-kappaB activation by binding linear polyubiquitin chains via its zinc finger 7. EMBO J. *31*, 3845-3855.

Voskuhl,R.R., Peterson,R.S., Song,B., Ao,Y., Morales,L.B., Tiwari-Woodruff,S., and Sofroniew,M.V. (2009). Reactive astrocytes form scar-like perivascular barriers to leukocytes during adaptive immune inflammation of the CNS. J. Neurosci. *29*, 11511-11522.

Vucic,D., Dixit,V.M., and Wertz,I.E. (2011). Ubiquitylation in apoptosis: a post-translational modification at the edge of life and death. Nat. Rev. Mol. Cell Biol. *12*, 439-452.

Wagner,B., Natarajan,A., Grunaug,S., Kroismayr,R., Wagner,E.F., and Sibilia,M. (2006). Neuronal survival depends on EGFR signaling in cortical but not midbrain astrocytes. EMBO J. *25*, 752-762.

Wajant,H., Pfizenmaier,K., and Scheurich,P. (2003). Non-apoptotic Fas signaling. Cytokine Growth Factor Rev. *14*, 53-66.

Waldner,H., Sobel,R.A., Howard,E., and Kuchroo,V.K. (1997). Fas- and FasL-deficient mice are resistant to induction of autoimmune encephalomyelitis. J. Immunol. *159*, 3100-3103.

Walz,W. (2000). Role of astrocytes in the clearance of excess extracellular potassium. Neurochem. Int. *36*, 291-300.

Watanabe-Fukunaga,R., Brannan,C.I., Copeland,N.G., Jenkins,N.A., and Nagata,S. (1992). Lymphoproliferation disorder in mice explained by defects in Fas antigen that mediates apoptosis. Nature *356*, 314-317.

Wertz,I.E. and Dixit,V.M. (2010). Signaling to NF-kappaB: regulation by ubiquitination. Cold Spring Harb. Perspect. Biol. *2*, a003350.

Wertz,I.E., O'Rourke,K.M., Zhou,H., Eby,M., Aravind,L., Seshagiri,S., Wu,P., Wiesmann,C., Baker,R., Boone,D.L., Ma,A., Koonin,E.V., and Dixit,V.M. (2004). De-ubiquitination and ubiquitin ligase domains of A20 downregulate NF-kappaB signalling. Nature *430*, 694-699.

Wicovsky,A., Salzmann,S., Roos,C., Ehrenschwender,M., Rosenthal,T., Siegmund,D., Henkler,F., Gohlke,F., Kneitz,C., and Wajant,H. (2009). TNF-like weak inducer of apoptosis inhibits proinflammatory TNF receptor-1 signaling. Cell Death. Differ. *16*, 1445-1459.

Won,M., Park,K.A., Byun,H.S., Sohn,K.C., Kim,Y.R., Jeon,J., Hong,J.H., Park,J., Seok,J.H., Kim,J.M., Yoon,W.H., Jang,I.S., Shen,H.M., Liu,Z.G., and Hur,G.M. (2010). Novel anti-apoptotic mechanism of A20 through targeting ASK1 to suppress TNF-induced JNK activation. Cell Death. Differ. *17*, 1830-1841.

Yamaguchi,N., Oyama,M., Kozuka-Hata,H., and Inoue,J. (2013). Involvement of A20 in the molecular switch that activates the non-canonical NF-small ka, CyrillicB pathway. Sci. Rep. *3*, 2568.

Yuan,C., Qi,J., Zhao,X., and Gao,C. (2012). Smurf1 protein negatively regulates interferon-gamma signaling through promoting STAT1 protein ubiquitination and degradation. J. Biol. Chem. *287*, 17006-17015.

Zarnegar,B.J., Wang,Y., Mahoney,D.J., Dempsey,P.W., Cheung,H.H., He,J., Shiba,T., Yang,X., Yeh,W.C., Mak,T.W., Korneluk,R.G., and Cheng,G. (2008). Noncanonical NF-kappaB activation requires coordinated assembly of a regulatory complex of the adaptors cIAP1, cIAP2, TRAF2 and TRAF3 and the kinase NIK. Nat. Immunol. *9*, 1371-1378.

Zeinstra,E., Wilczak,N., Streefland,C., and De,K.J. (2000). Astrocytes in chronic active multiple sclerosis plaques express MHC class II molecules. Neuroreport *11*, 89-91.

Zepp,J., Wu,L., and Li,X. (2011). IL-17 receptor signaling and T helper 17-mediated autoimmune demyelinating disease. Trends Immunol. *32*, 232-239.

Zhao,W., Tilton,R.G., Corbett,J.A., McDaniel,M.L., Misko,T.P., Williamson,J.R., Cross,A.H., and Hickey,W.F. (1996). Experimental allergic encephalomyelitis in the rat is inhibited by aminoguanidine, an inhibitor of nitric oxide synthase. J. Neuroimmunol. *64*, 123-133.

Zhou,Y., Sonobe,Y., Akahori,T., Jin,S., Kawanokuchi,J., Noda,M., Iwakura,Y., Mizuno,T., and Suzumura,A. (2011). IL-9 promotes Th17 cell migration into the central nervous system via CC chemokine ligand-20 produced by astrocytes. J. Immunol. *186*, 4415-4421.

Zhu,B., Luo,L., Chen,Y., Paty,D.W., and Cynader,M.S. (2002). Intrathecal Fas ligand infusion strengthens immunoprivilege of central nervous system and suppresses experimental autoimmune encephalomyelitis. J. Immunol. *169*, 1561-1569.

Zhu,S., Pan,W., Shi,P., Gao,H., Zhao,F., Song,X., Liu,Y., Zhao,L., Li,X., Shi,Y., and Qian,Y. (2010). Modulation of experimental autoimmune encephalomyelitis through TRAF3-mediated suppression of interleukin 17 receptor signaling. J. Exp. Med. *207*, 2647-2662.

Zlokovic,B.V. (2008). The blood-brain barrier in health and chronic neurodegenerative disorders. Neuron *57*, 178-201.

Erklärung

Hiermit erkläre ich, dass ich die von mir eingereichte Dissertation zum Thema:

Astrocyte-specific function of A20 and FasL in experimental autoimmune encephalomyelitis

selbstständig verfasst, nicht schon als Dissertation verwendet habe und die benutzten Hilfsmittel und Quellen vollständig angegeben wurden.

Weiterhin erkläre ich, dass ich weder diese noch eine andere Arbeit zur Erlangung des akademischen Grades doctor rerum naturalium (Dr. rer. nat.) an anderen Einrichtungen eingereicht habe.

Magdeburg, den 10.12.2014

Xu Wang

Curriculum vitae

Persönliche Daten

Name	Xu Wang
Adresse	602, Fermersleber Weg 45C
	39112 Magdeburg
Geburtsdatum	16.02.1986
Geburtsort	Linyi, Shandong, Volksrepublik China
Familienstand	Verheiratet
Telefon	0049-15214328025
E-Mail	xu.wang@med.ovgu.de

Hochschulausbildung

2003 - 2007	Bachelor of Science, von Northeast Forestry University, Harbin, Volksrepublik China
2007 - 2010	Master of Science, von Northeast Forestry University, Harbin, Volksrepublik China

Beruflicher Werdegang

seit 2010	Wissenschaftlicher Mitarbeiter des Instituts für Medizinische Mikrobiologie und Krankenhaushygiene, Otto-von-Guericke-Universität Magdeburg.